NASA CR-145005

Report No. 3179

BBN Job No. 10815

NASI-13857

ACOUSTICAL MODELING STUDY OF THE OPEN TEST SECTION OF THE NASA LANGLEY V/STOL WIND TUNNEL

Istvan L. Ver
Douglas W. Andersen
Donald B. Bliss

(NASA-CR-145005) ACOUSTICAL MODELING STUDY OF THE OPEN TEST SECTION OF THE NASA LANGLEY V/STOL WIND TUNNEL (Bolt, Beranek, and Newman, Inc.) 116 p HC $5.50 CSCL 20A

N76-27958

G3/71 Unclas 44509

Submitted to:

National Aeronautics and Space Administration

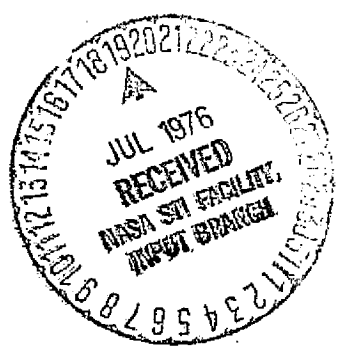

SUMMARY

Bolt Beranek and Newman Inc. has been requested by the NASA Langley Research Center to carry out an acoustical and aerodynamic scale-model study of the open test section of the NASA Langley V/STOL Wind Tunnel. The goal of the acoustic model study was to identify effective sound absorbing treatment of strategically located surfaces in the open tunnel test section which would enlarge that portion of the test section where free field conditions are simulated while the aerodynamic study sought to find measures to control low frequency jet pulsations which occur when the tunnel is operated in its open test section configuration.

The results of the acoustical modeling study indicated that: (1) lining of the raised ceiling and the test section floor immediately below it results in a substantial improvement, (2) any further increase of the sound absorbing treatment beyond this yields only marginal improvement.

The aerodynamic model study indicated that: (1) the low frequency jet pulsations are most likely caused or maintained by coupling of aerodynamic and aeroacoustic phenomena in the closed tunnel circuit, (2) replacing the hard collector cowl with a geometrically identical but porous fiber metal surface of 100 mks rayls flow resistance does not result in any noticable reduction of the test section noise caused by the impingement of the turbulent flow on the cowl.

TABLE OF CONTENTS

TABLE OF CONTENTS *cont.*

LIST OF FIGURES

LIST OF FIGURES *(cont.)*

LIST OF FIGURES *(cont.)*

LIST OF TABLES

INTRODUCTION

The NASA Langley V/STOL Wind Tunnel in its open test section mode of operation has the potential for use in aeroacoustic research. Noise surveys [1, 2]* indicate that for a given air speed the fan noise in the test section of the V/STOL tunnel is considerably lower than the noise in other open test section tunnels where the driving fans have a direct line of sight to the test section.

However, low fan noise is only a necessary but not sufficient requirement for using a tunnel for aeroacoustic research. In addition to this requirement, one also must make provisions to minimize the reflection of the sound from tunnel surfaces so that these reflections do not interfere with the measurement of the direct sound emanating from the aerodynamic noise source under test and thereby permitting the evaluation of its radiation pattern.

The prime purpose of the scale-model study described in this report was to find cost effective ways to reduce unwanted reflections and reverberation in the open tunnel test section by lining certain strategically located surfaces with sound absorbing material.

Parallel, and in addition to this acoustical model study, an aerodynamic model study of limited scope was also conducted with the purpose of finding ways to reduce low frequency jet pulsations through changes in collector cowl geometry, and to experimentally evaluate whether or not the test section noise due to the impingement of the turbulent flow on the collector cowl can be reduced

*Numbers in brackets refer to references listed at the end of this report.

by replacing the rigid collector cowl by a porous cowl of the same geometry.

The acoustical model study is described in Section A and the aerodynamic model study in Section B of this report.

A ACOUSTIC MODEL STUDY

The purpose of the acoustical model study was to experimentally evaluate the effect of lining certain, strategically located, interior tunnel surfaces on the sound field in the open tunnel test section. The methods and instrumentation used in this study was very similar to that used in a previous study modeling the open test section of the NASA Langley Full-Scale Wind Tunnel [3]. The discussions on scaling room acoustic performance, choice of scaling factor and instrumentation in Ref. 3 also apply to this case and the reader not familiar with the techniques of acoustical scale-modeling may find it helpful to study Sections III and IV of that report and the appropriate references contained within it.

1. Description of the Acoustical Model

A conceptual sketch of the NASA Langley V/STOL Wind Tunnel is shown in Fig. 1. In the framework of the present study we were concerned about only the room acoustics of the open tunnel test section. Accordingly, we have built a 1:10-scale model of this test section including all acoustically significant features of the full-scale test section. The rest of the tunnel circuit was not modeled. However, a short piece of the nozzle and collector was attached and terminated by effective anechoic treatment.

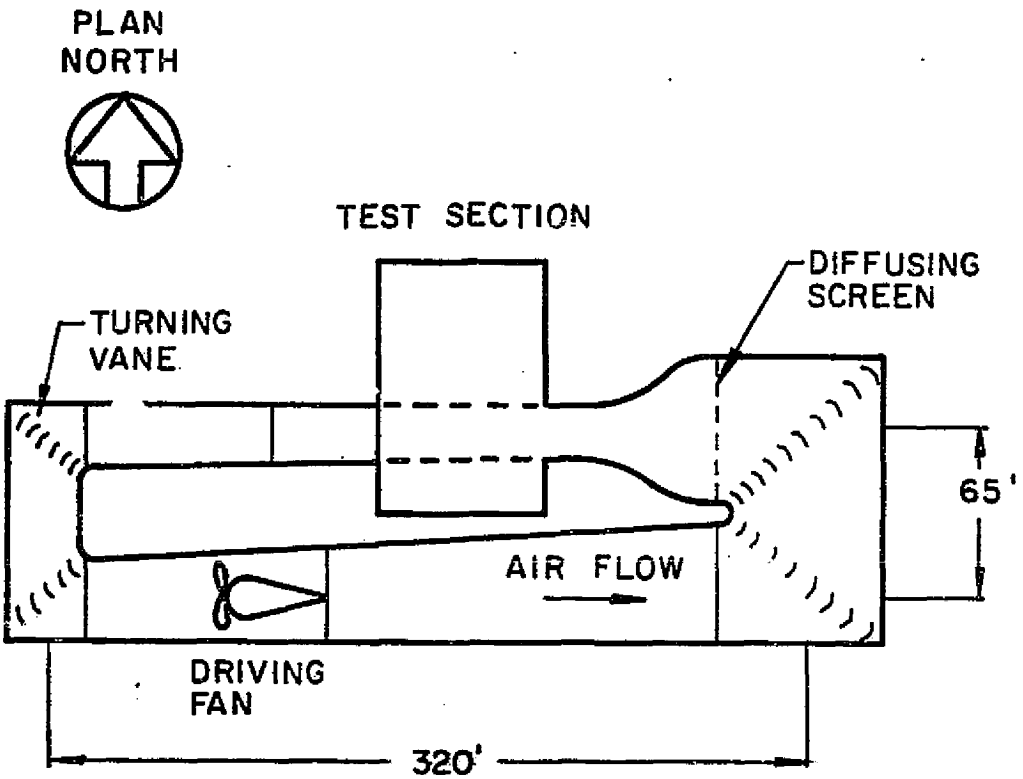

FIG. 1. PLAN VIEW OF THE V/STOL WIND TUNNEL

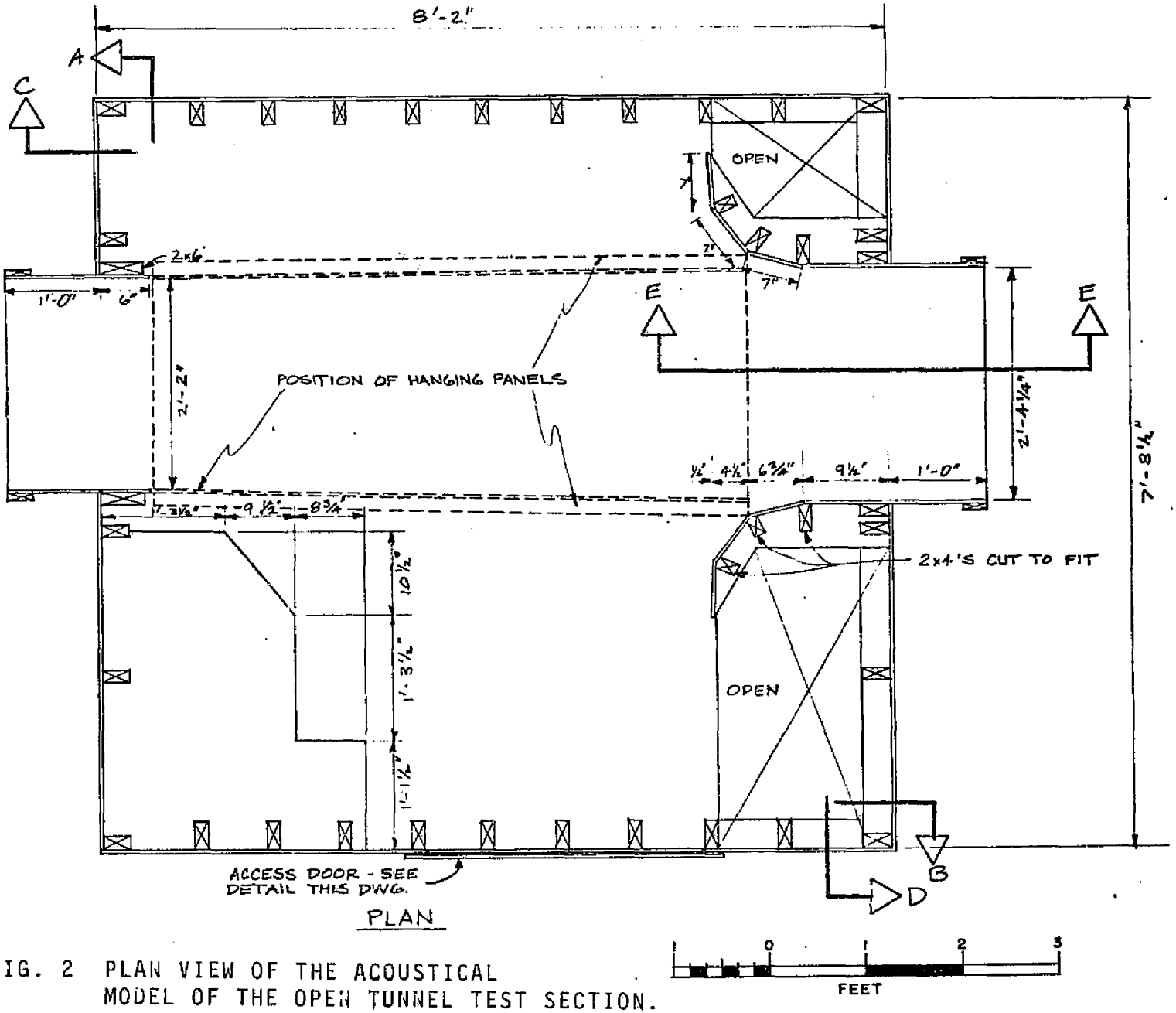

FIG. 2 PLAN VIEW OF THE ACOUSTICAL MODEL OF THE OPEN TUNNEL TEST SECTION.

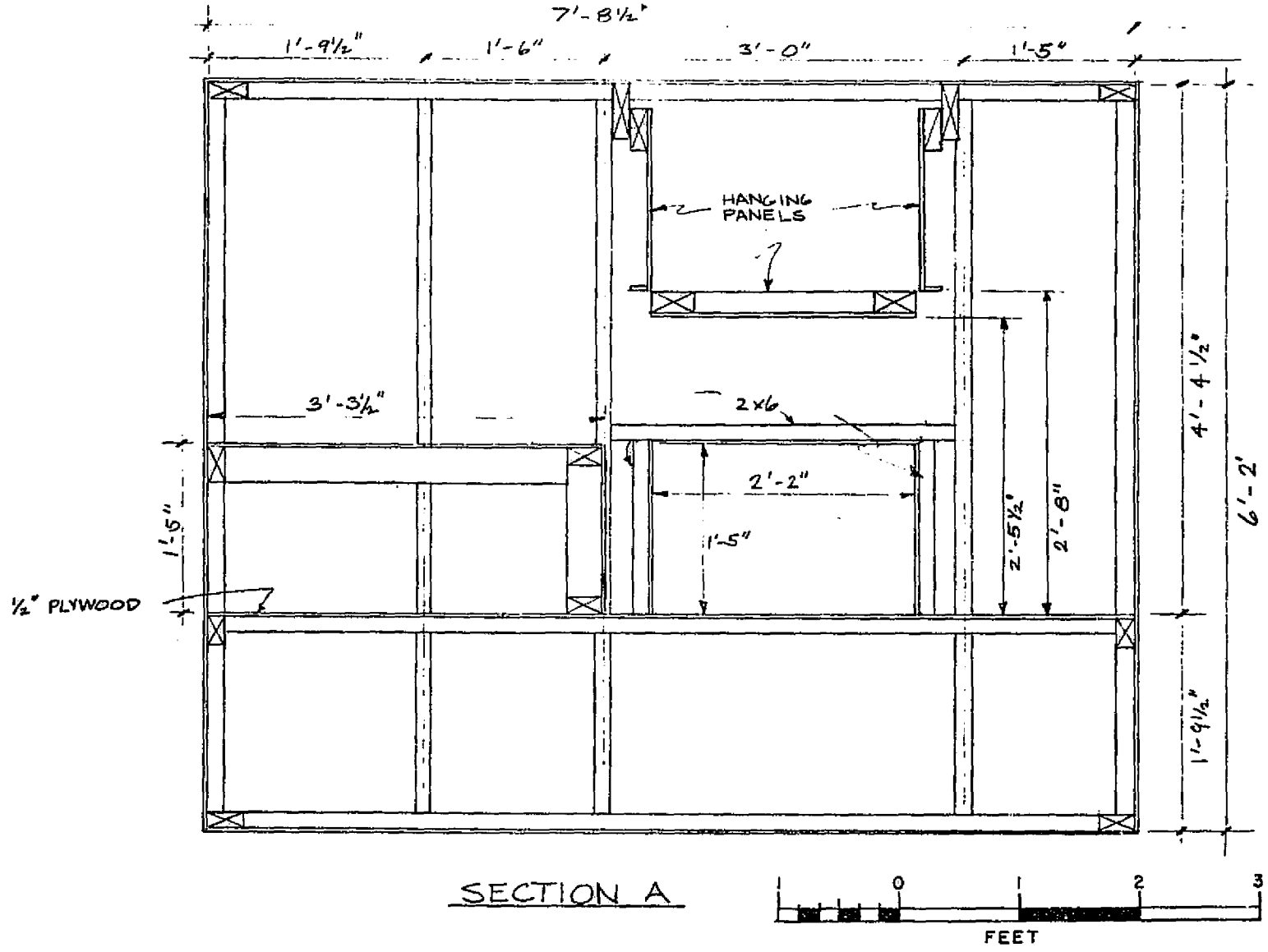

FIG. 3a SECTION A OF FIG. 2

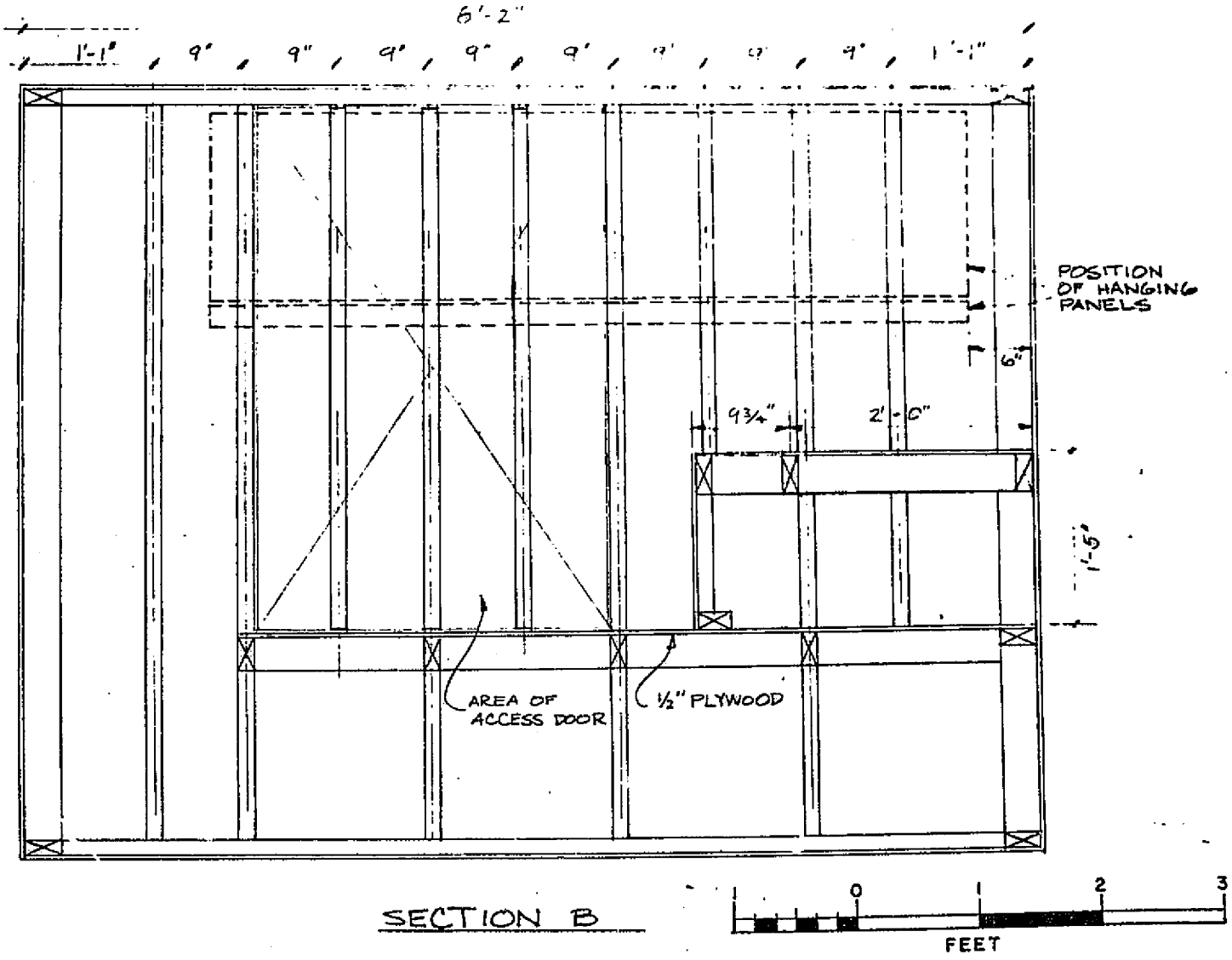

FIG. 3b SECTION B OF FIG. 2

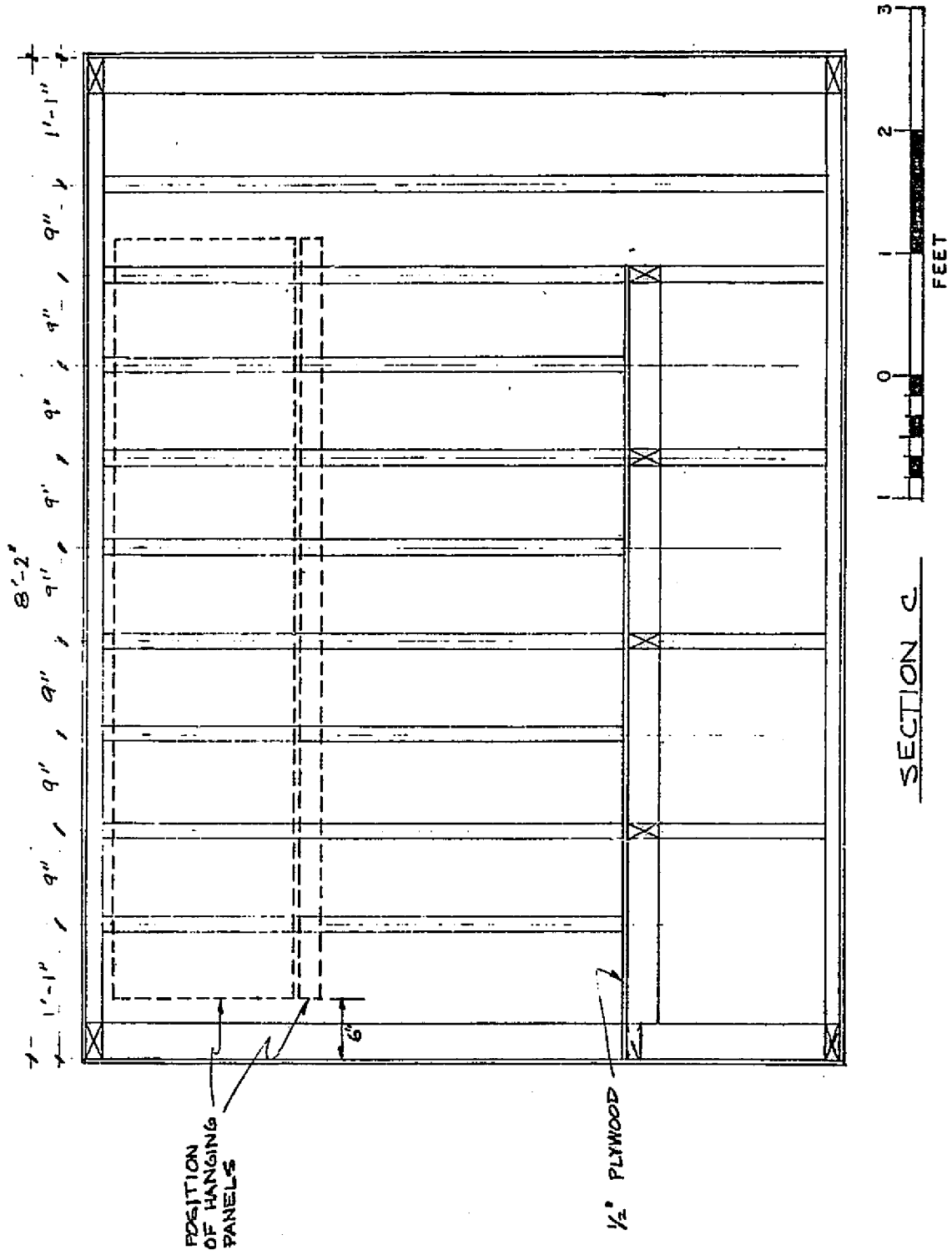

FIG. 3c SECTION C OF FIG. 2

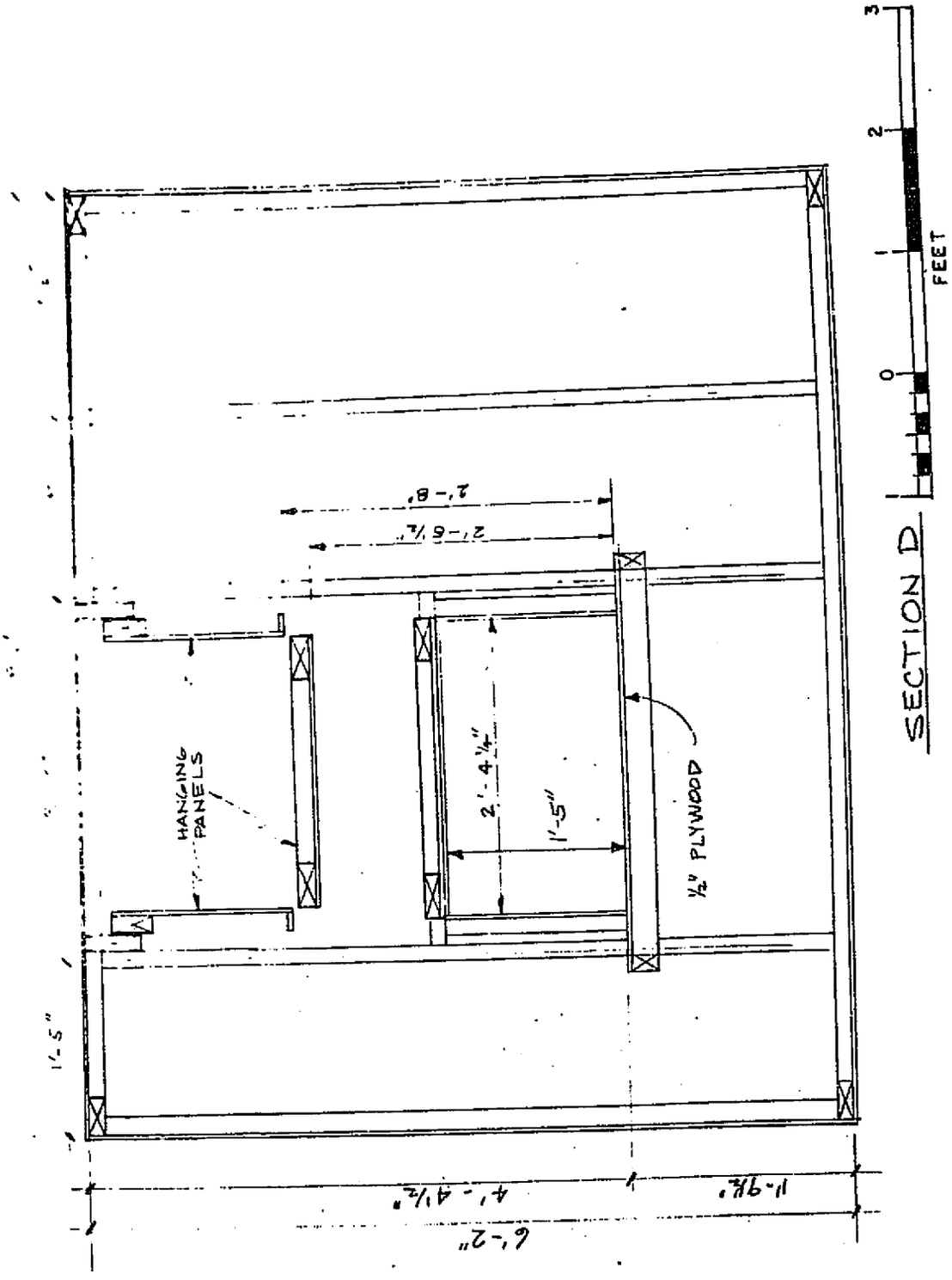

FIG. 3d SECTION D OF FIG. 2.

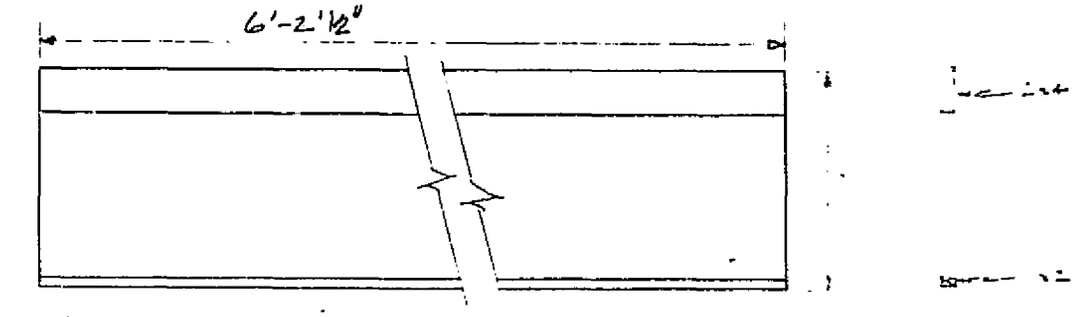

HANGING PANEL DETAIL (MAKE 2)

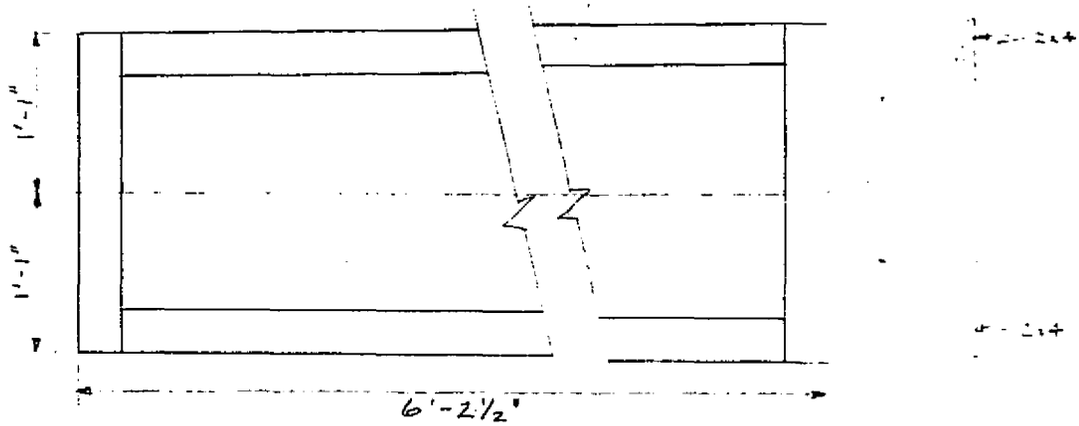

HANGING CEILING DETAIL (MAKE

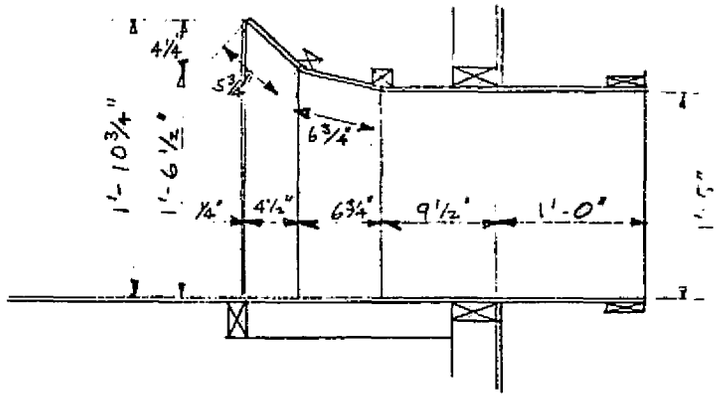

SECTION E-E

FIG. 3e SECTION L OF FIG. 2.

The significant dimensions of the scale-model test section are shown in Fig. 2 and Figs. 3a to 3e respectively. The photographs in Fig. 4a and Fig. 4b show views of the completed test section model from the nozzle and diffuser duct respectively. These photographs also show the ceiling panel in its raised position, the crossing jet noise source and the microphone. Fig. 5 shows a side-view of the model test section; again showing the nozzle opening and the lined ceiling and side wall panels in their raised positions.

2. Experimental Method

As in any experimental study, the first step is to plan a series of experiments to yield quantitative or qualitative information which, if appropriately processed, provide the answer to the problem at hand.

The problem in our case was to find a cost effective way to simulate free field conditions within a large portion of the open test section for the sound emanating from sources at typical test positions. The criteria we have chosen to decide the spatial extent around the source where free field propagation conditions are achieved by lining certain interior surfaces with a sound absorbing material was to find how the sound pressure level decreases with increasing radial distance from a small omnidirectional sound source.

As long as the sound pressure level decreases by a slope of 6 dB per doubling of the distance between the source and receiver the existing conditions are equivalent to free field. Deviation from this slope indicates that reflections from specific nearby

surfaces or multiply reflections responsible for the existence of a semi-diffuse sound field far from the source, interfere with the direct sound wave.

The "hall radius" defined as the radial distance from the source where the reverberent sound field has the same intensity as the direct sound, is the traditional measure to describe the spatial extent of the free field conditions in a "well behaved" reverberation room where there are no strong individual reflections from nearby hard surfaces, and the reverberant field is completely uncorrelated with the direct sound.

Since the existing open test section of the V/STOL tunnel has large reflecting surfaces near to both the source and the receiver (i.e. the raised ceiling, the hard floor, hard collector cowl, etc.) and the walls have a heat insulation treatment which in certain frequency ranges is an effective sound absorber, it is expected that the sound pressure level vs distance curves obtained experimentally will not follow exactly the smooth pattern of 6 dB decrease per distance doubling up to the hall radius and leveling off beyond. Accordingly, the individual sound pressure level vs. distance curves contain more relevant information than the hall-radius obtained by trying to fit a smooth theoretical level vs distance curve (valid only in reverberation rooms) over the data point obtained in the environment of the model tunnel test section.

Because the hall radius, as a single number, is much easier to comprehend and to compare than the rugged sound level vs distance curves, each containing a large number of data points, we will use it in spite of its above discussed limitations as a simple measure for the spatial extent of free field dominance.

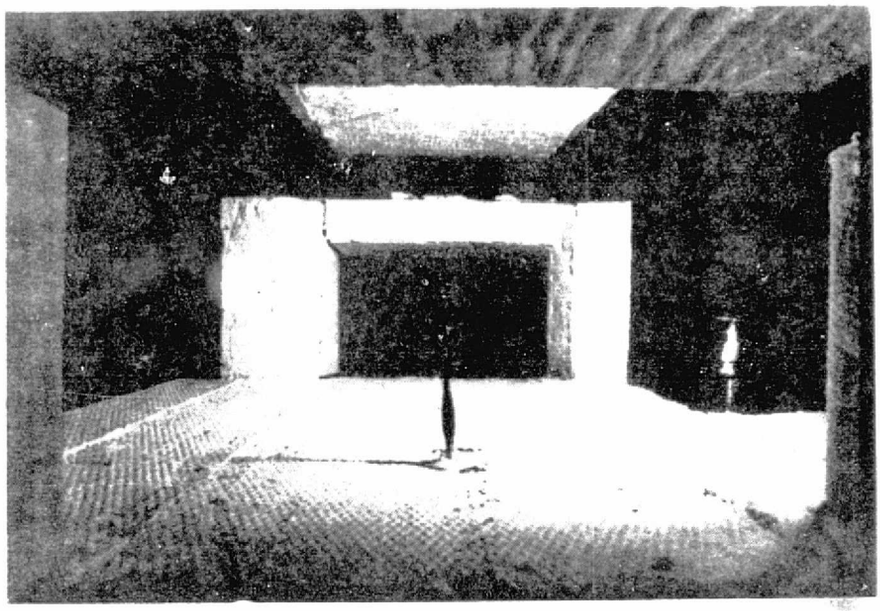

a

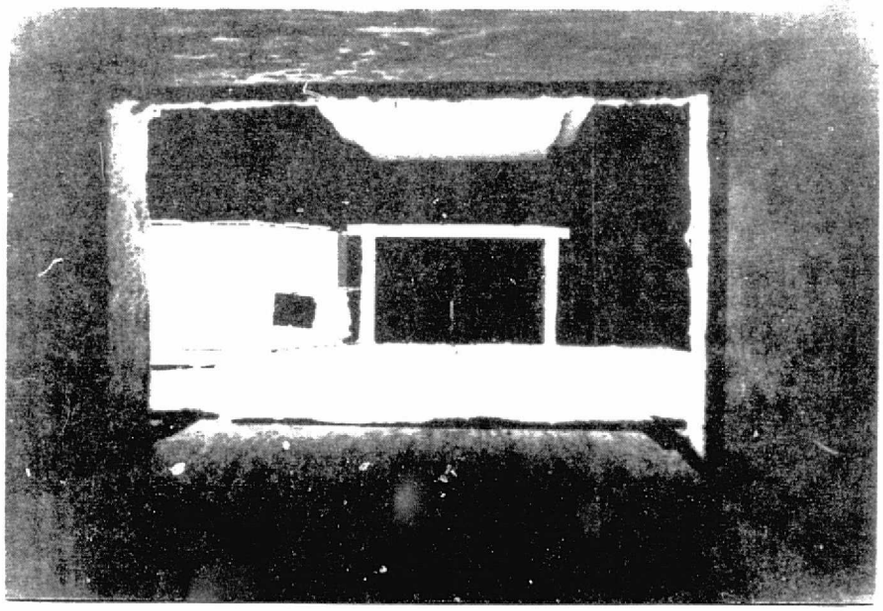

b

FIG. 4 PHOTOGRAPHS OF THE ACOUSTICAL MODEL OF THE TUNNEL TEST SECTION.

a) View from the Nozzle Opening
b) View from the Collector Duct

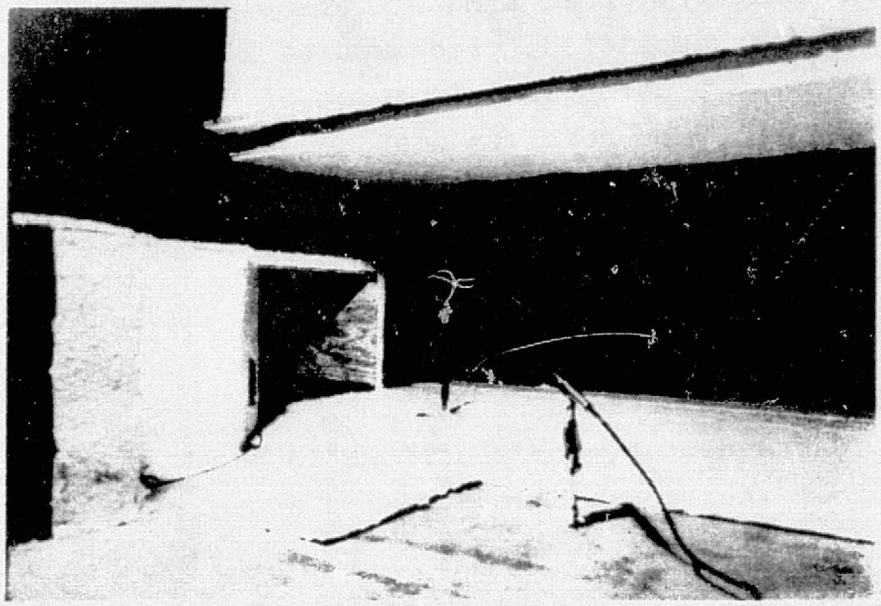

FIG. 5 SIDE VIEW OF THE ACOUSTICAL MODEL OF THE TEST SECTION SHOWING THE RAISED LINED CEILING PANELS AND SIDE WALLS AND THE NOZZLE OPENING.

3. Experimental Setup

The block diagram of the experimental setup is shown in Fig. 6. Except for the crossing-jet noise source, which is described in Ref. 4, all other components are commercially available units. The crossing-jet noise source radiates a stationary broadband sound in an omnidirectional manner. The electric signal from the microphone is amplified, processed by a 1/3-octave band real time analyzer and plotted as a function of frequency on a X-Y plotter with the source receiver distance and direction of traverse as parameter. Based on these recorded data one can plot for each frequency band sound pressure vs distance curves for each direction of traverse for a given acoustical environment.

The above procedure is carried out first for a configuration modeling the existing conditions of the open test section of the V/STOL tunnel. Subsequently, the procedure is repeated after each enlargement of the acoustically treated areas.

4. Modeling of the Sound Absorbing Treatment

To predict the extent of improvement in simulating free field conditions in the test section of the full-scale V/STOL tunnel obtained by lining certain strategically located surfaces it is necessary to model both the existing sound absorbing surfaces and the additional linings one may want to apply at full-scale.

The existing open test section has a canvas-faced glass fiber heat insulation treatment directly applied against the inside surface of the walls of the test section enclosure. A sample of this heat insulation treatment was supplied by NASA and was evaluated by BBN for its normal incidence sound absorption coefficient in BBN's impedance tube. Fig. 7 shows the measured normal incidence sound absorption coefficient as a function of frequency obtained with

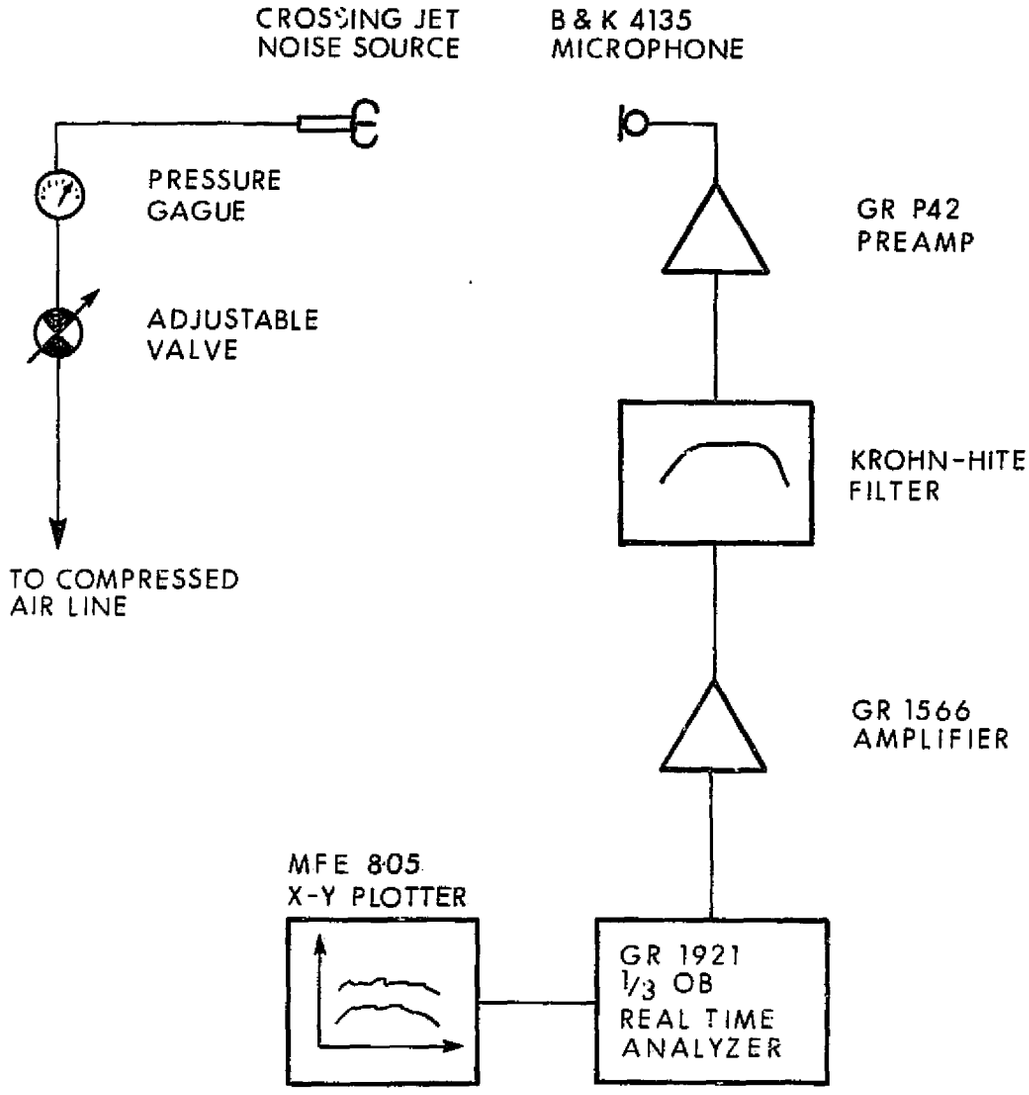

FIG. 6 BLOCK DIAGRAM OF THE INSTRUMENTATION USED IN THE ACOUSTICAL MODELING STUDY.

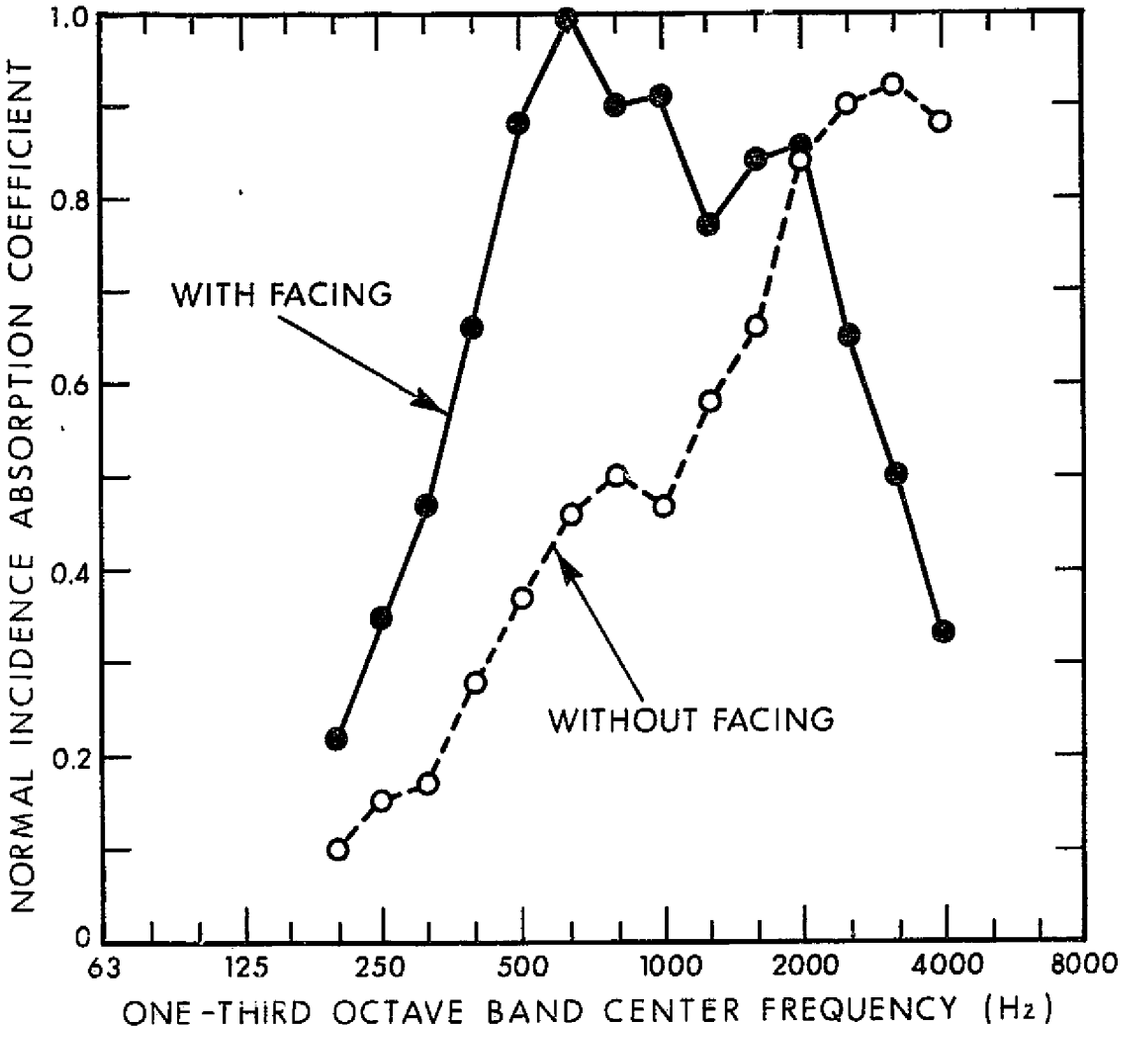

FIG. 7 MEASURED NORMAL INCIDENCE ABSORPTION COEFFICIENT OF THE EXISTING HEAT INSULATION TREATMENT.

and without the canvas facing. As expected, the impervious canvas facing, acting as a membrane, increases the sound absorption coefficient at low frequencies (below 2000 Hz). However, at high frequencies (above 2000 Hz) the inertia of the canvas controls its motion and only a small portion of the incident sound is transmitted into the porous sound absorbing layer behind. Accordingly, the absorption coefficient in this frequency range decreases rapidly with increasing frequency with the canvas facing while without it would tend to unity.

This full-scale heat insulation treatment was modeled acoustically by a layer of flame-proofed double-faced Style 1200 flannel having a total flow resistance of 400 mks rayls covered by a layer of 0.0033 lb/ft^2 surface-weight Mylar foil. In this combination the flannel, which was directly attached to the hard sealed plywood walls, modeled the glass fiber insulation and the Mylar membrane modeled the impervious canvas facing.

The additional sound absorbing treatments used in the model were a layer of 0.5 inches thick type PF-105 glass fiber* of high specific flow resistance to be used at the hung ceiling and on the floor and 2 layers of double faced flannel† nailed onto the two-by-fours.

The model sound absorbing treatments used in this study are depicted in Fig. 8.

5. The Experiment

To generate the sound pressure level vs distance curves (and from these evaluate the hall radius) the crossing-jet noise source was placed at two different positions; both 8.5 in. above floor level and above the tunnel center line. The primary source

*The flow resistance of this layer is approximately 1000 mks rayls = 25ρc

†The total flow resistance of this double layer is 800 mks rayls = 2ρc

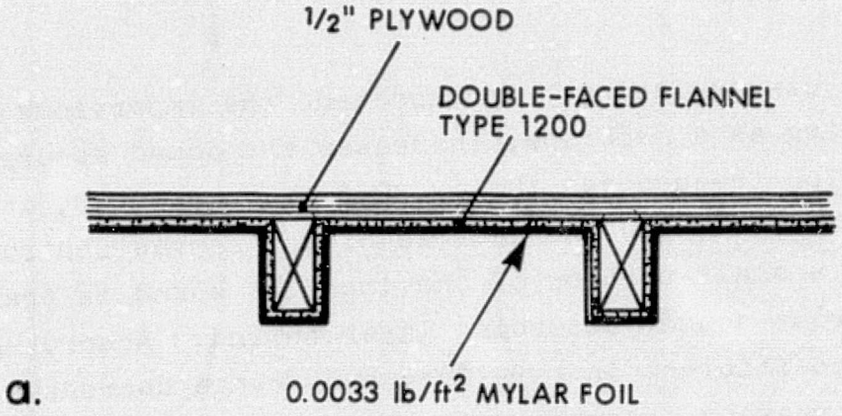

a.

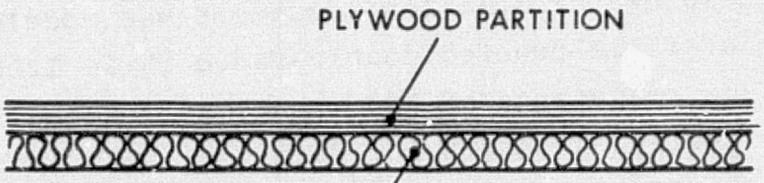

b.

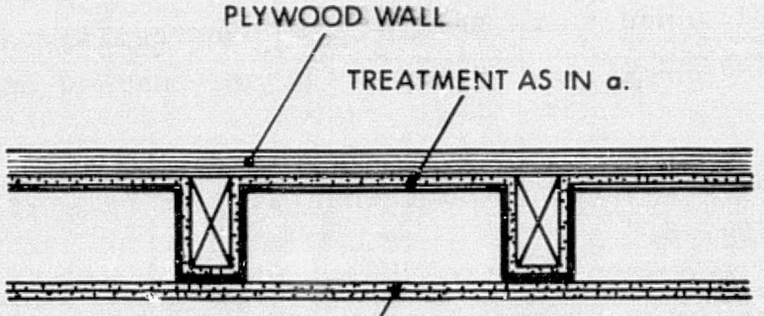

c.

FIG. 8 ACOUSTIC TREATMENTS USED IN THE MODEL

a. Configuration to Model Existing Heat Insulation Treatment.

b. Configuration to Model a 6 in. Thick Full-Scale Treatment.

c. Configuration to Model Additional Wall Treatment to Provide Broadband Sound Absorption.

position, designated as Pos. 1, was 21.25 in. downstream of the nozzle exit plane which corresponds to 17.7 ft. at full-scale. The secondary source position, designated as Pos. 2, was 26.5 in. (corresponding to 22 ft. at full-scale) downstream of the primary position. A high pressure air container with a pressure reducing valve served as an air supply for the crossing-jet noise scurce. The valve was set to maintain a constant line pressure of 40 psi. The 1/3-octave band sound pressure levels were measured at 6 in. intervals along each of the various directions from the source. These traverses for each of the two source positions are identified by letters A to G' in Fig. 9 and in Table I.

TABLE I

SUMMARY OF TRAVERSE DIRECTIONS

SOURCE LOCATION	TRAVERSE IDENTIFICATION	
	IDEN. LETTER	DESCRIPTION
POS. 1	A	Upstream
	B	Toward Near Wall
	C	Downstream
	D	45° Downstream, Toward Far Corner
	E	Toward Far Wall
	F	Straight Upwards
POS. 2	A'	Upstream
	C'	Downstream
	E'	Toward Far Wall
	G'	45° Upstream, Toward Central Room

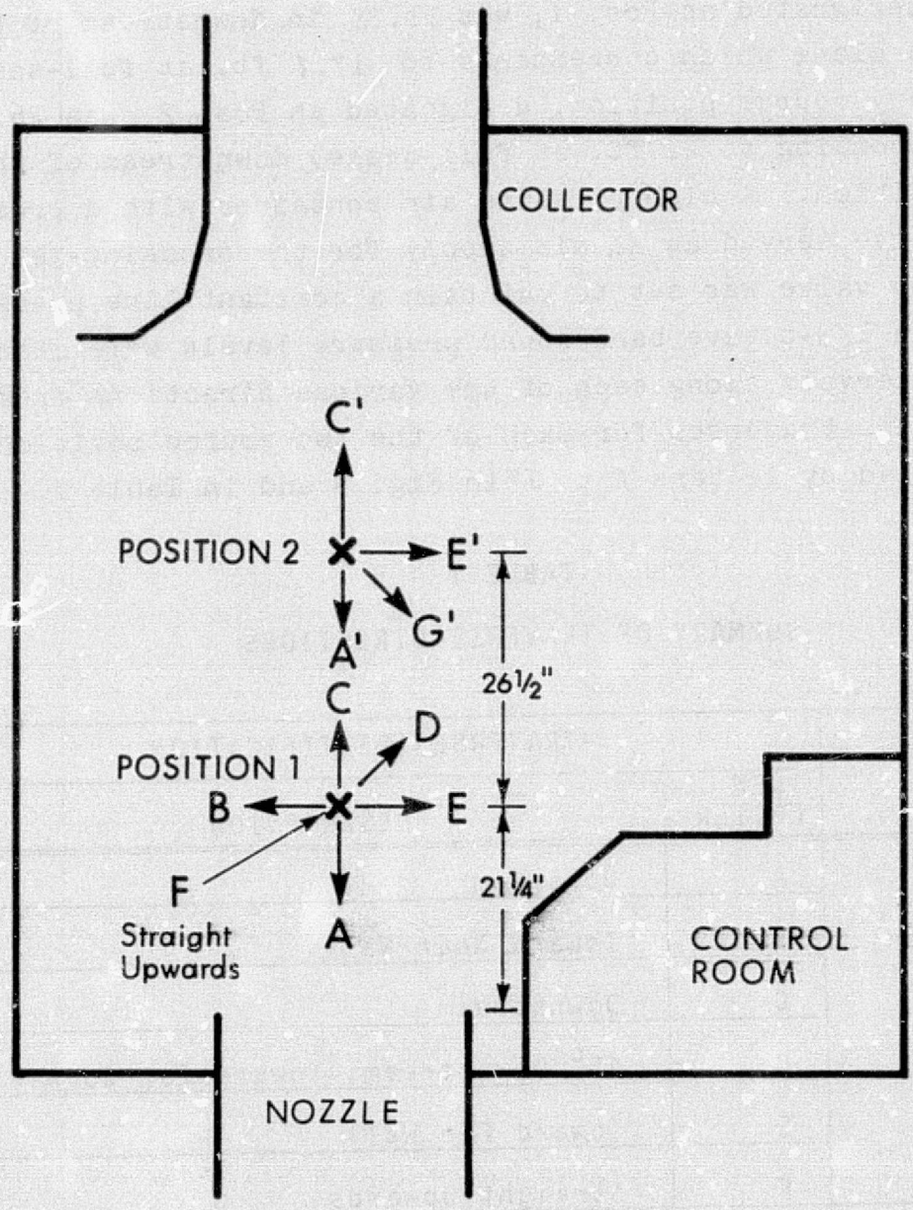

FIG. 9 IDENTIFICATION OF SOURCE POSITIONS AND TRAVERSE DIRECTIONS.

5.1 Model configurations tested

The acoustical study of the model test section was carried out for eight different configurations of sound absorbing treatments. These treatments are identified by numbers 1 through 8, where the number 1 designates the existing conditions. The numbers 2 through 8 identify additional treatment of increasing extent of area coverage; with 8 corresponding to a full sound absorbing treatment. The different acoustical conditions experimentally evaluated are summarized briefly in Table II and discussed in more detail below.

TABLE II

MODEL TEST SECTION CONFIGURATIONS
STUDIED EXPERIMENTALLY

CONFIGURATION NUMBER	BRIEF DESCRIPTION OF ACOUSTICAL CONDITIONS
1	Model of existing conditions
2	Treatment #1, plus raised ceiling & floor below treated*
3	Treatments 1, 2, plus collector cowl treated*
4	Treatments 1,2,3, plus control room wall treated*
5	Treatments 1 to 4, plus floor lining extended 18 in. to both sides
6	Treatments 1 to 5, plus side walls up to height of raised ceiling treated
7	Treatments 1 to 6, plus rest of walls & high ceiling treated
8	Treatments 1 to 7, plus rest of floor*, roof of control room* and outside surfaces of raised test section walls* treated

*The asterisks indicate treatment with 0.5 in. thick PF 105 blanket.

Configuration 1 models the existing conditions of the full-scale tunnel test section, including the heat insulation treatment as depicted in Fig. 8a. The double-faced flame-proofed type 1200 flannel is stapled onto the plywood walls and the 0.0033 lb/ft^2 Mylar foil is adhered to the outside surface of the flannel by a very small amount of sprayed-on adhesive.

Configuration 2 retains the treatment described above, but the lower surface of the raised ceiling (of the closed test section) and the projection of this ceiling panel on the test section floor are covered with a 0.5 in. thick PF 105 blanket as depicted in Fig. 8b.

Configuration 3 differs from Configuration 2 only by the treatment of the entire interior surface of the collector cowl by a 0.5 in. thick PF 105 blanket.

Configuration 4, in addition to the features of Configuration 3, has the exterior surfaces of the control room lined with 0.5 in. thick PF 105.

Configuration 5 differs from Configuration 4 only by the addition of an 18 in. wide strip of 0.5 in. thick PF 105 blanket to both sides of the existing floor lining described under Configuration 2.

Configuration 6 is identical to Configuration 5, except for covering the walls of the test section enclosure up to the height of the raised ceiling with two layers of Type 1200 double-faced flame-proofed flannel as depicted in Fig. 8c.

Configuration 7 differs from Configuration 6 only by extending the sound absorbing treatment of Fig. 8c to the full height of the walls and over the ceiling.

Configuration 8 is identical to Configuration 7 except that the sound absorbing wall treatment of Fig. 8b is now extended to cover the entire floor, the roof of the control room and the outside surfaces of the raised test section walls. Accordingly, this last configuration practically corresponds to the maximum amount of sound absorbing treatment possible.

6. Experimental Results

The experimental results were obtained in the form of sound pressure level vs frequency curves with the source receiver distance as parameter. A graph, representative of all raw data obtained from the X-Y plotter in form of 1/3-octave band spectra with the source-receiver distance as parameter, is shown in Fig. 10 for Source Position 1 test section Configuration 5 and Traverse E.

The raw data, consisting of a very large number of curves similar to that of Fig. 10, was obtained as data was gathered for the two source positions for all traverse directions for each of the eight different configurations of the sound absorbing treatment of the test section. The raw data was evaluated by plotting the normalized 1/3-octave band sound pressure level at each octave-band center frequency as a function of source-receiver distance for a given source position and traverse direction for all the eight different room conditions on a single graph. The sound pressure level data were normalized to the level measured at 6 in. distance in each case.

A typical normalized sound pressure level vs distance curve obtained this way for Source Position 1, traverse direction E and at 5000 Hz is shown in Fig. 11. In this figure the thin solid line represents the theoretical slope of 6 dB level decrease

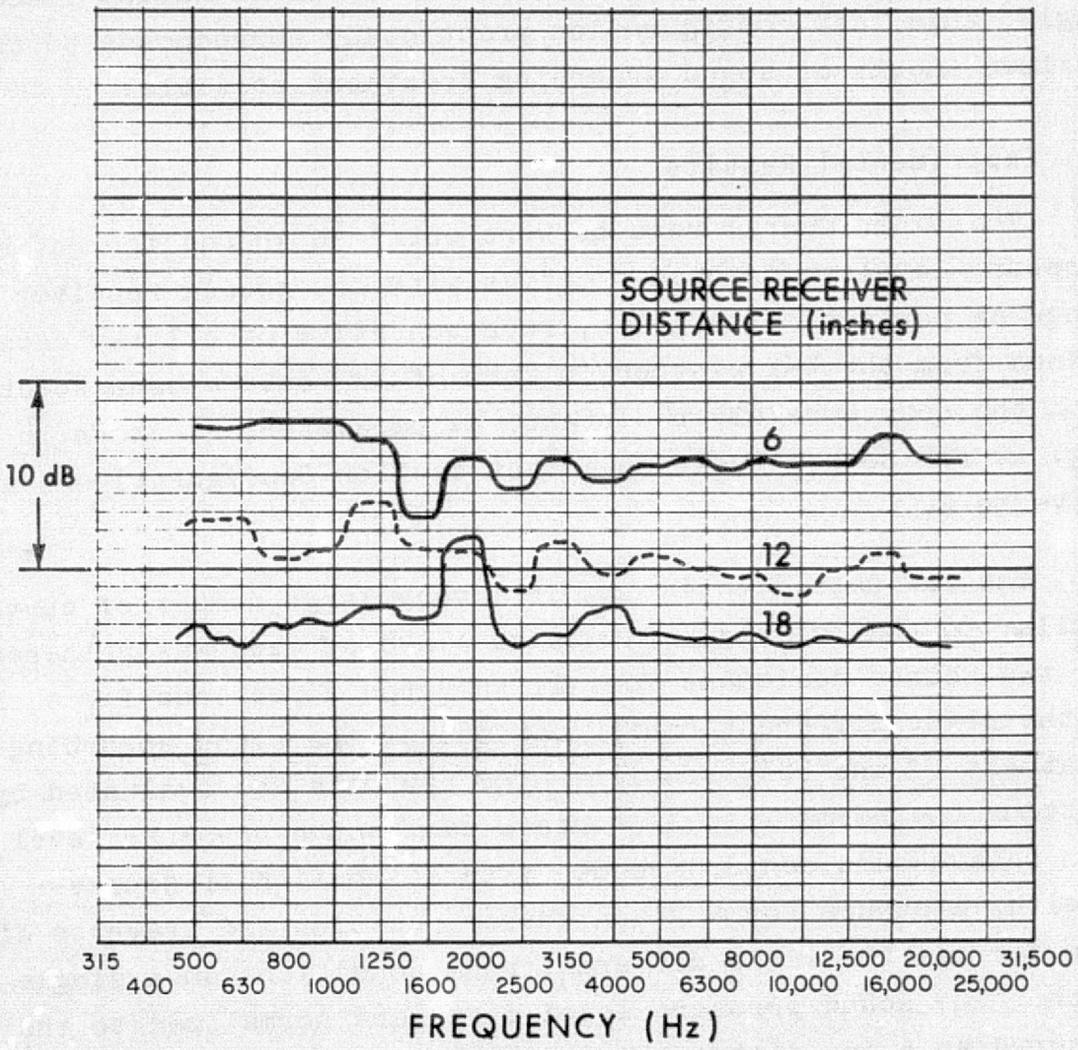

FIG. 10 TYPICAL RAW DATA FROM THE X-Y PLOTTER
(1/3-octave band spectra vs distance;
Source Pos. 1, Configuration 5, Traverse E)

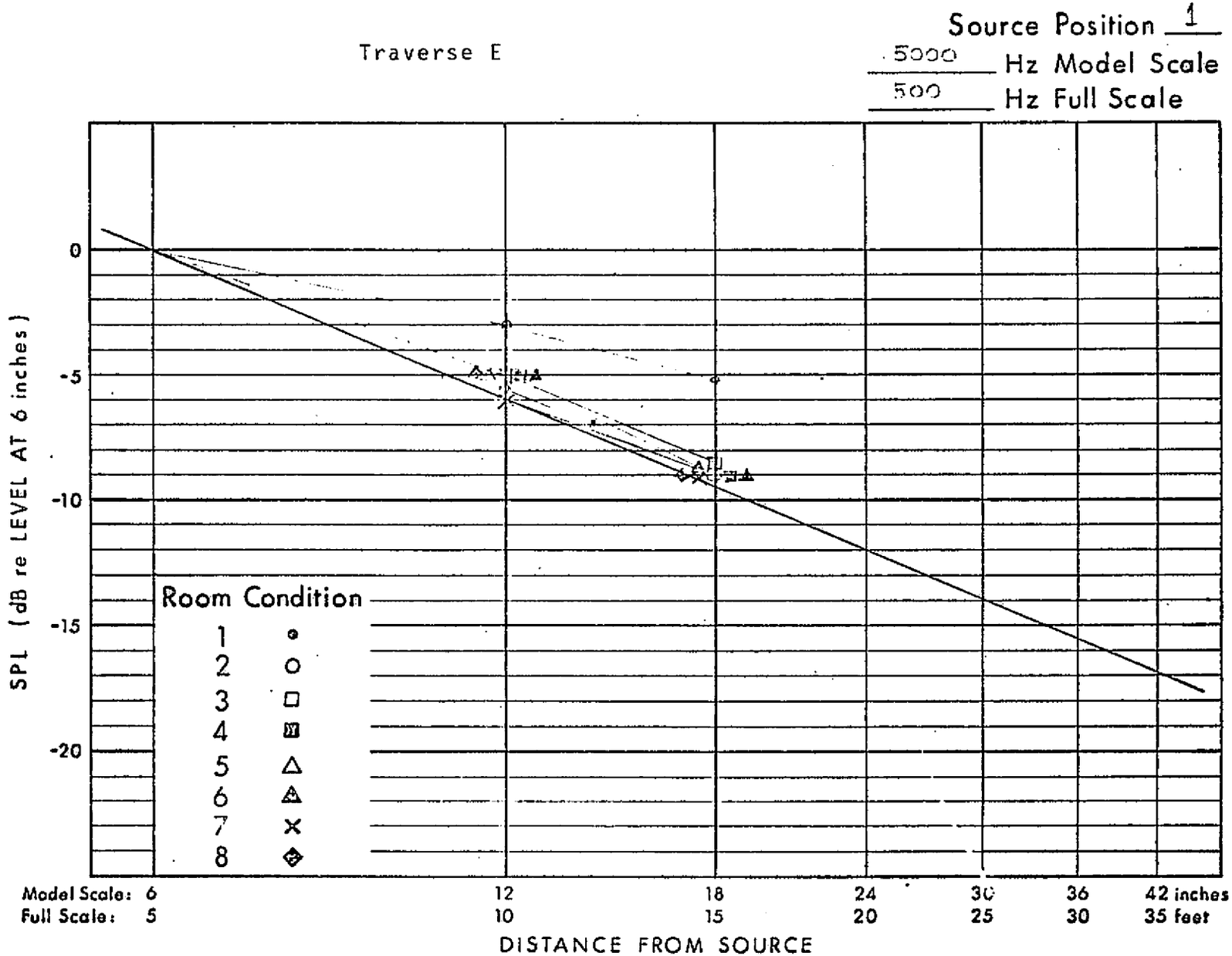

FIG. 11 TYPICAL NORMALIZED SPL VS DISTANCE CURVE WITH TEST SECTION CONFIGURATION AS PARAMETER.

with each doubling of the source-receiver distance one would obtain under ideal free field conditions for spherical spreading. The results obtained for Configuration 1, which models the existing conditions at full-scale, is represented by the dotted line and solid circles. The fact that this curve deviates substantially from that expected for free field conditions indicate that nearby reflecting surfaces contribute substantially to the sound pressure at each microphone location. This is then confirmed by results obtained (see open circles in Fig. 11) after lining the raised ceiling and the floor below it, as required for Configuration 2. A further conclusion one can draw from Fig. 11 is that any further increase in sound absorbing treatment above that of Configuration 2 brings only diminishing improvement for this specific traverse and frequency. As we will see later, this conclusion is generally valid for all other traverses and frequency ranges.

In evaluating the effects of additional sound absorbing treatment we concentrated our efforts on Source Position 1. A few additional measurements were also performed for Source Position 2. The normalized sound pressure level vs distance curves obtained from the measured data are collected in Data Appendix A, and are represented in the series of Figs. from A-1 to A-60. The data is organized according to source position, traverse direction and frequency. The frequency range extends over 6 octaves from 630 Hz to 20,000 Hz.

7 Conclusions

The experimental data presented in Appendix A is voluminous. Accordingly, in addition to observing general trends, we have also attempted to condense it by evaluating the hall radius as a function of frequency with the room condition as parameter for each traverse direction.

Though the acoustical conditions in the open tunnel test section are far from being reverberant, and the variation of the sound pressure level with increasing distance from the source does not exactly follow the smooth pattern of 6 dB decrease per distance doubling up to the hall radius and leveling off beyond, we still attempted to determine an *approximate hall radius* by finding the best fit of the theoretical curve to the normalized SPL vs distance curves. An example of the difficulties inherent in this procedure, especially at low frequencies, in the abnormally large hall radius at 1250 Hz (model scale) for several of the microphone traverses. The approximate hall radius vs frequency curves obtained by this procedure for the two source positions and for each of the traverse directions are shown in Figs. 12 to 21. Note, that in many cases the approximate hall radius is larger than the maximum source-receiver distance used; indicating that semi-free field conditions extend up to a short distance from the wall. The maximum source-receiver distance used for a specific traverse is indicated in the figures by a dotted line. If there are no symbols shown, this indicates that at those frequencies the approximate hall radius is larger than the maximum source-receiver distance used in the experiment.

Analyzing the graphs presented in Data Appendix A and Figs. 12 to 21, the following general trends are observed:

- At low model-scale frequencies below 2500 Hz (i.e. 250 Hz at full-scale) the thickness of the lining of the nearby reflecting surfaces is not thick enough to provide effective sound absorption and the sound reflected from these surfaces interferes with the direct sound.
- At and above 2500 Hz (i.e. 250 Hz at full-scale) the additional sound absorbing treatments resulted in a substantial increase of test section area where free field conditions are effectively simulated.
- The largest improvement is achieved by lining the raised ceiling and the test section floor below. (See Configuration 2.)
- Any further increase in sound absorbing treatment above that of Configuration 2 yields only diminishing results.

Accordingly, one can conclude that the lining of the two surfaces nearest to the sound source, namely the raised ceiling panel and the area it projects on the test section floor, constitutes the most effective measure to extend the spatial region where free field conditions are simulated.

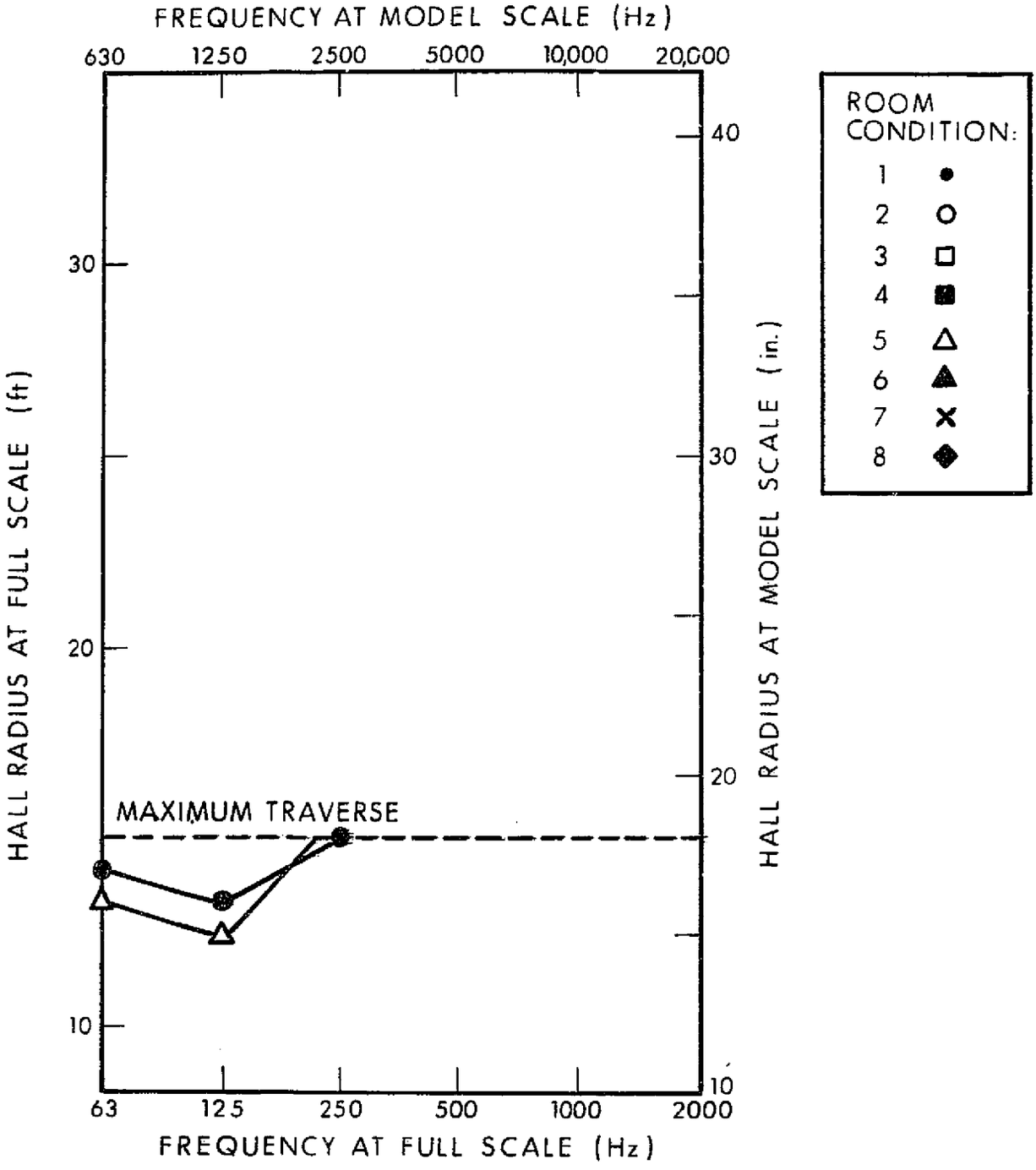

FIG. 12 APPROXIMATE HALL RADIUS VS FREQUENCY WITH ROOM CONDITION AS PARAMETER.

SOURCE POSITION 1 TRAVERSE A

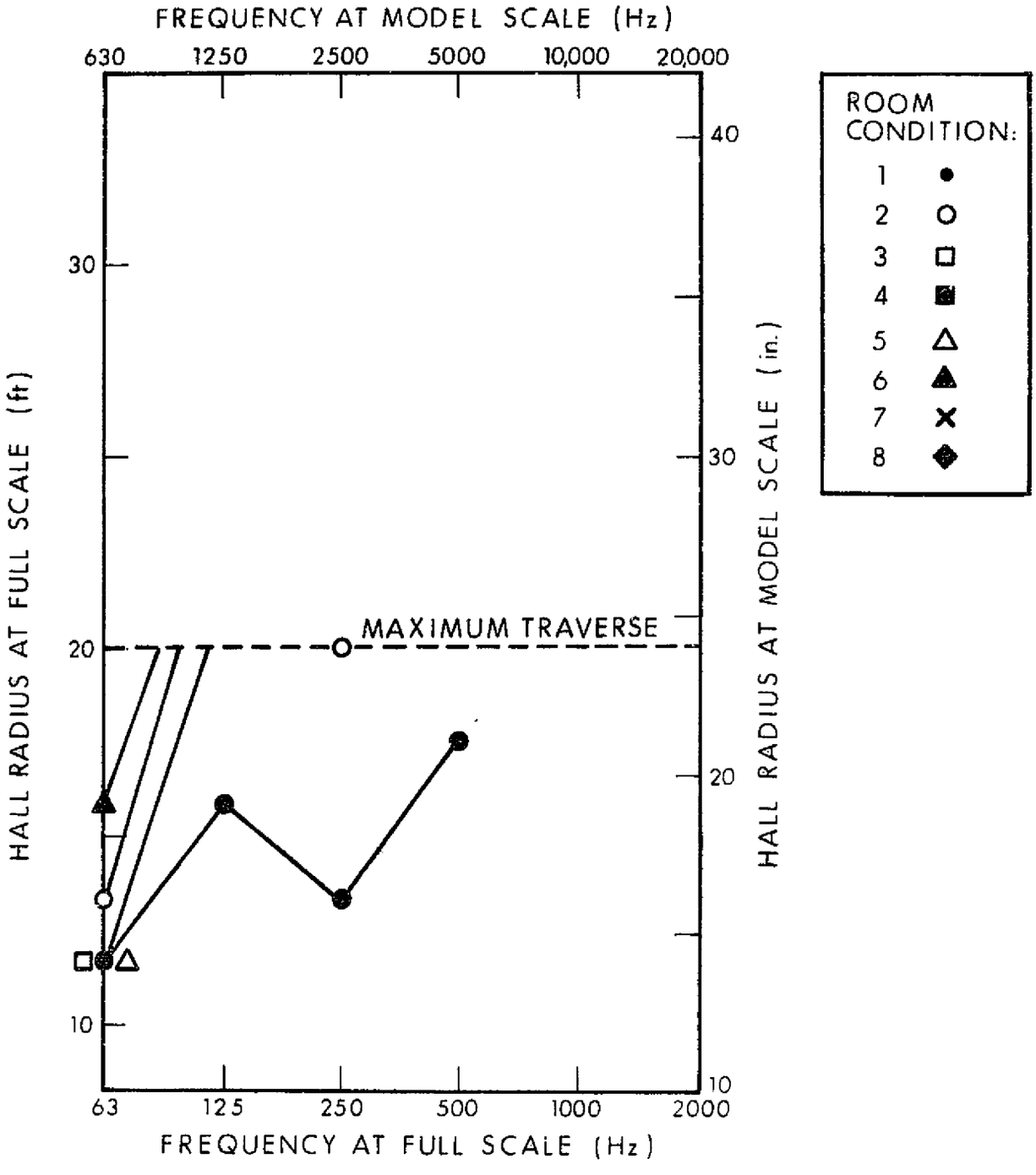

FIG. 13 APPROXIMATE HALL RADIUS VS FREQUENCY WITH ROOM CONDITION AS PARAMETER.

SOURCE POSITION 1 TRAVERSE B

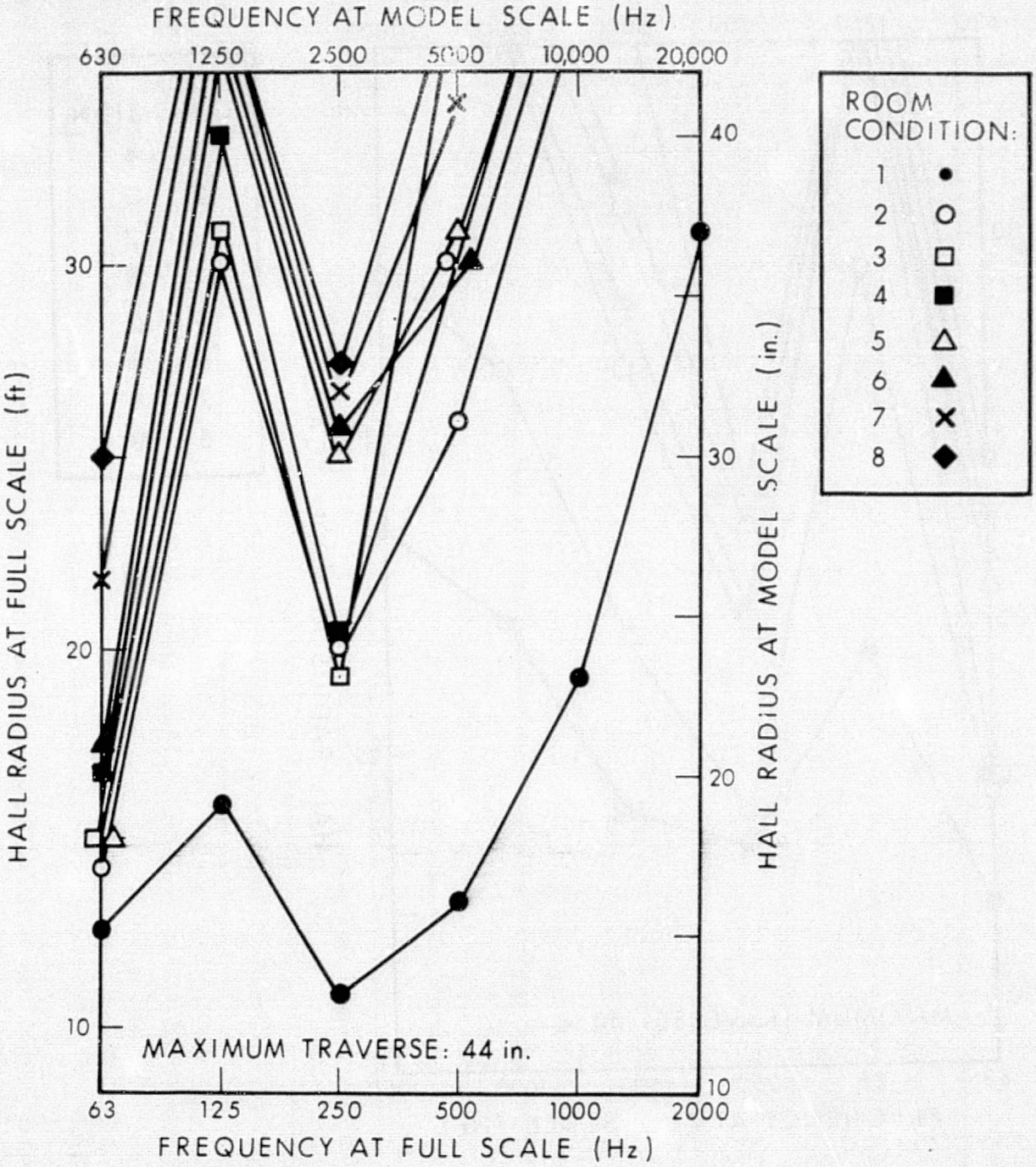

FIG. 14 APPROXIMATE HALL RADIUS VS FREQUENCY WITH ROOM CONDITION AS PARAMETER.

SOURCE POSITION 1 TRAVERSE C

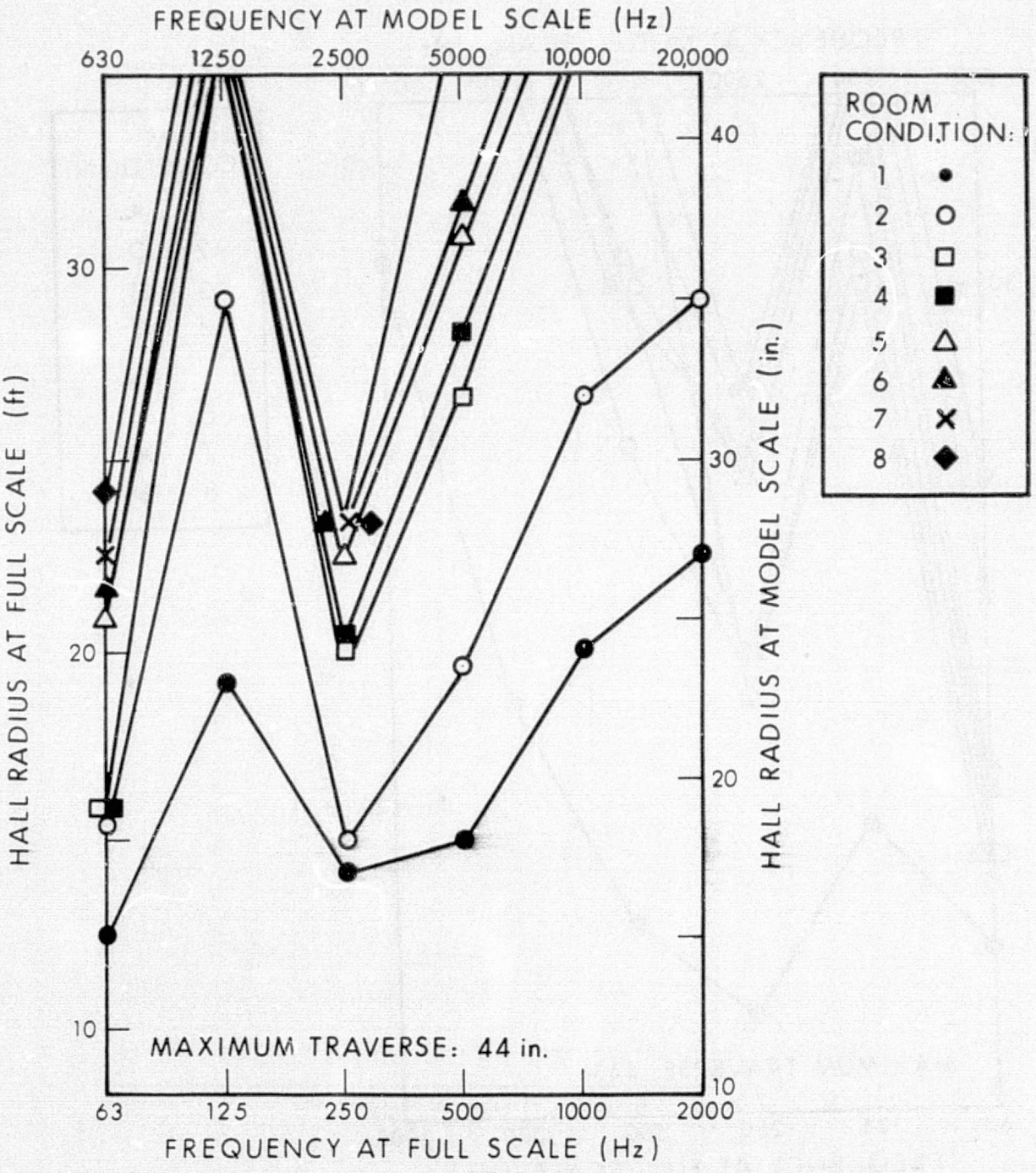

FIG. 15 APPROXIMATE HALL RADIUS VS FREQUENCY WITH ROOM CONDITION AS PARAMETER.

SOURCE POSITION 1 TRAVERSE D

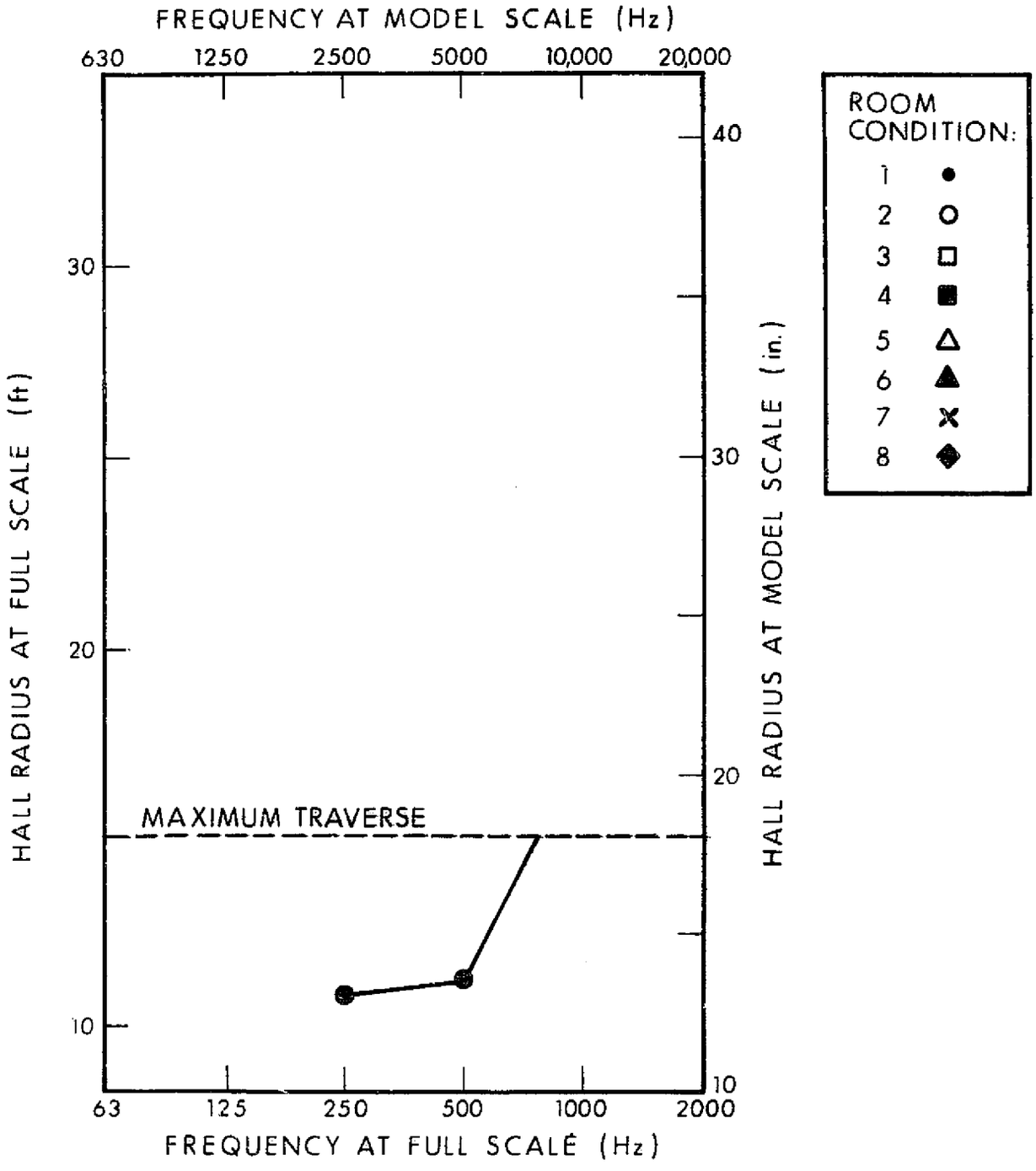

FIG. 16 APPROXIMATE HALL RADIUS VS FREQUENCY WITH ROOM CONDITION AS PARAMETER.

SOURCE POSITION 1 TRAVERSE E

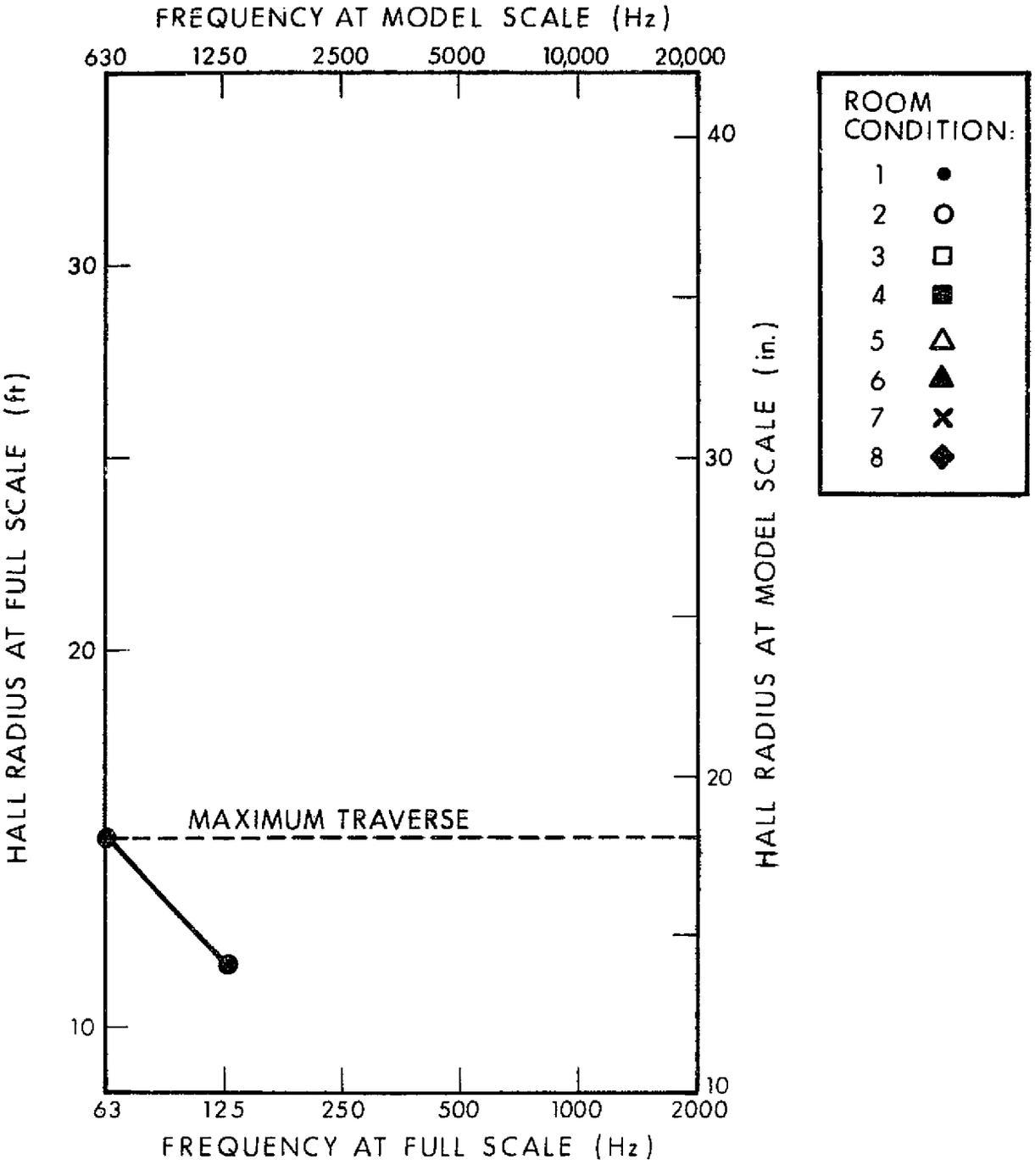

FIG. 17 APPROXIMATE HALL RADIUS VS FREQUENCY WITH ROOM CONDITION AS PARAMETER.

SOURCE POSITION 1 TRAVERSE F

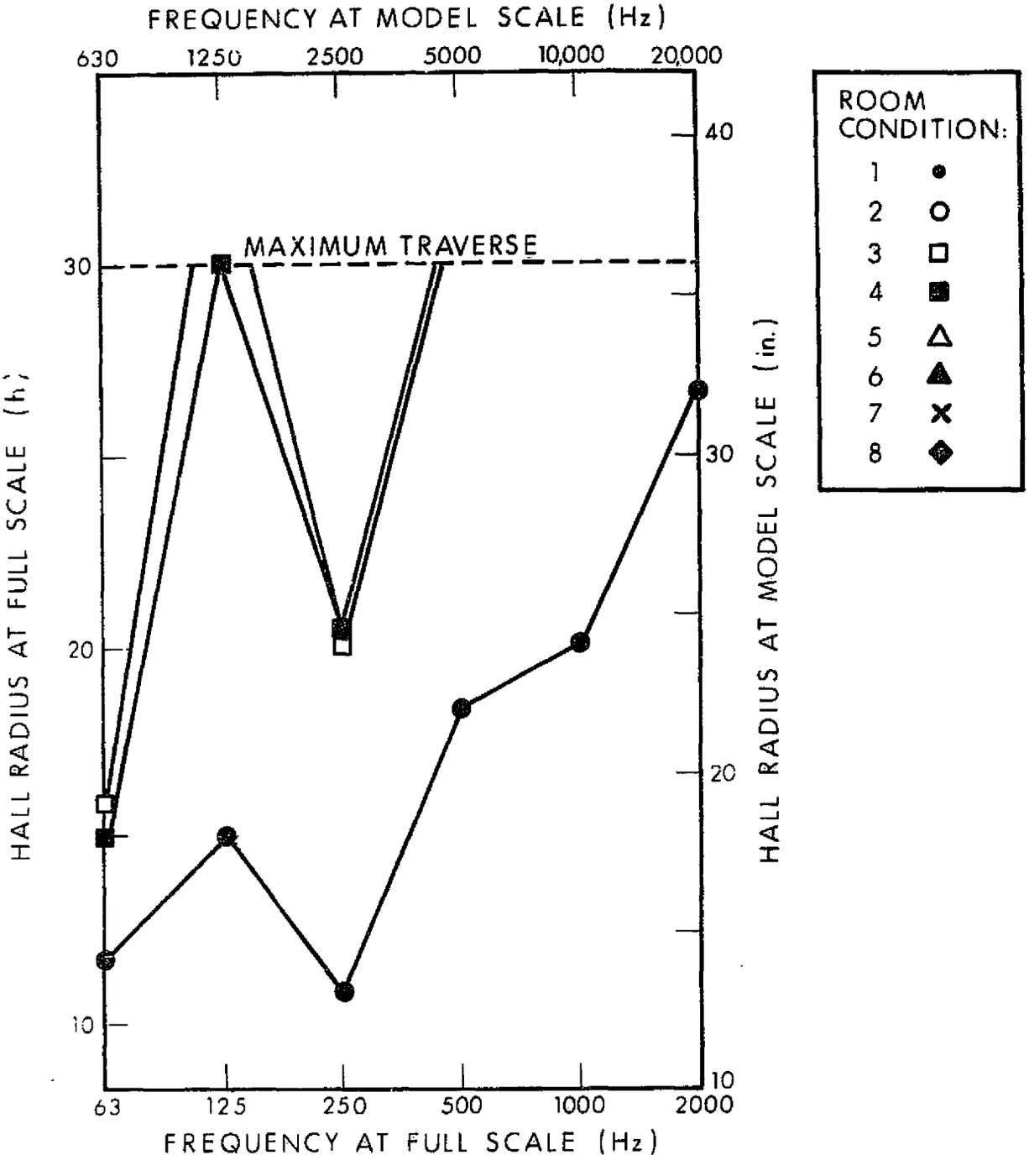

FIG. 18 APPROXIMATE HALL RADIUS VS FREQUENCY WITH ROOM CONDITION AS PARAMETER.

SOURCE POSITION 2 TRAVERSE A'

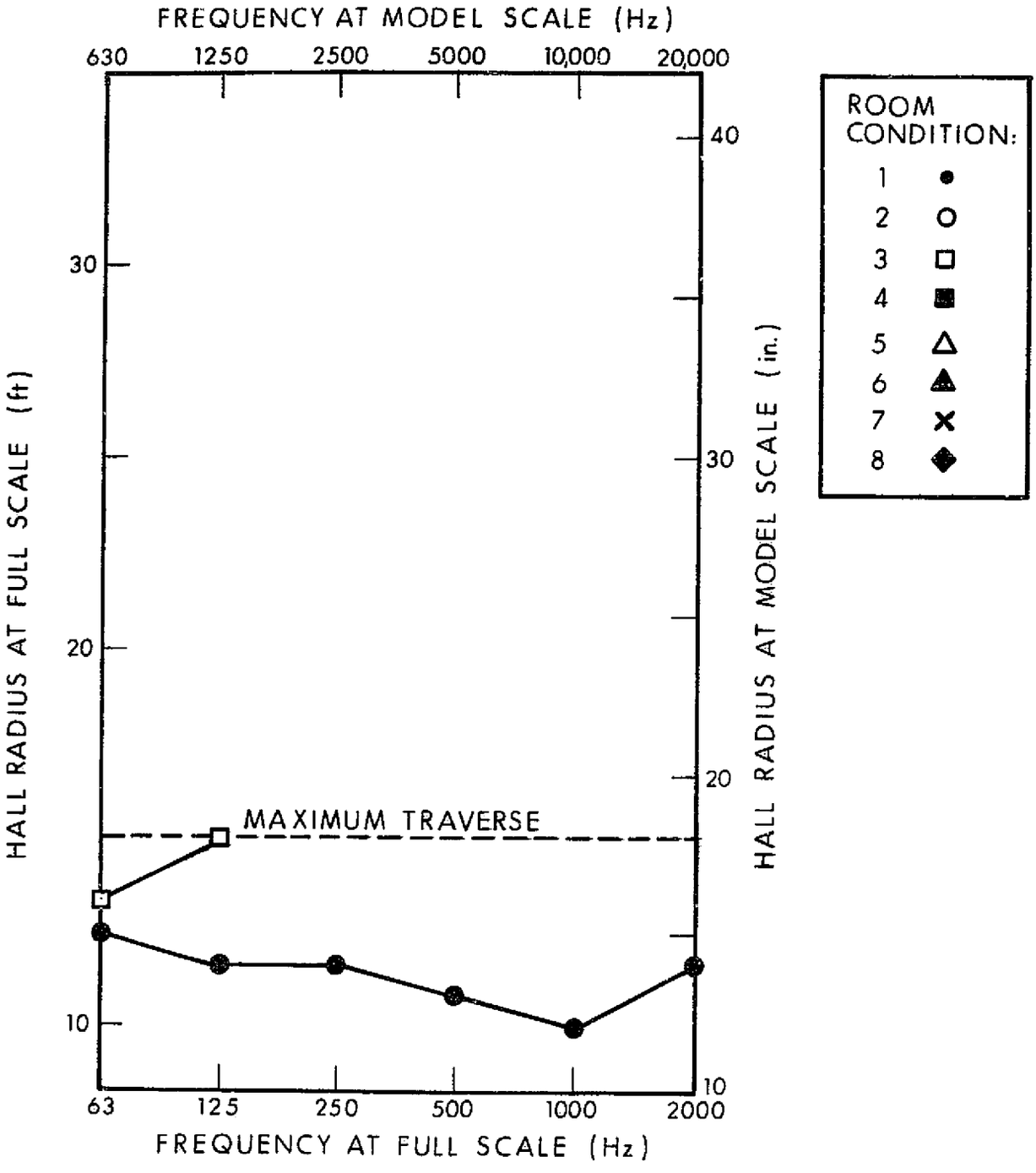

FIG. 19 APPROXIMATE HALL RADIUS VS FREQUENCY WITH ROOM CONDITION AS PARAMETER.

SOURCE POSITION 2 TRAVERSE C'

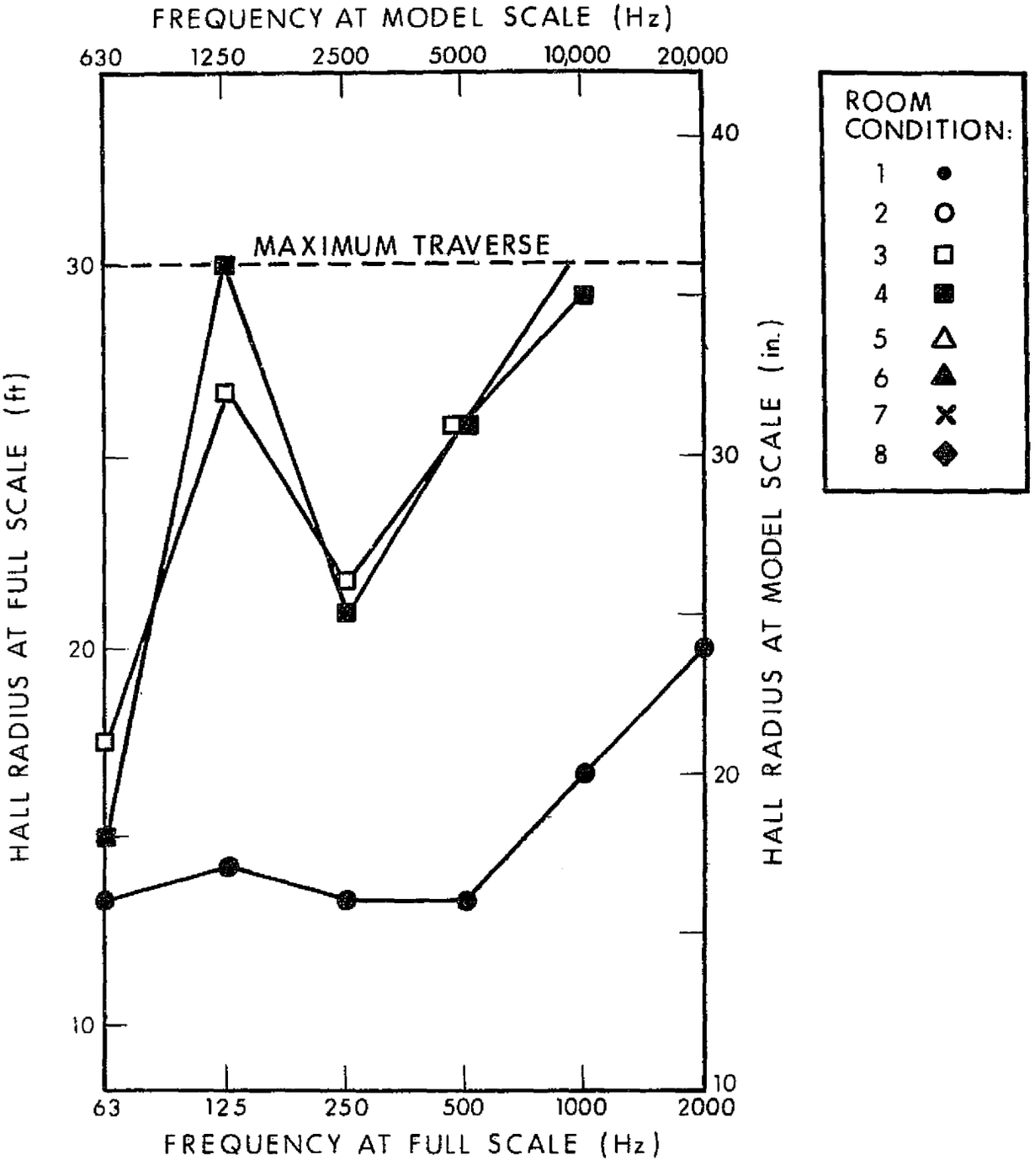

FIG. 20 APPROXIMATE HALL RADIUS VS FREQUENCY WITH ROOM CONDITION AS PARAMETER.

SOURCE POSITION 2 TRAVERSE E'

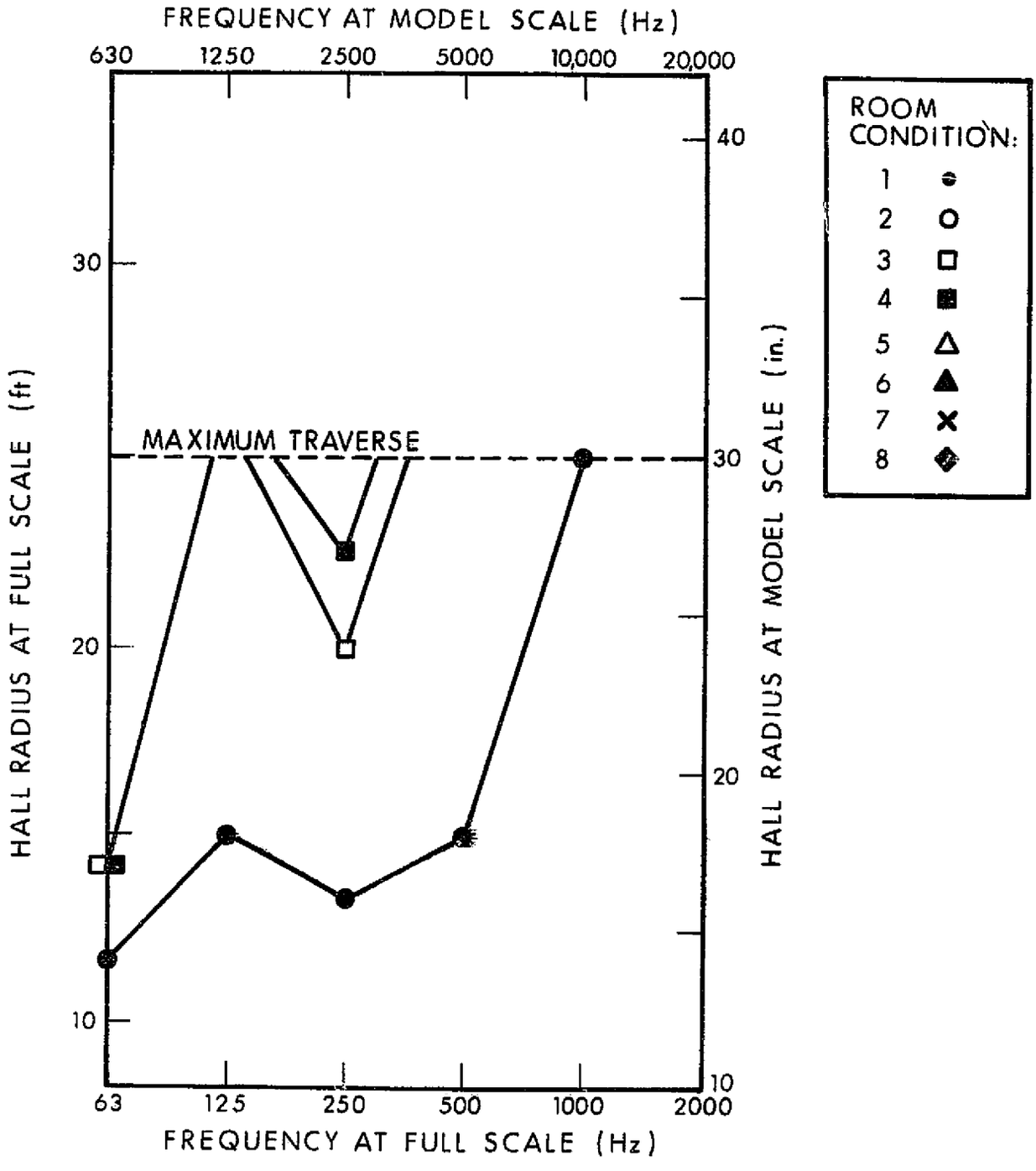

FIG. 21 APPROXIMATE HALL RADIUS VS FREQUENCY WITH ROOM CONDITION AS PARAMETER.

SOURCE POSITION 2 TRAVERSE G'

8 Implementation at Full-Scale

The results of our scale-model experiments indicated that lining of the raised ceiling and the test section floor below it constitutes the most effective measure to enlarge the hall radius. Accordingly, we recommend that NASA should consider the implementation of these specific noise control measures. Only after these measures have been implemented at full-scale and their effectiveness is confirmed should one consider whether any further treatment is desirable.

Possible ways to implement these recommended measures are discussed below.

8.1 Raised ceiling panel

The interior surface of the raised ceiling panel is exposed to high speed airflow. However, it is not required to carry any concentrated load as it is required for the test section floor below. Accordingly, the functional criteria for selecting a sound absorbing treatment are minimum added weight and sufficient protection from flow erosion. The arrangement is depicted in Fig. 22. The open-cell acoustical foam which constitutes the sound absorbing material is selected because of its light weight. The felt metal in this case serves as a smooth protecting surface for the foam behind. In contrast to perforated metal surfaces, where the flow can generate pure tone noise due to the regularity of the perforation pattern, the smooth felt metal surface would prevent the generation of such undesirable noise. If stability considerations require it, the felt metal layer can be bonded onto a honeycomb to increase its stiffness.

8.2 Test section floor

The floor of the closed test section can be lowered. Lowering the floor by 5 inches would permit the installation of a 5 in. thick sound absorbing layer, the top surface of which would then be level with the top surface of the concrete floor of the open test section. The acoustical treatment can be permanent or temporary.

For a permanent treatment it is necessary that the top surface is capable of withstanding concentrated loads, provide sufficient protection for the porous sound absorbing material from the turbulent flow and, in addition, it must be transparent for the sound so it can freely penetrate the porous sound absorbing material below. These requirements are contradictory in nature, and one must strike a compromise. The sound absorbing treatment depicted in Fig. 23 is the result of such a compromise.

If the sound absorbing treatment is not permanent, individual plates utilizing the construction depicted in Fig. 22 can be used to cover the surface of the lowered test section floor. Regarding high frequency absorption, this treatment is much superior to the permanent treatment.

The final design of these sound absorbing treatments, which takes into account functional, safety, aerodynamic and acoustical requirements, shall be carried out with close cooperation between the design engineer and the acoustical consultant.

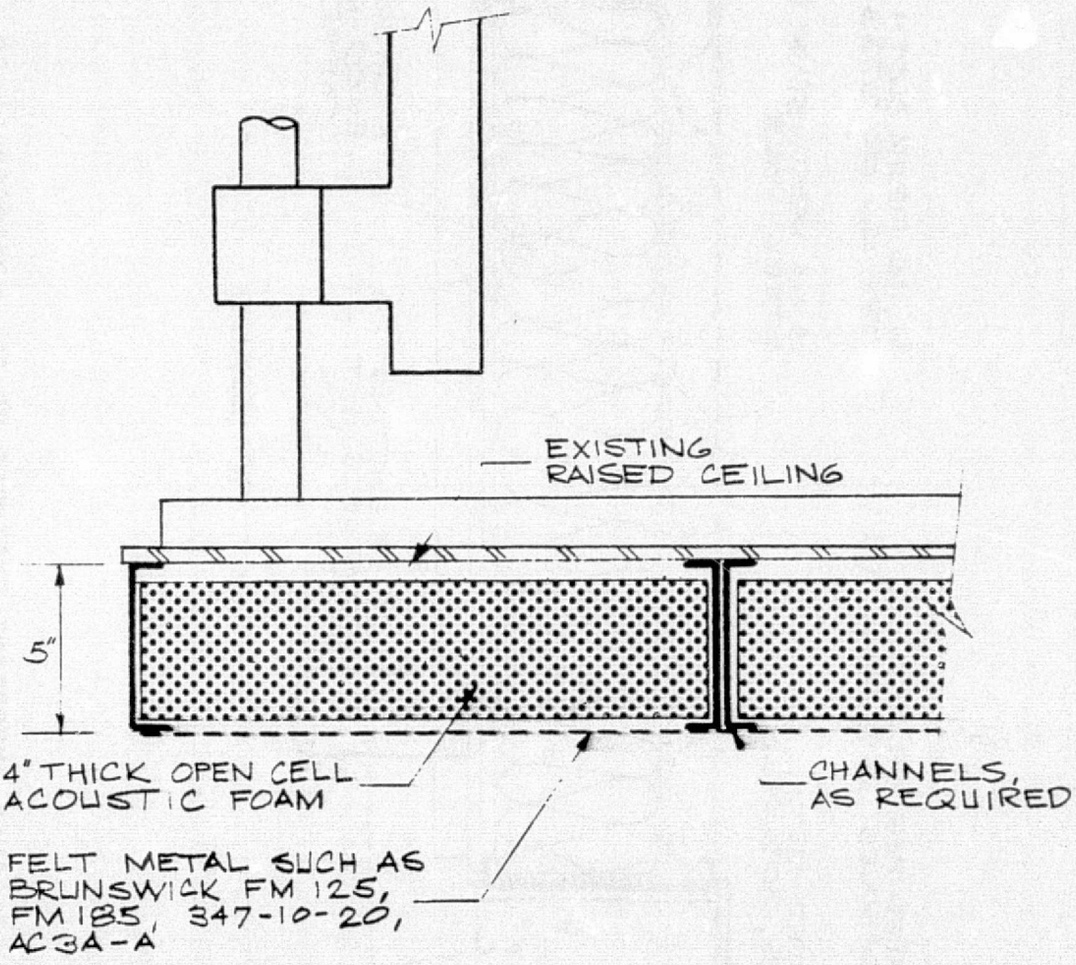

FIG. 22 ACOUSTICALLY IMPORTANT FEATURES OF THE PROPOSED CEILING TREATMENT.

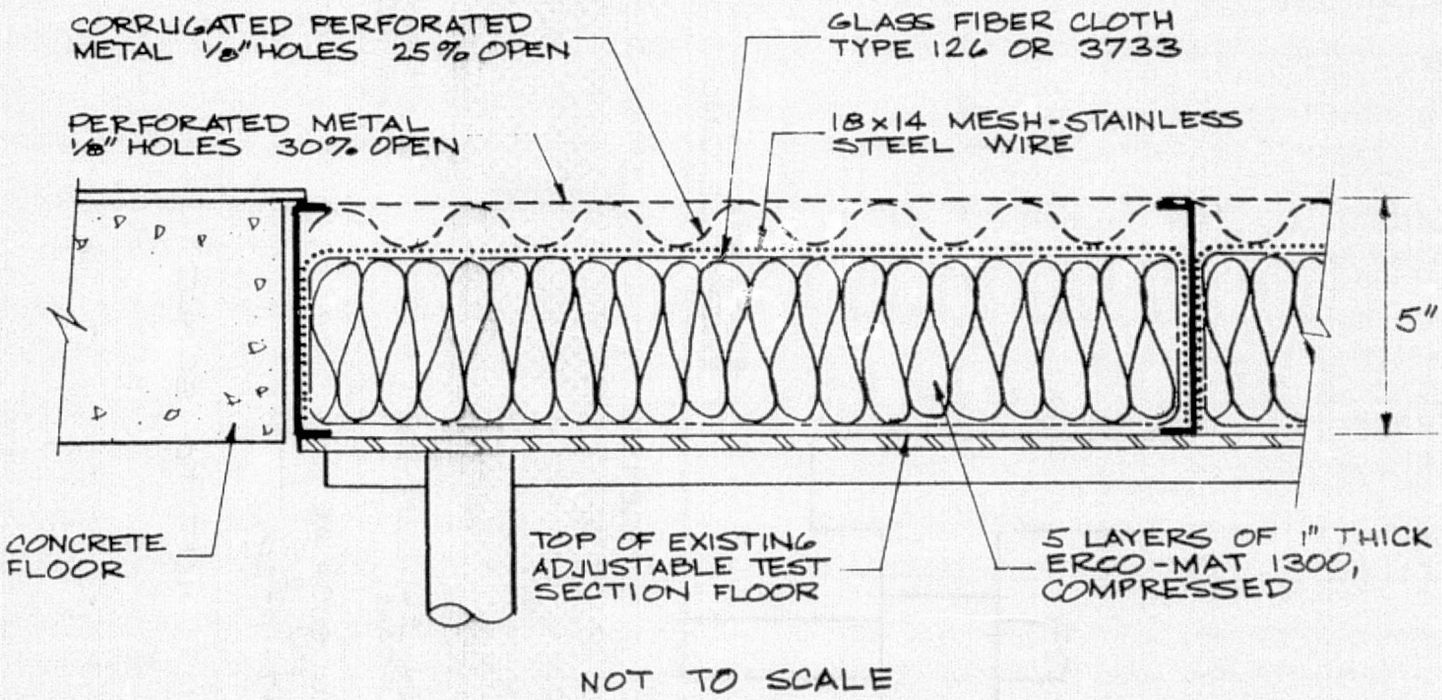

FIG. 23 ACOUSTICALLY IMPORTANT FEATURES OF THE PROPOSED FLOOR TREATMENT.

B AERODYNAMIC MODEL STUDY

1. Statement of the Problem

There is interest in converting the V/STOL Tunnel at NASA Langley into an acoustic facility. The tunnel can currently be run either as a conventional closed test section tunnel or in an open jet mode. In addition to applying acoustic treatment to various portions of the facility, it is important to see whether the noise associated with the free jet collection process can be reduced. Besides the acoustical aspect of this problem, the V/STOL tunnel is known to have a jet pulsation problem which occurs in varying degrees of severity at about 1 Hz for values of dynamic pressure between q=3 and q=11. At higher values of q the pulsations apparently do not occur.

Recently BBN has developed a novel idea for a wind tunnel collector design which differs from the commonly used bellmouth configuration. It was believed that this new design might suppress the jet pulsation problem experienced in the V/STOL Tunnel. Furthermore, it was desirable to determine whether treating a wind tunnel collector surface with a porous fiber metal would reduce the broadband noise arising from the impingement of turbulent flow on the collector. The following sections describe the aerodynamic model, the instrumentation used and document the results of tests performed on the open configuration of the V/STOL Tunnel test section.

2. The Aerodynamic Model

An existing model of an open jet wind tunnel test section and surrounding room was modified to resemble the V/STOL tunnel. This model was originally used for a collector design project conducted for NASA Ames. The model, illustrated in Fig.24, was attached to the nozzle of BBN's small open jet acoustic wind tunnel. Flow

from the model diffuser exits into the BBN tunnel room and flows into the BBN tunnel collector; thus the remainder of the V/STOL Tunnel closed circuit was not simulated. Since the model was a modification of a previous design, not all the dimensions of the test room were duplicated exactly. Nevertheless, all aspects of the model which could be pertinent were duplicated at a scale of 1:16.3. Specifically, the following were constructed to scale: the nozzle exit, the collector, the first diffuser section, the raised ceiling and side walls, (which are stored in the upper part of the test section and are lowered when the tunnel runs in the closed test section mode), and the distance to the nearest side wall.

In addition to the scale-model of the existing cowl configuration, two other collector shapes were assembled. These collector configurations are illustrated in Figs. 25 and 26. The two additional collectors were variations on the BBN collector design idea which employs surfaces that are angled towards the flow. The "small slant collector" was a simple modification of a collector model used in the previous study. The "large slant collector" was constructed from plywood and poster board; this collector was purely experimental and could not be used without first removing the ceiling piece. A 4.5 ft. extension to the diffuser (available from the previous collector design project) was also used in some tests to change the acoustic properties of the model. Finally, the model of the present V/STOL tunnel collector was also modified by covering its surfaces with fiber metal. Two versions of this model were studied: one with the back of the collector closed and filled with fiberglass and one having the back completely open.

A substantial portion of the interior wall surfaces of the model room were covered with 2" thick open cell foam to serve as an acoustic treatment. This step was taken to reduce the excitation of room modes in the model, the goal being to listen directly to the aerodynamic noise generation at the collector rather than the acoustic response of the room. The foam covered the side walls and a portion of the floor away from the jet. The model ceiling was left uncovered since it was constructed primarily of plexiglas for purposes of flow visualization. Part of the ceiling is hinged to provide access to the model.

3. Experimental Setup

Flow velocity is measured by a pitot tube located in the model nozzle. Measurements were conducted in a speed range of 59 to 155 ft/sec (q=4.2 to 28.6 lb/ft^2). Acoustic measurements were made using a 1" B&K microphone with an omni-directional cap and a wind screen. The microphone was placed at two locations within the model as indicated in Fig. 24. A foam barrier was sometimes used to shield the microphone from noise sources in the nozzle. A hot wire was located at various positions around the jet and collector during one phase of the testing.

Low frequency noise spectra were recorded using a Federal Scientific UA6A constant bandwidth analyzer (500 line system). A General Radio real time one-third octave band analyzer was used for the noise measurements taken to 10 kHZ. Because of dynamic range problems these spectra were taken twice: once flat and once A-weighted through a sound level meter.

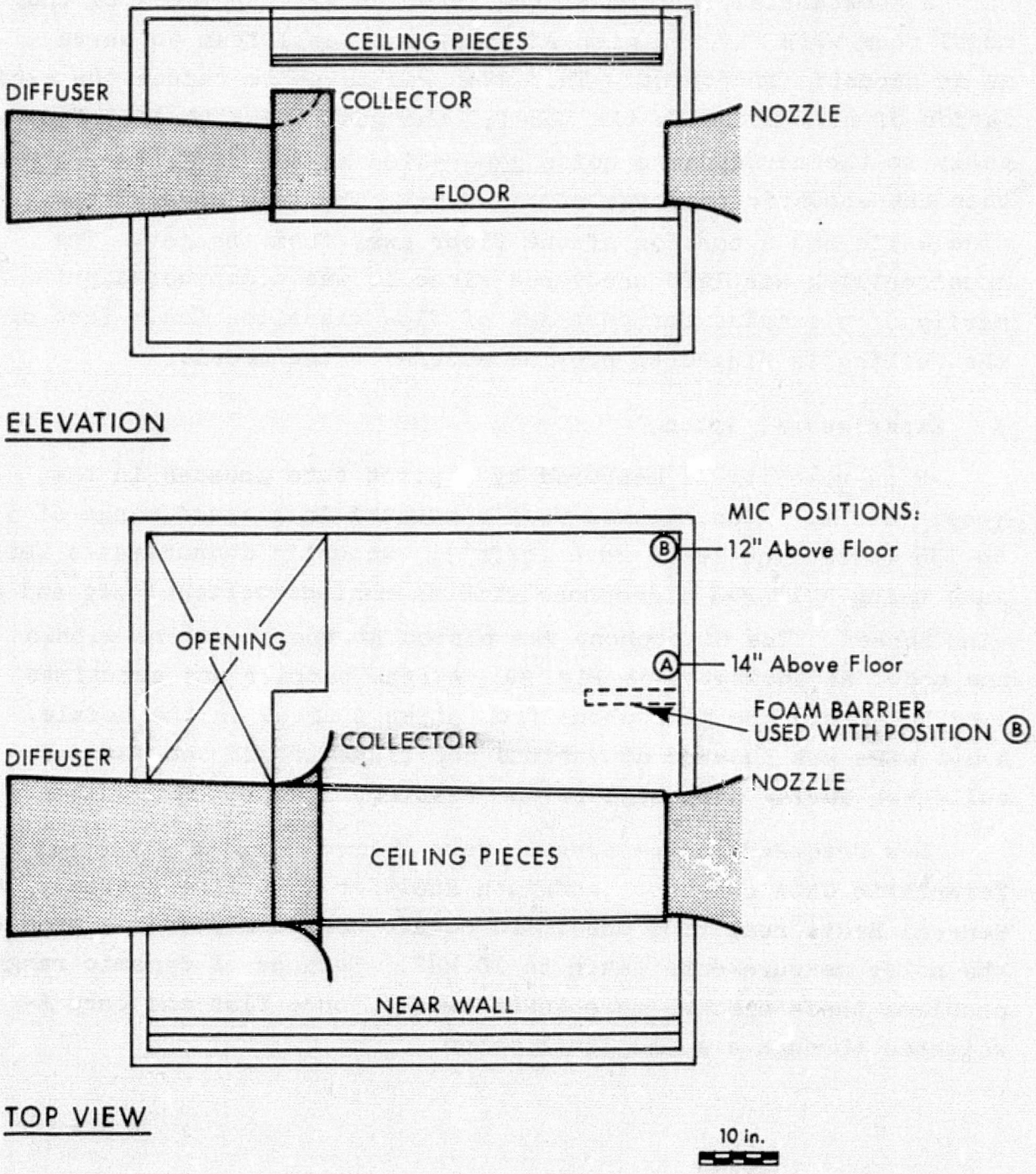

FIG. 24 AERODYNAMIC MODEL OF THE NASA LANGLEY V/STOL TUNNEL.

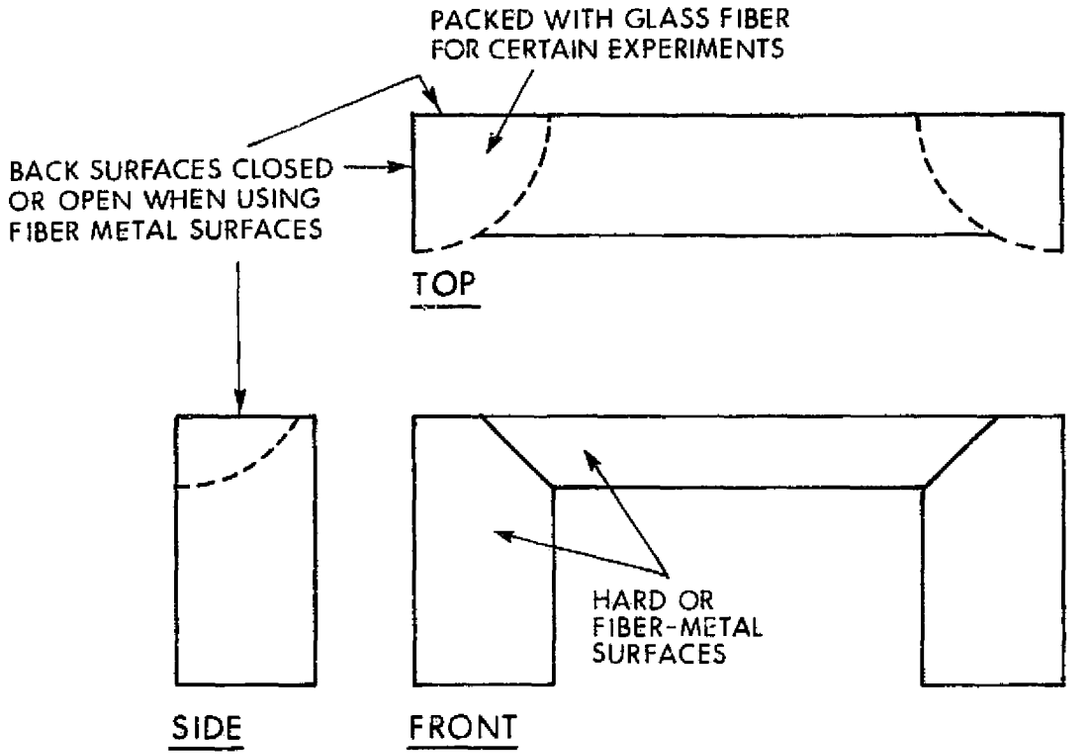

(a) Model of V/Stol Tunnel Collector

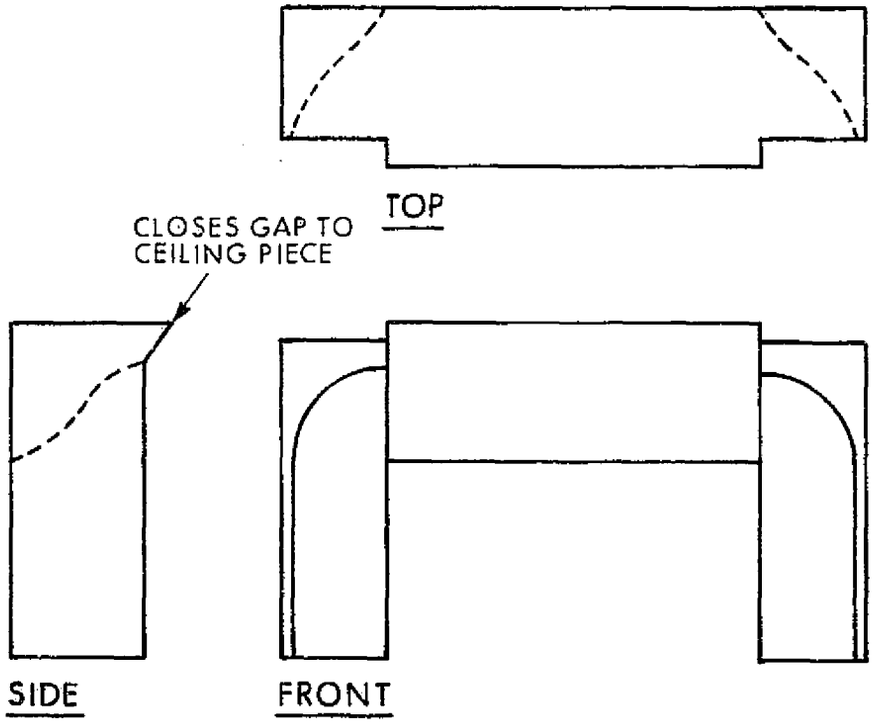

(b) Small Slant Collector

FIG. 25 GEOMETRY OF THE COLLECTOR MODELS TESTED.

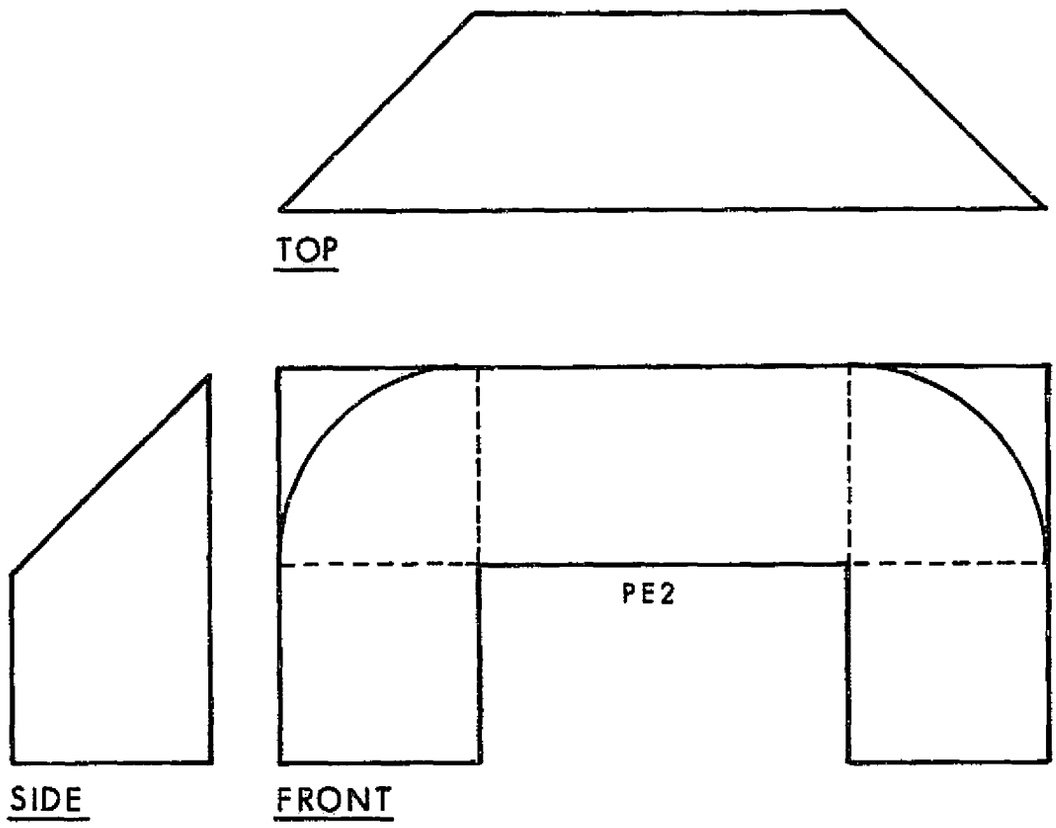

FIG. 26 GEOMETRY OF THE LARGE SLANT COLLECTOR MODEL TESTED.

The acoustic check of the model was done by driving a 10 in. diameter loudspeaker, sealed in an enclosure, with white noise through a power amplifier. The acoustic spectra were obtained using the UA6A.

Hot-wire measurements were made using a one-half mil wire with a Disa constant temperature anemometer system and a linearizer. The output was read on a D.C. voltmeter and spectra were obtained using the type UA6A analyzer The hot-wire was calibrated using the model free jet speed as measured by the pitot tube.

4. Flow Observations

Tufts were attached to the model of the V/STOL Tunnel collector, to the ceiling panel, and to the floor in the vicinity of the collector. Additional observations of the flow were made using a single tuft attached to a wire and held by an experimenter enclosed in the model room.

The location of the flow attachment line along the collector surface was determined to be similar to that observed in the full scale V/STOL Tunnel. Because of the long jet length, large scale turbulent eddies are apparent in the collector region and the flow attachment line is therefore not sharply defined. The flow outside the attachment line returns to the room to replace the fluid removed by the viscous/turbulent entrainment of the jet, setting up recirculation patterns in the room.

Flow along the side wall nearest the jet is opposite to the jet flow direction, indicating a compact recirculation cell in this region. On the opposite side the flow recirculation pattern is large and not clearly defined. The flow along the raised ceiling piece is in the same direction as the jet flow from the nozzle to point just upstream of the collector, indicating that the effect of jet entrainment dominates in this region. Around the collector,

however, the flow in the ceiling piece reverses direction, being dominated by the flow which has impinged on the collector and is being returned to the room. A portion of this return flow also passes behind the collector through the gap between the collector and the ceiling piece.

Since the diffuser entry plane is approximately five jet heights downstream of the nozzle, the potential core is essentially gone by the time the flow reaches the collector and diffuser. Although the flow in the diffuser is turbulent, the tufts showed no evidence of separation on the diffuser walls or in the corners.

The tufts on the collector showed no evidence of discrete pulsations but, because of the difference in scale, jet pulsations on the model would occur at about 16 Hz and it is unlikely the tufts could follow this oscillation frequency.

5. Summary of Tests Performed and Results

5.1 Low Frequency Microphone Measurements

Narrow band (1 Hz bandwidth) measurements were made on the model with the V/STOL tunnel model collector in place in a frequency range from 5 to 500 Hz in a velocity range from 59 to approximately 150 ft/sec. A representative set of spectra are shown in Fig. 27 A set of peaks (between about 15 to 30 Hz) which begin at low speed, reach a maximum, and decrease at higher speed were at first believed to be candidates for the low speed V/STOL tunnel pulsation problem. However, subsequent testing of the small slant and large slant collector (shape 1) showed only small changes in the spectrum, appearing to be primarily a redistribution of energy among the peaks. As indicated below, these low frequency peaks were subsequently shown to be the consequence of an acoustical or mechanical room resonance and were therefore unrelated to the pulsation problem.

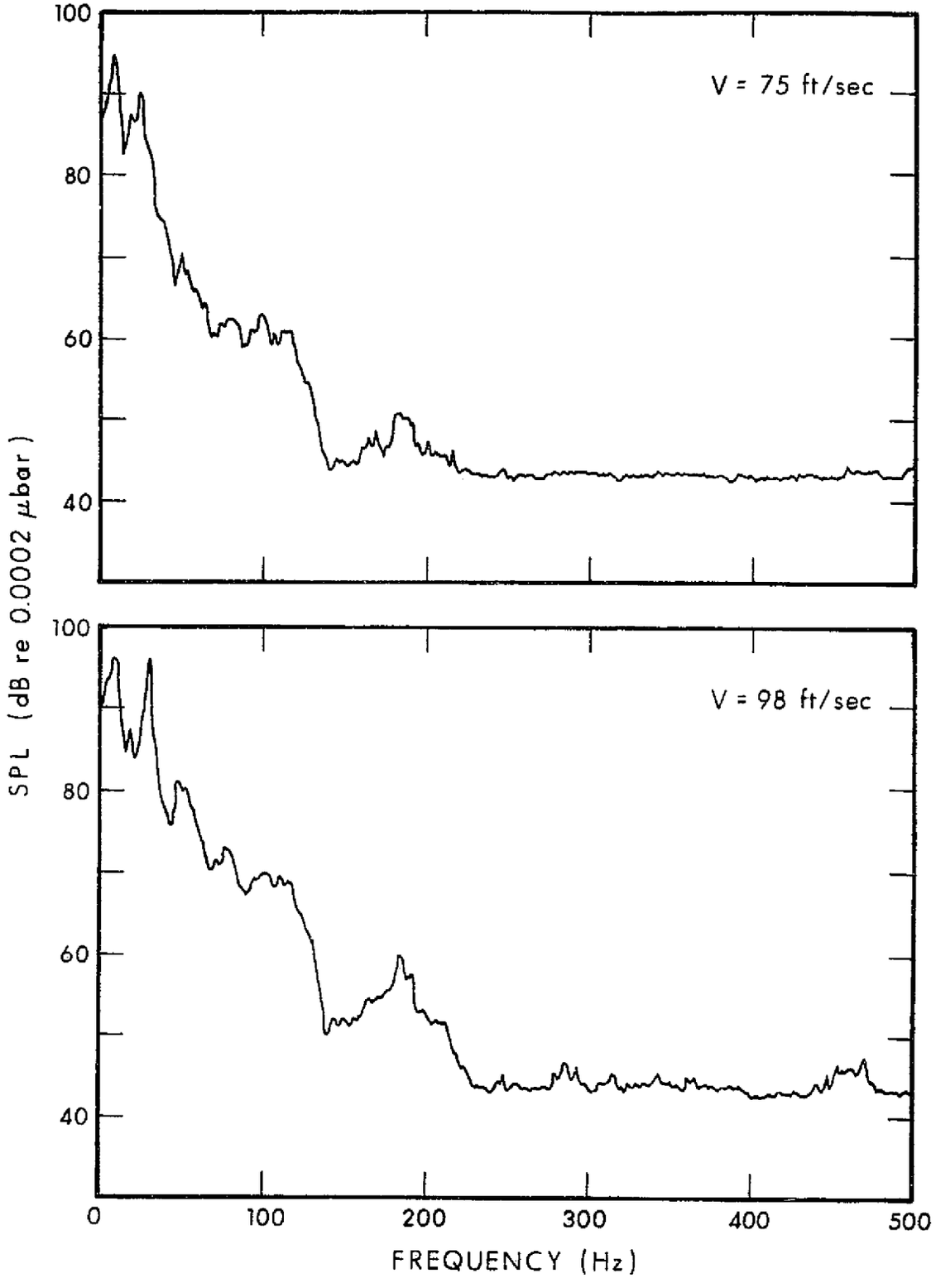

FIG. 27 TYPICAL SPECTRA FROM LOW FREQUENCY ACOUSTIC TESTS V/STOL TUNNEL MODEL COLLECTOR. NOTE BEHAVIOR OF LOW FREQUENCY PEAKS. MIC. POSITION A.

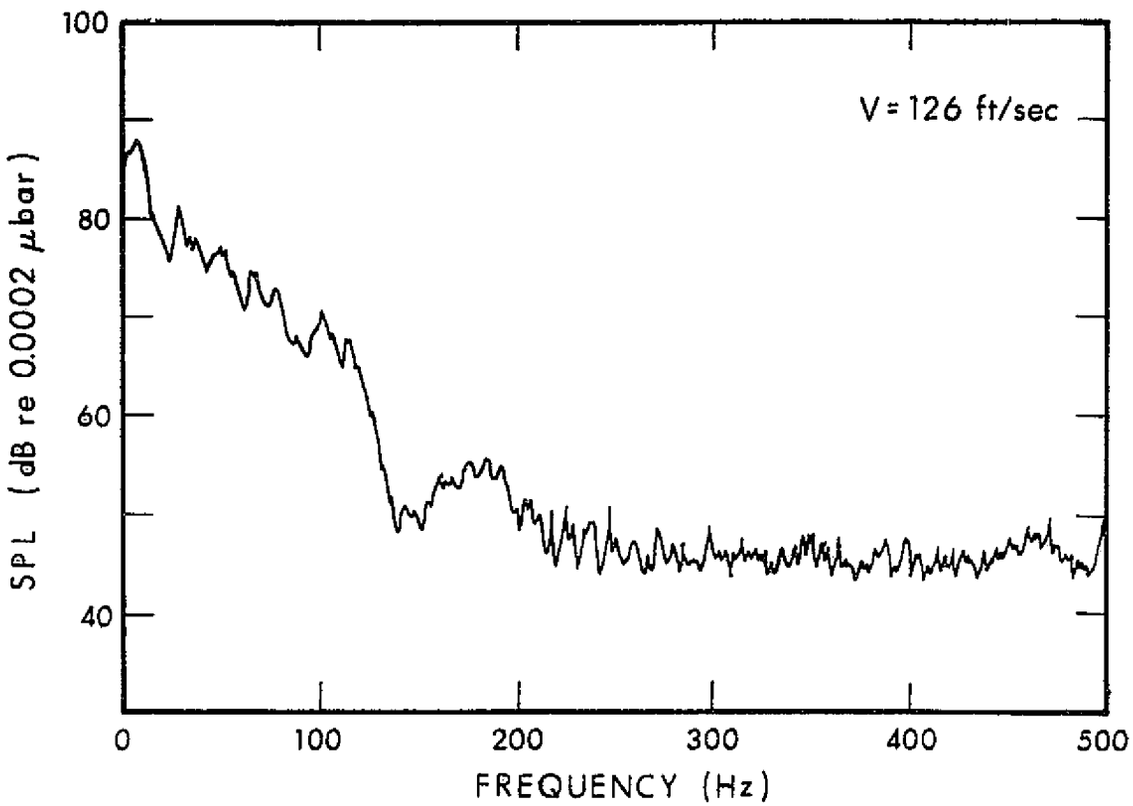

FIG. 27 continued.

5.2 Hot-Wire Measurements

Hot-wire measurements were made of the model free jet flow, including the potential core, the shear layers, and flow associated with the impingement process at the collector. Fig.28. shows spectra taken at a point in the shear layer 12 in. downstream of the nozzle and 6 in. above the floor aligned with the nozzle side surface. Fig. 29 shows a spectrum taken at a point near the flow attachment line on the collector. Fig. 30 shows a spectrum taken farther in from the collector and near the edge of the potential core (note the expanded frequency scale). All of these spectra are characterized by their extreme regularity with no evidence of aerodynamic pulsations in the flow. The hot-wire was then held at many points in and around the free jet flow and the instantaneous spectrum was constantly monitored in order to conduct a thorough search for flow pulsations. Flow speeds in a range of 59 to 100 ft/sec. were investigated but no discrete pulsations were discovered. The implication is that some feature of the model required to simulate the aerodynamic pulsations was not included. It is now believed that the missing feature may be the remainder of the tunnel circuit.

5.3 Acoustic Response of the Model

A sealed enclosure loadspeaker was placed in the tunnel room model and driven with a broadband noise source. The output of the microphone located at position A was recording the acoustical response. A typical result is shown in Fig.31. The results of this testing strongly suggested that the low frequency peaks observed previously were acoustical or mechanical resonances

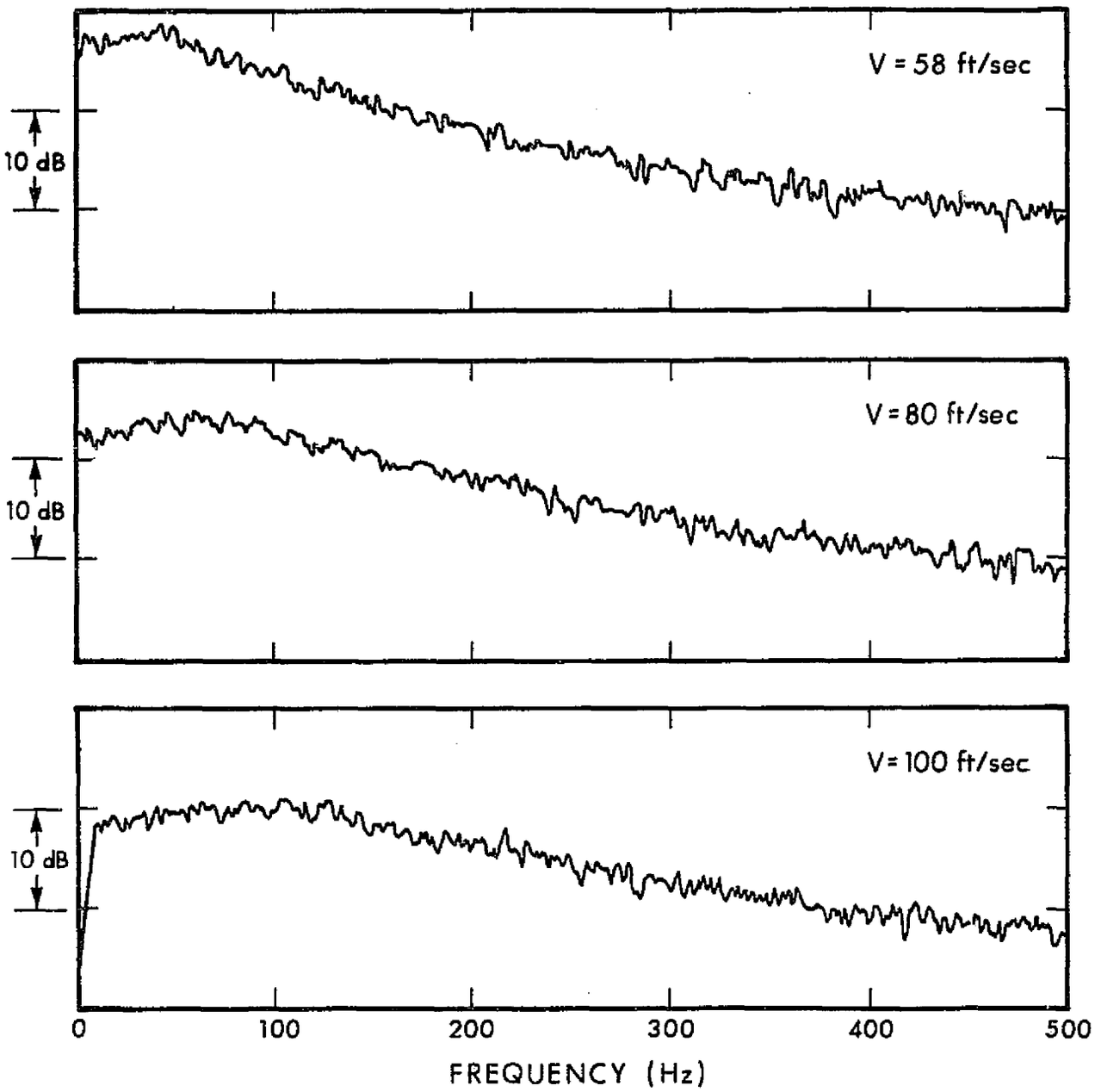

FIG. 28 TYPICAL HOT-WIRE VELOCITY SPECTRUM IN THE SHEAR LAYER.

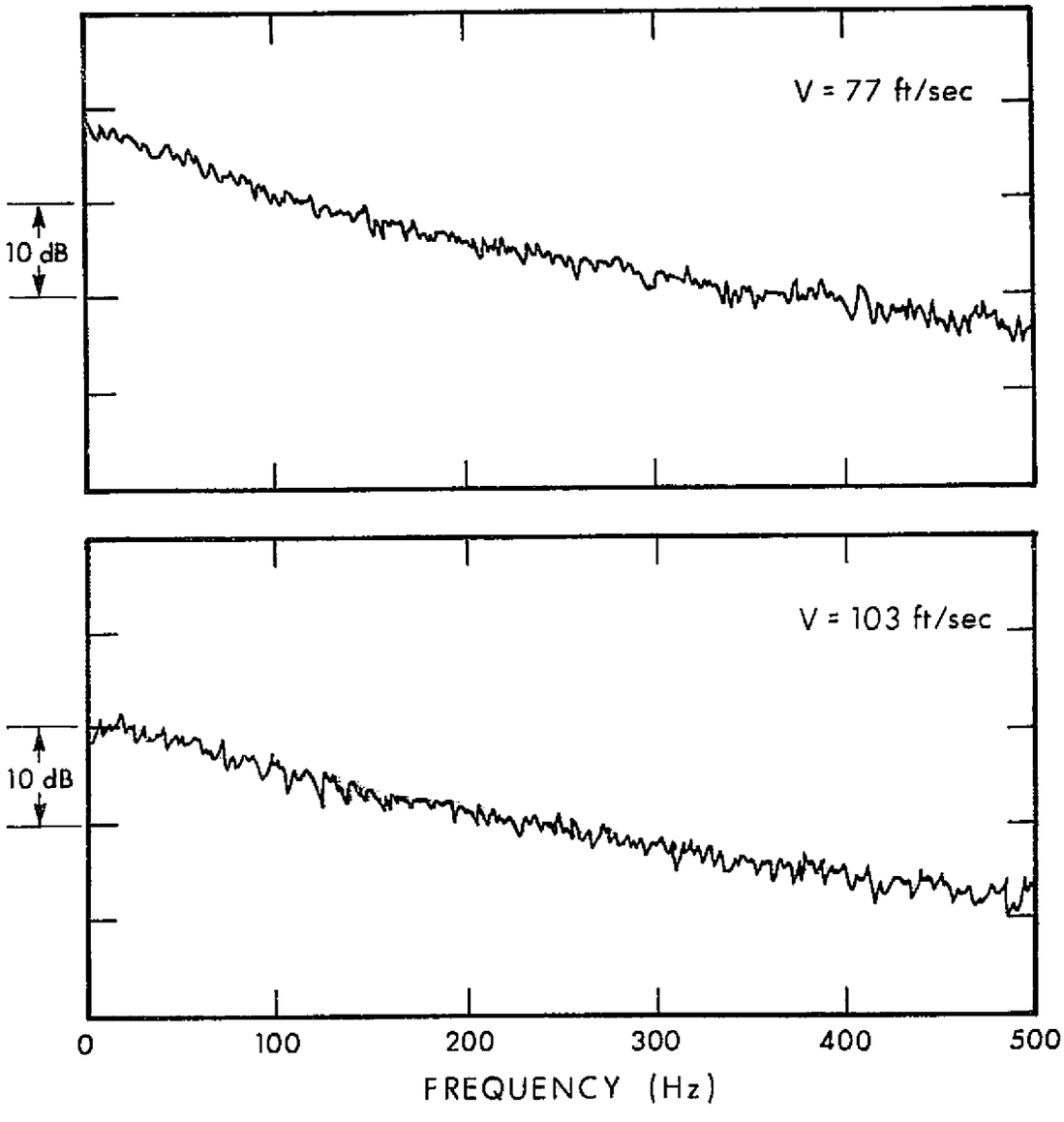

FIG. 29 TYPICAL HOT-WIRE VELOCITY SPECTRA IN FRONT OF THE COLLECTOR.

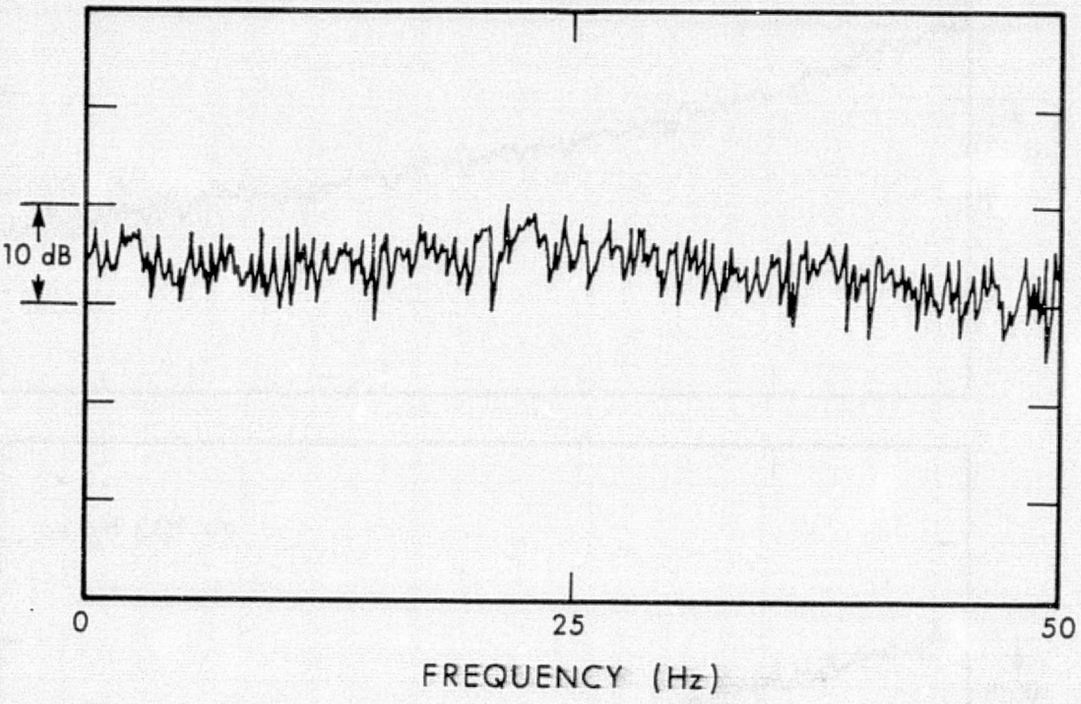

FIG. 30 HOT WIRE VELOCITY SPECTRUM UPSTREAM OF COLLECTOR NEAR THE INNER EDGE OF THE POTENTIAL CORE (NOTE EXPANDED FREQUENCY SCALE)

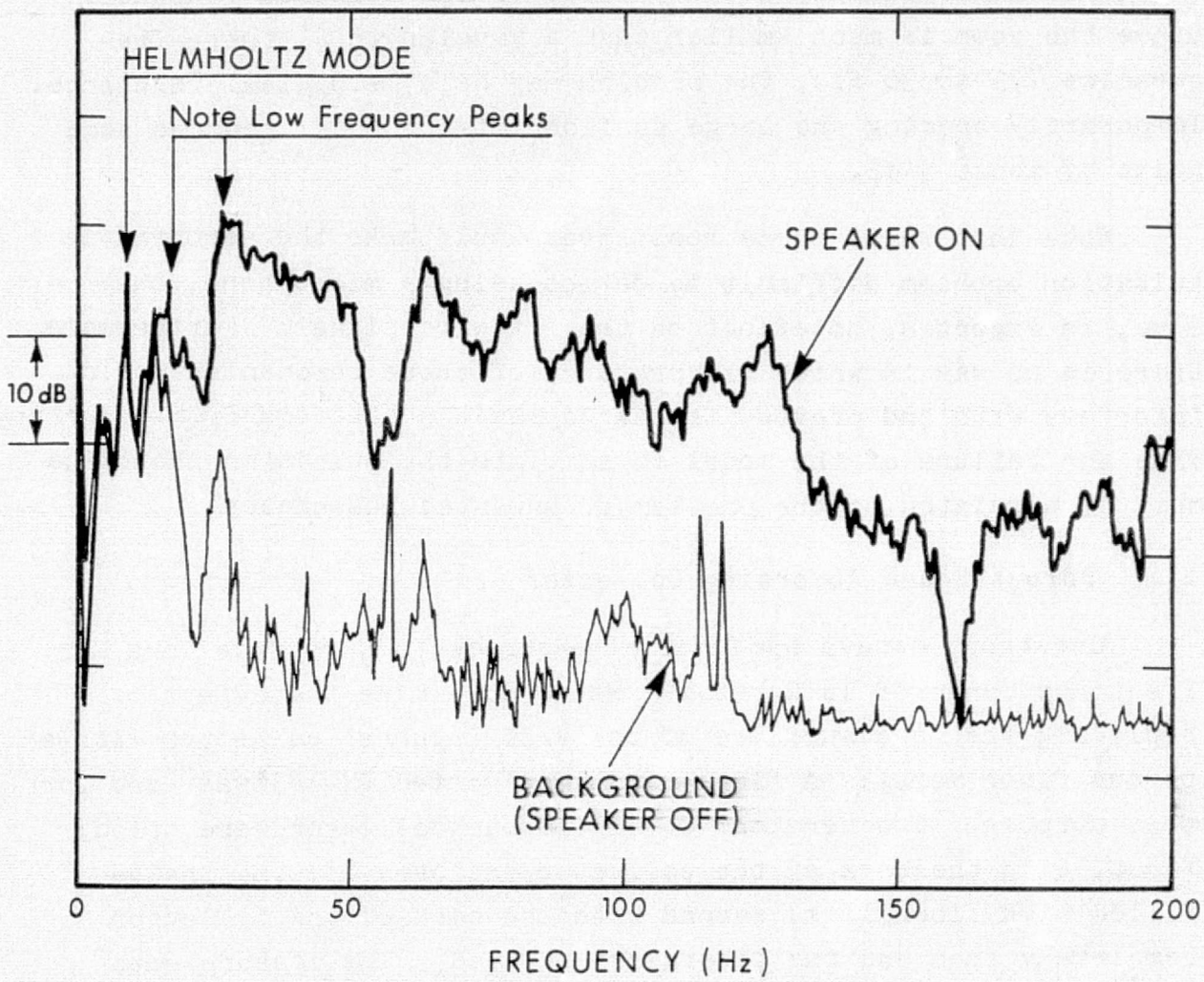

FIG. 31 TYPICAL RESULTS OF ACOUSTIC CHECK ON MODEL BEHAVIOR.

excited acoustically by the broadband noise generated by the shear layer impinging on the collector. Blocking the nozzle or diffuser had relatively little effect on the measured response. Since the room is much smaller than a wavelength at these frequencies (15 to 30 Hz), the problem may be a mechanical resonance. Temporarily bracing the large subfloor of the model reduced some peaks by about 5 dB.

Note that while these resonances would make the aerodynamic pulsation problem difficult to detect using a microphone, they have, as expected, no effect on the hot wire signal. Furthermore, there is no way in which the presence of these resonances could interfere with and prevent the aerodynamic puslations from occurring. Thus the failure of the model to simulate the pulsation phenomena must be unrelated to the problem of unwanted resonances.

5.4 Porous Sound Absorbing Collector Cowl

One-third octave band noise measurements were made in a frequency range of 16 Hz to 10 kHz to determine the effect of replacing the hard surfaces of the V/STOL tunnel collector with a porous fiber metal. A fiber metal designated FM-185*was used for this purpose. Two versions of the porous collector were tried; first, with the back of the collector enclosed and the inside filled with fiberglass; second with the back of the collector completely open and the fiberglass removed. The measurements were made for q = 0.8" H_2O (V = 59 ft/sec), q = 1.6" (V= 83.6 ft/sec), q = 3.2" (V = 118 ft/sec), and q = 4.8" (V= 145 ft/sec). The microphone was located in position B with a foam barrier in place

*This material is manufactured by the Brunswick Corporation in layers of 0.02 in. thickness and has a flow resistance of 100 mks rayl=0.25 ρc.

(see Fig.24) in order to diminish the effect of a high frequency noise emanating from the nozzle. Figures 32 and 33 present the results for the lowest and highest speeds tested, respectively. For diagnostic purposes measurements were also made with the collector removed entirely and with the diffuser length extended by 4.5 ft. In the case of no collector, the flow impinges directly on the relatively sharp edges of the diffuser and a considerable increase in the noise level is obtained. Extending the diffuser length has the effect of lowering the diffuser exit velocity by a factor of 1.8, which would substantially reduce the strength of noise sources at the diffuser exit plane.

Except for increased noise levels with the collector removed and some changes in low frequency behavior with the diffuser extended, there are no other really significant differences in the spectrum shown in Figs.32 and 33. Accordingly, we can conclude that replacing the rigid collector by a geometrically identical but porous collector of this specific flow resistance had virtually no effect on the noise generated by the flow impinging on it.

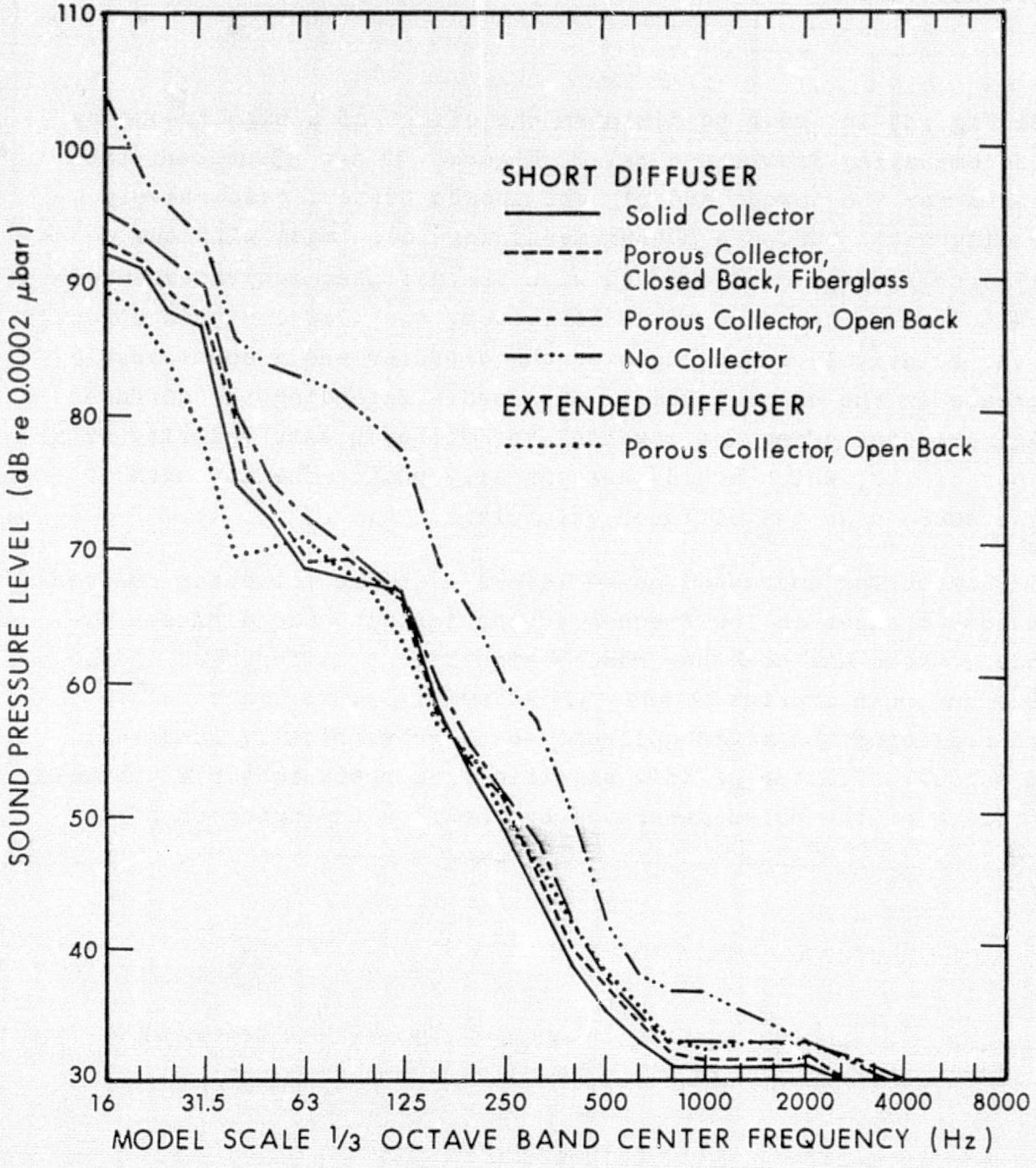

FIG. 32 NOISE LEVELS AT MIC. POSITION B, FOAM RUBBER IN PLACE, q=0.8 IN. H_2O, V=59 FT/SEC.

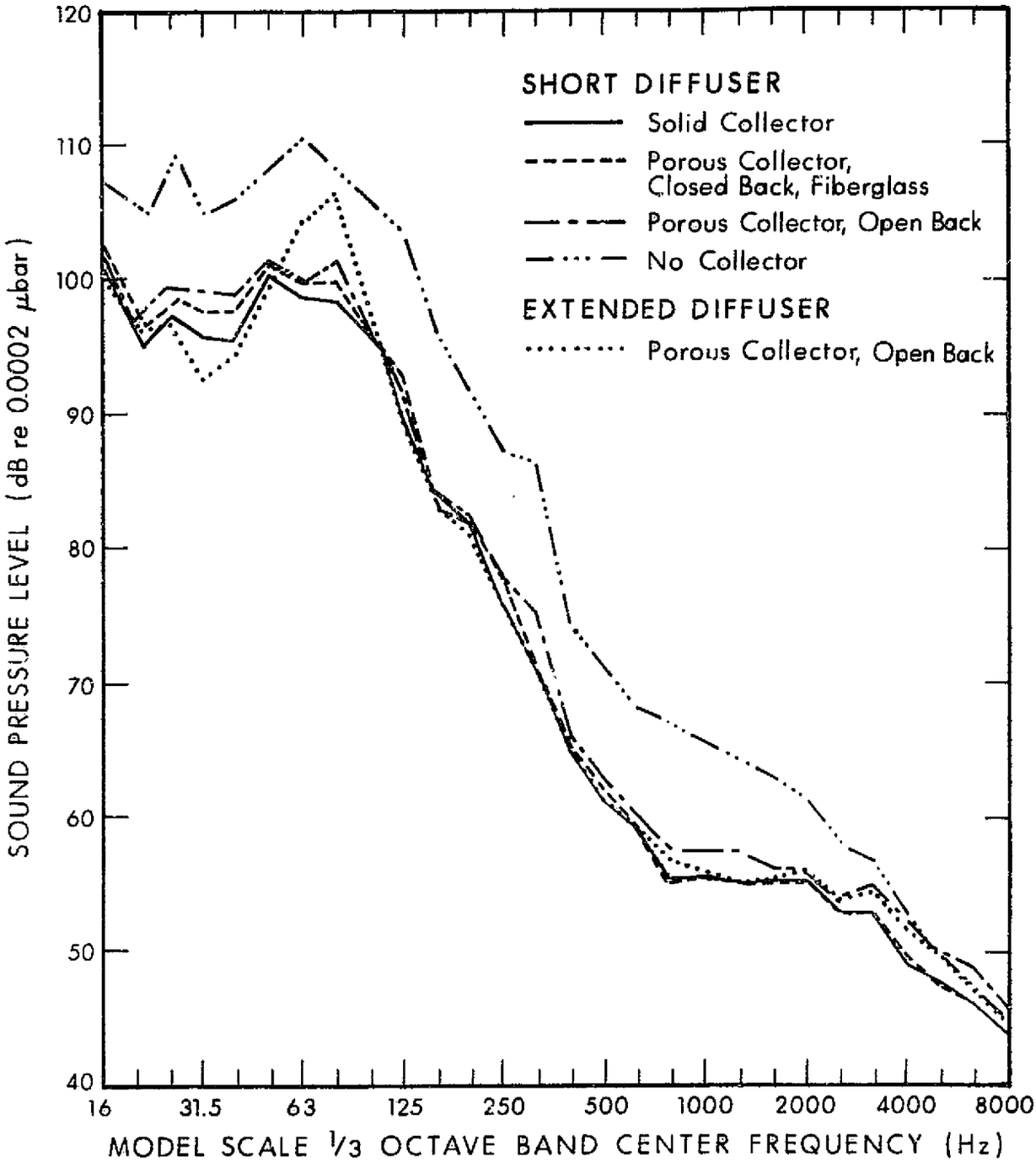

FIG. 33 NOISE LEVELS AT MIC. POSITION B, FOAM BARRIER IN PLACE, q=4.8 IN. H_2O, V=145 FT/SEC

6 Conclusions of the Aerodynamic Model Test

The purpose of the aerodynamic model test was to provide information on the cause of low frequency jet pulsations, test various scale-model collector cowl configurations promising to reduce or eliminate low frequency jet pulsations and to test whether or not a porous sound absorbing collector cowl can reduce the intensity of the flow impingement noise. The basic assumption made by both parties in conceiving these model investigations was that the cause for low frequency jet pulsations are phenomena restricted to the test section and the rest of the tunnel circuit do not contribute to the generation of these pulsations. The results of this preliminary study led us to conclude that:

(1) The low frequency jet pulsations are most probably caused or maintained by a coupling of aerodynamic and aeroacoustic phenomena in the tunnel circuit and the test section, (e.g. acoustic feedback through the tunnel circuit or periodic flow separation phenomena at turning vanes screens, etc.)

(2) There is a need to conduct an acoustical and aerodynamical survey of the full-scale tunnel to provide sufficient quantitative information about the aerodynamic and acoustic phenomena to be modeled later in a more detailed scale-model study.

(3) Because the low frequency jet pulsations in the model could not be produced in spite of modeling all the essential geometrical and aerodynamic features of the open test section, no conclusion could be drawn whether or not any of the tested new collector cowl configurations would eliminate low frequency jet pulsations in full-scale or scale-model tunnels containing the full return loop.

(4) The measured data indicate that replacing the hard collector cowl by a geometrically identical but porous low-flow resistance fiber metal surface of 100 mks rayls flow resistance do not result in any noticeable reduction of the test section noise caused by the impingement of the turbulent flow on the cowl.

7. Topics Recommended for Further Study

The pulsation phenomena is more complex than originally anticipated and in fact the entire tunnel circuit may be involved. One possibility is that a standing wave mode in the tunnel circuit forms part of the feedback loop in the pulsation process. The remainder of the feedback loop would involve waves on the free jet impinging on the collector. The jet waves would be triggered by the standing wave in the tunnel circuit and the flow pulsations produced when the jet waves strike the collector would reinforce the standing wave mode. At certain flow speeds resonant conditions could occur. No doubt other mechanisms can also be put forth. It is recommended that diagnostic tests on the full scale V/STOL Tunnel be performed to determine as precisely as possible the characteristics of the pulsation process. These diagnostic tests should include:

(1) hot-wire measurements of the velocity spectra in the free jet, the shear layer and around the collector to quantitatively determine the frequency of jet pulsations

(2) fluctuating pressure spectra at points around the circuit and cross correlation of these pressures to determine the nature of the feedback loop, if any, including phase determination and wave speeds.

(3) Flow quality measurements around the tunnel circuit especially at turning vanes and screens.

These measurements must be made accurately up to very low frequencies (i.e. 0.5 Hz). In addition to yielding quantitative information about the pulsation process these measurements shall provide information about the physical process responsible for the pulsation. This physical insight gained from the careful evaluation of the full-scale facility will indicate the nature of a promising measure to reduce or eliminate pulsations and would also indicate whether such a measure can be evaluated in model test or only at full-scale.

Because of our experience in diagnostic measurements in complex aeroacoustic phenomena, we strongly believe that the diagnostic tests should be carried out by a combined NASA-BBN team. Since we are dealing here with a complex phenomena the nature of which is not yet understood, the effective solution of the problem (which would yield needed design information for any new open circuit tunnels) would require a study with a more extended scope than the present investigations. Since any change in collector shape or any modification of the present collector's surfaces will be a major undertaking, it should be determined in advance whether collector configuration changes can fix the pulsation problem.

LIST OF REFERENCES

1. Vér, I.L., "Acoustical Evaluation of the NASA Langley V/STOL Wind Tunnel", BBN Rept. 2288, Dec. 1971, NASI-9559, Task 13.

2. Vér, I.L., C.I. Malme and E.B. Meyer, "Acoustical Evaluation of the NASA Langley Full-Scale Wind Tunnel", BBN Rept. 2100, January 1971, NASI-9559, Task 7.

3. Vér, I.L., "Acoustical Modeling of the Test Section of the NASA Langley Research Center's Full-Scale Wind Tunnel", BBN Rept. 2280, Nov. 1971, NASI-9559, Task II.

4. Vér, I.I., "Some Acoustical Characteristics of a Crossing-Jet Noise Source", *J. Accust. Soc. Am.*, Vol. 57, No. 5, 1975, pp. 1205-1206.

APPENDIX A

COLLECTION OF NORMALIZED SOUND PRESSURE LEVEL VS DISTANCE CURVES WITH THE ROOM CONDITION AS PARAMETER

SOURCE POSITION 1

TRAVERSE A - UPSTREAM DIRECTION

Figure No.	Model-Scale Frequency, Hz
A-1	630
A-2	1250
A-3	2500
A-4	5000
A-5	10,000
A-6	20,000

FIG A-1 TRAVERSE A ; UPSTREAM DIRECTION

Source Position 1
630 Hz Model Scale
63 Hz Full Scale

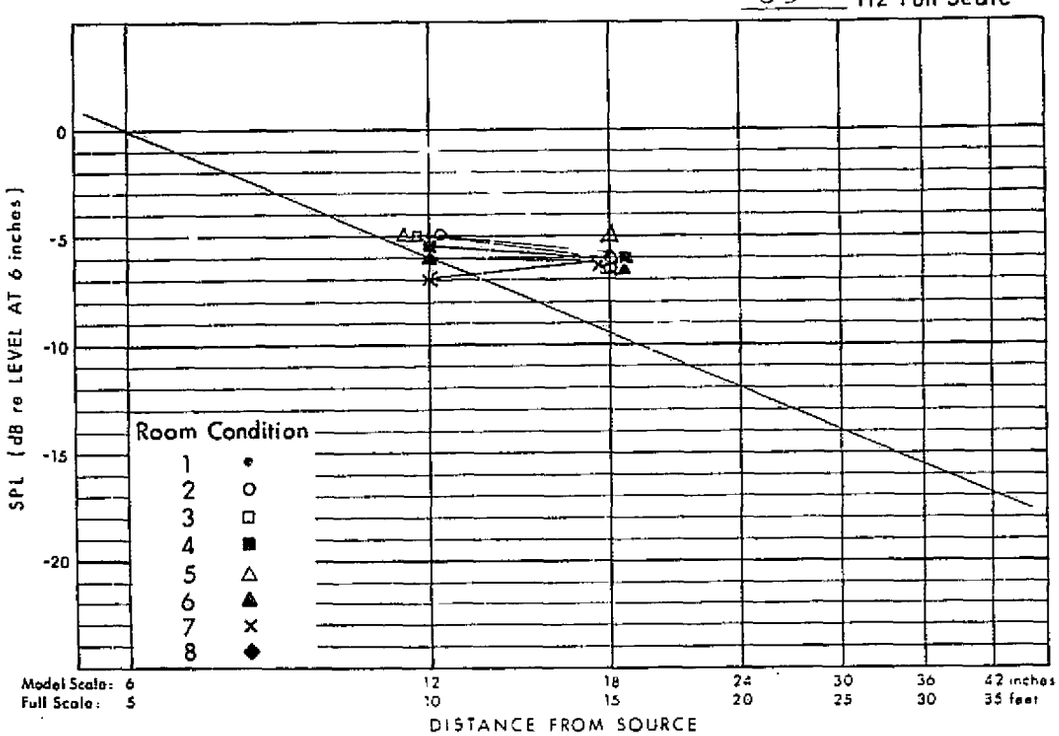

Fig A-2 TRAVERSE A ; UPSTREAM DIRECTION

Source Position 1
630 Hz Model Scale
63 Hz Full Scale

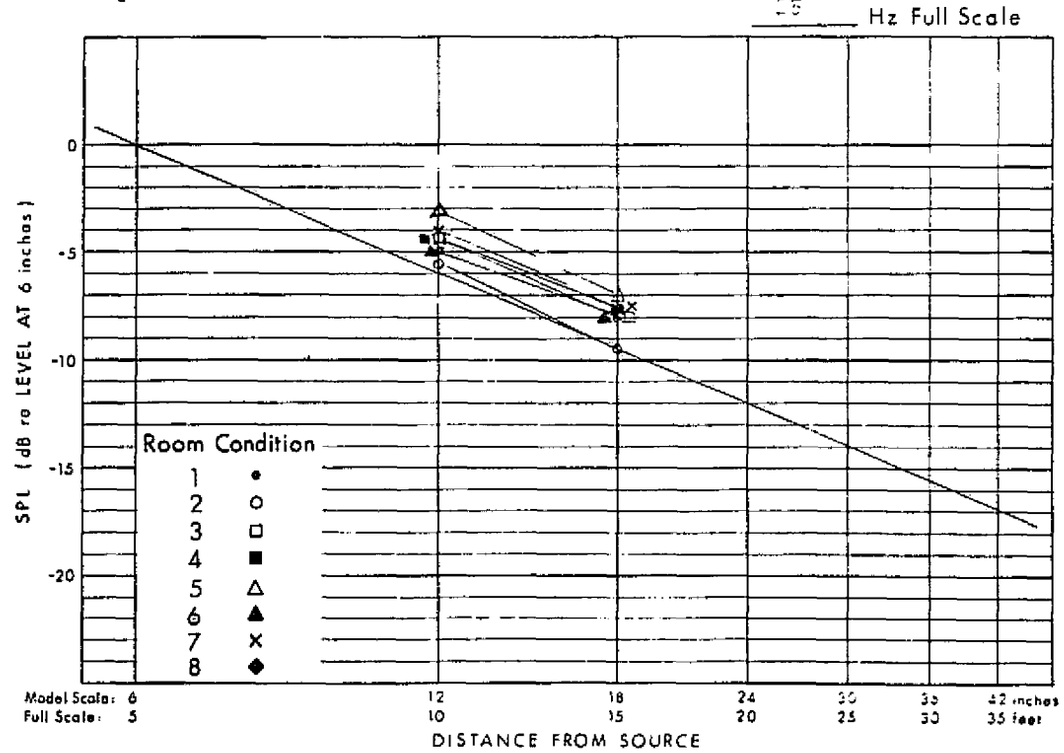

Source Position 1

2500 Hz Model Scale

250 Hz Full Scale

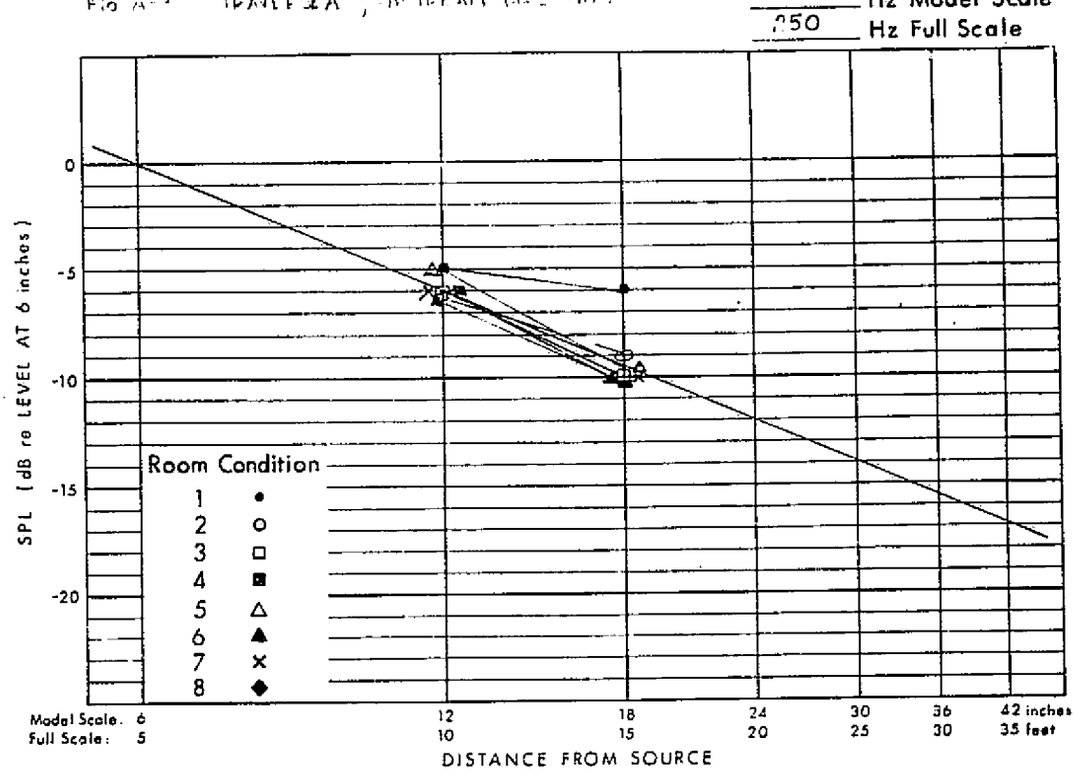

Source Position 1

5000 Hz Model Scale

500 Hz Full Scale

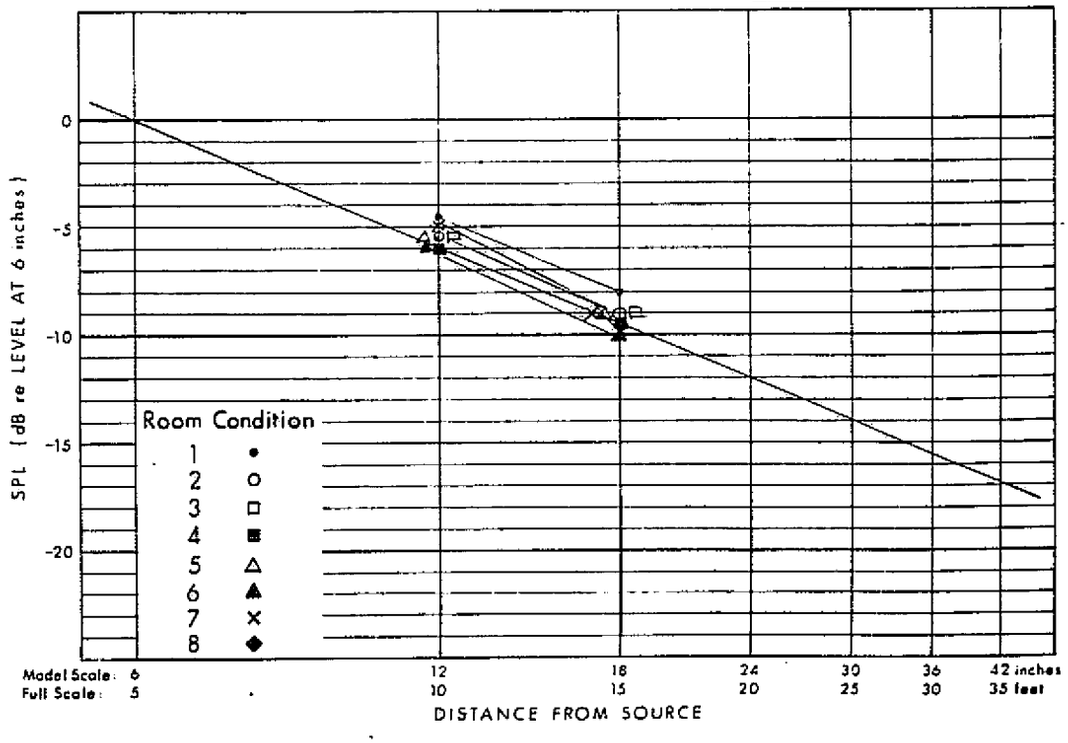

Fig A-5 TRAVERSE A ; UPSTREAM DIRECTION

Source Position 1
10,000 Hz Model Scale
1000 Hz Full Scale

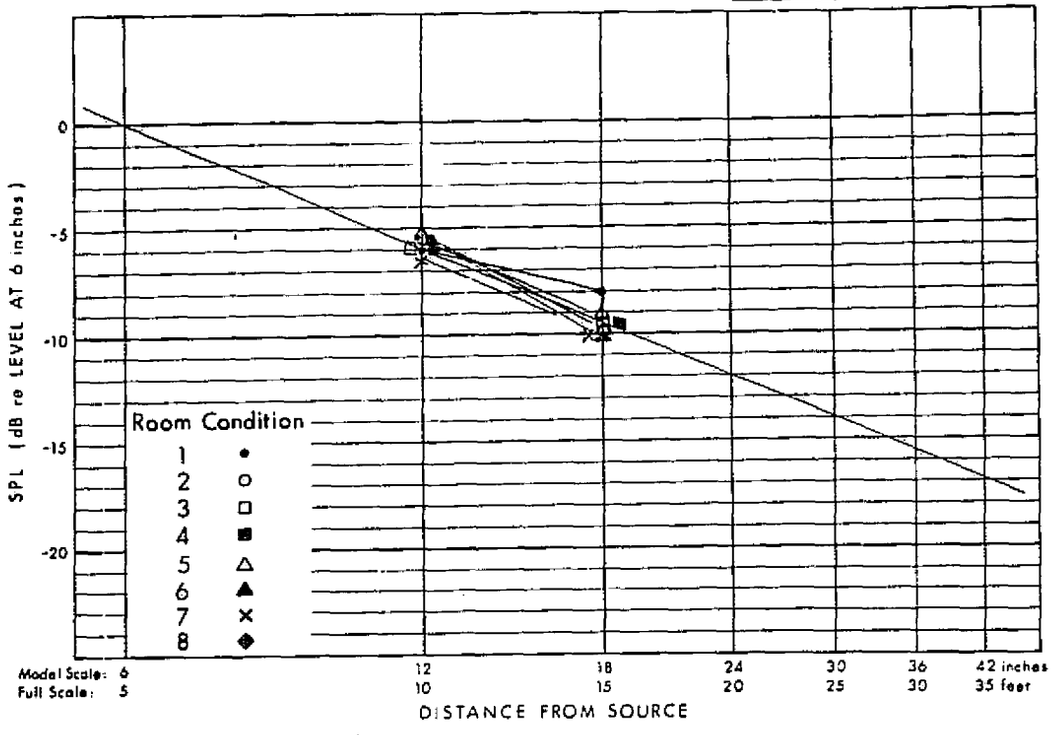

Fig A-6 TRAVERSE A UPSTREAM DIRECTION

Source Position 1
20,000 Hz Model Scale
2000 Hz Full Scale

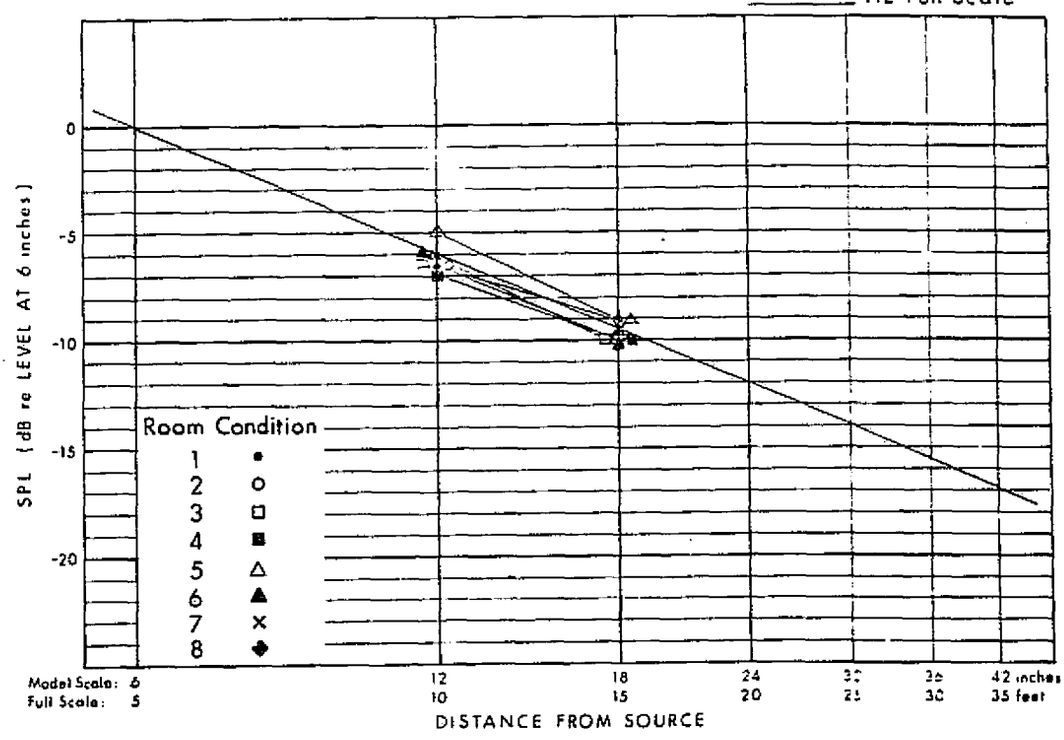

TRAVERSE B - 90° TOWARD NEAR WALL

Figure No.	Model-Scale Frequency, Hz
A-7	630
A-8	1250
A-9	2500
A-10	5000
A-11	10,000
A-12	20,000

Source Position 1
630 Hz Model Scale
63 Hz Full Scale

Fig. A-7 TRAVERSE B

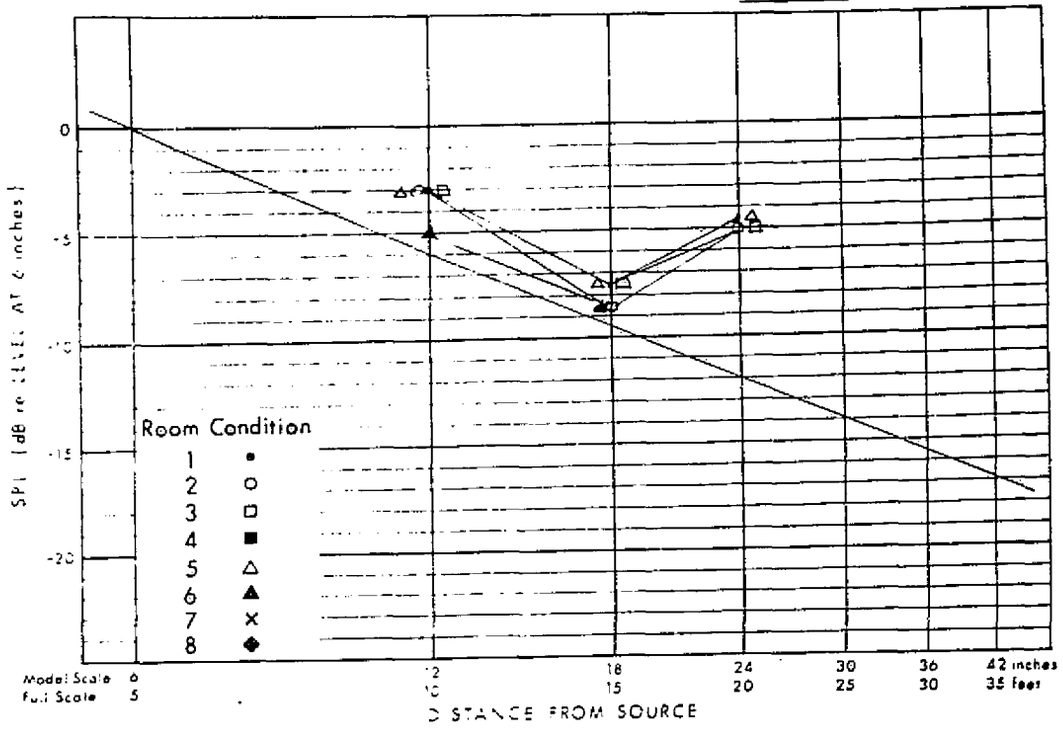

Source Position 1
1250 Hz Model Scale
125 Hz Full Scale

Fig A-8 TRAVERSE B

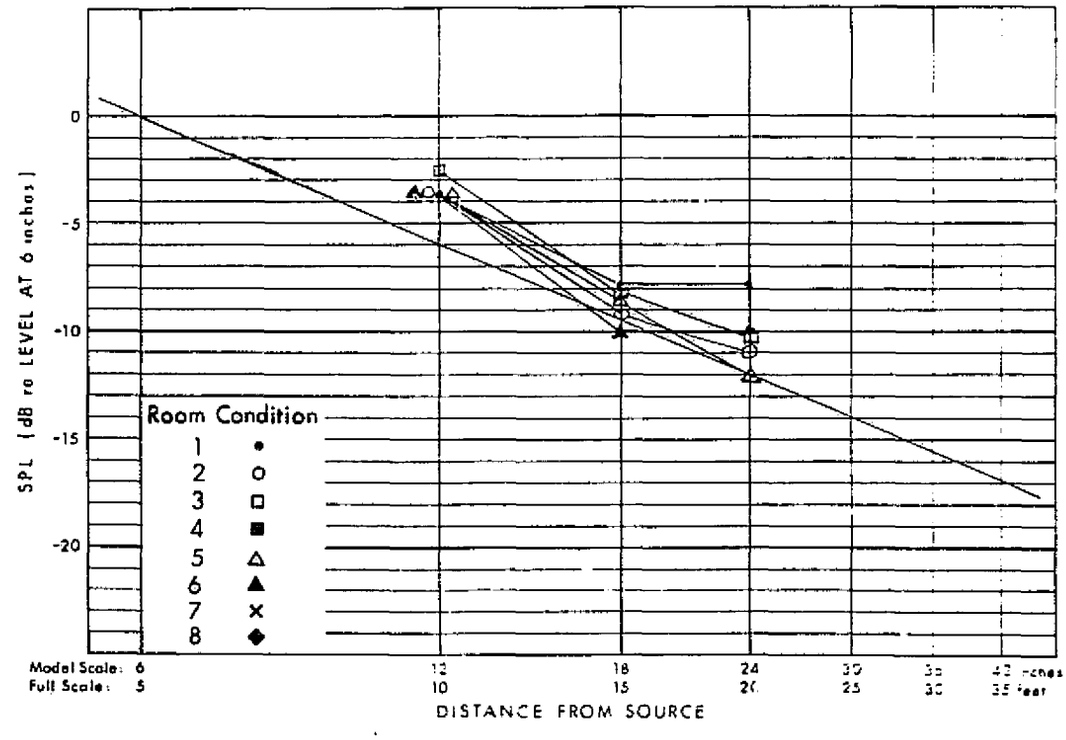

Fig. A-9 TRAVERSE B

Source Position 1
2500 Hz Model Scale
250 Hz Full Scale

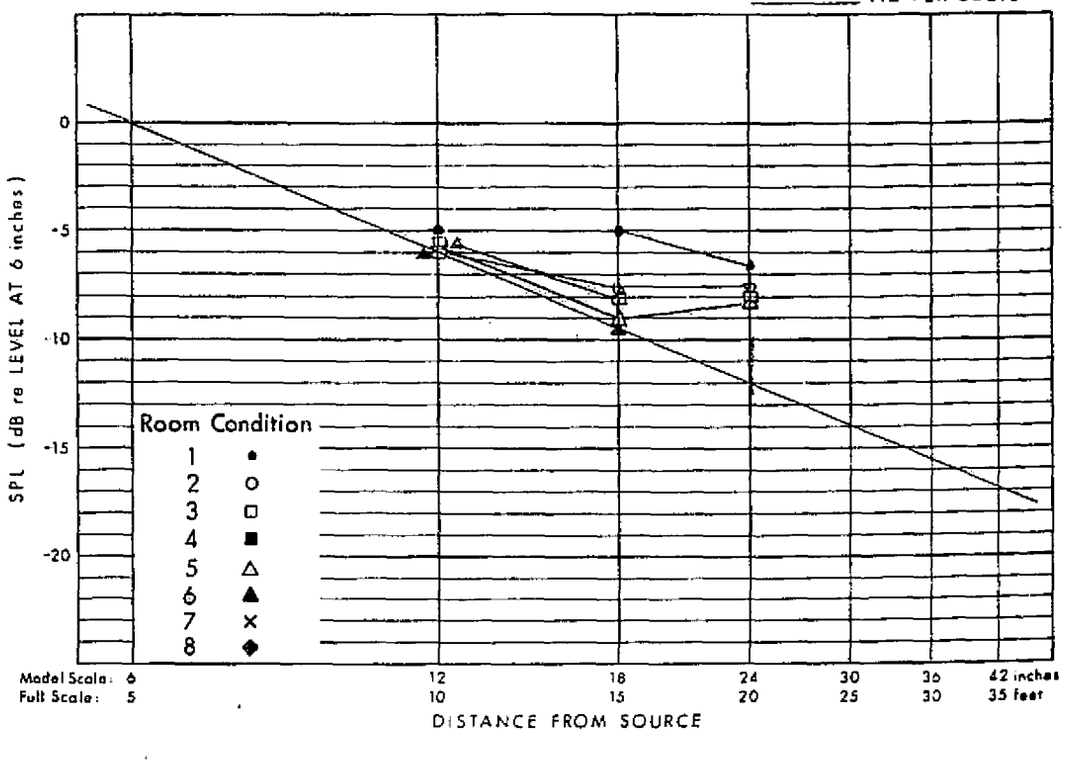

Fig. A-10 TRAVERSE B

Source Position 2
5000 Hz Model Scale
500 Hz Full Scale

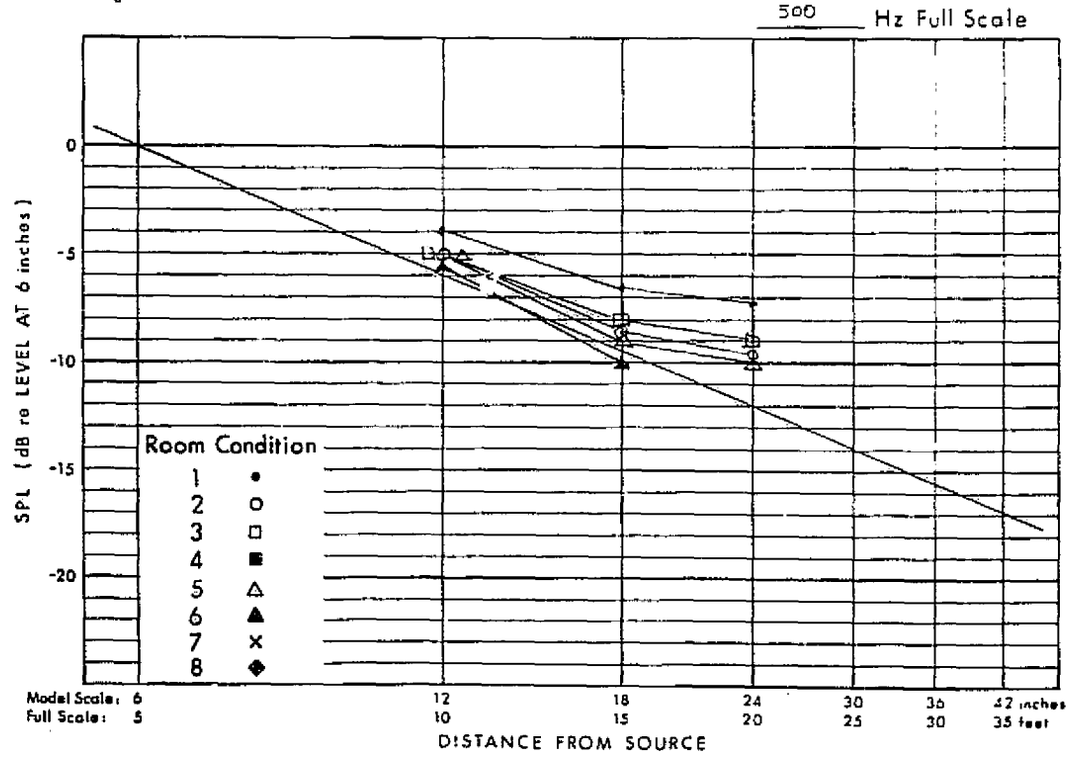

Fig A-11 TRAVERSE B

Source Position 1
10,000 Hz Model Scale
1000 Hz Full Scale

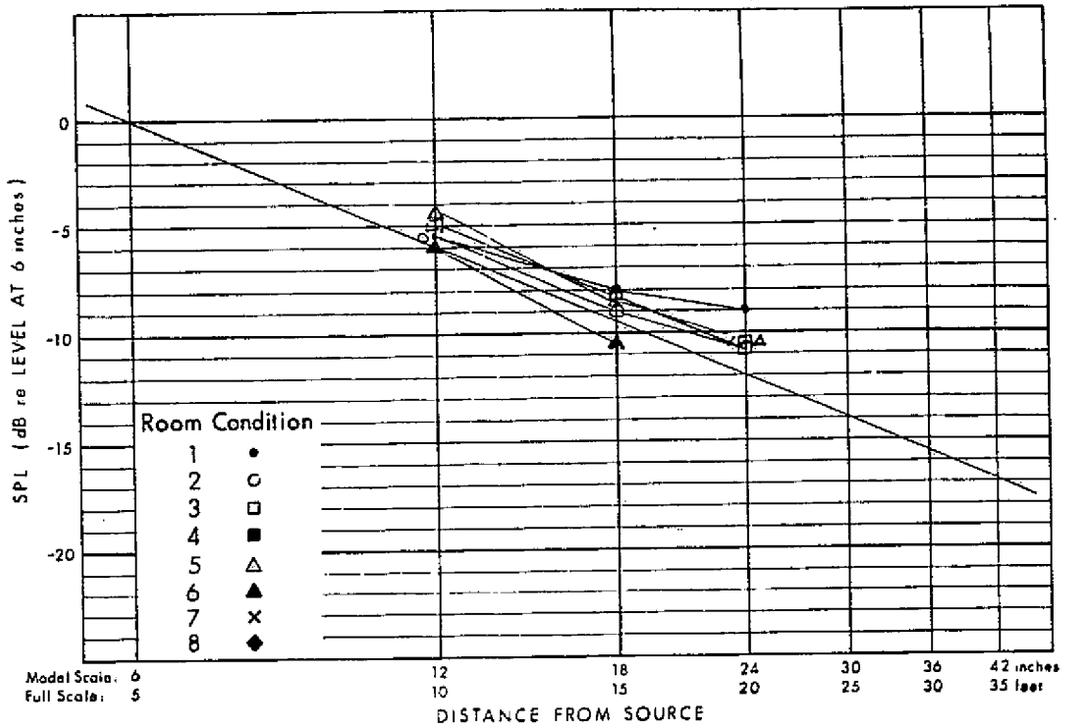

Fig A-12 TRAVERSE B

Source Position 1
20 000 Hz Model Scale
2000 Hz Full Scale

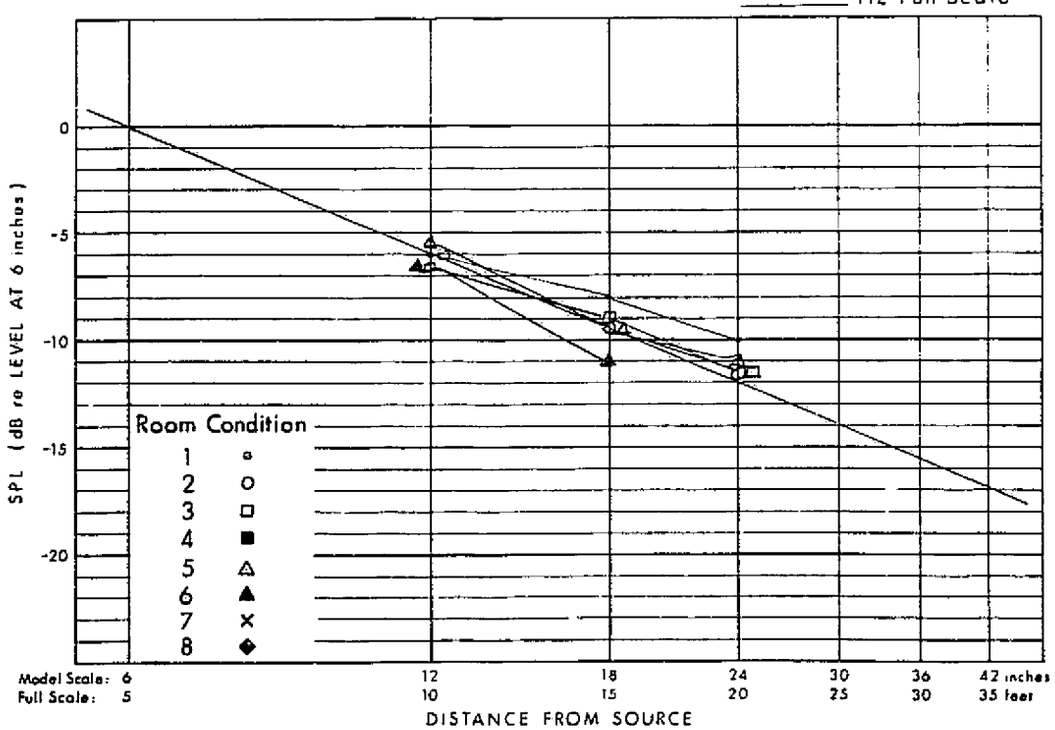

TRAVERSE C - DOWNSTREAM

Figure No.	Model-Scale Frequency, Hz
A-13	630
A-14	1250
A-15	2500
A-16	5000
A-17	10,000
A-18	20,000

Fig. A-13 TRAVERSE C

Source Position 1
630 Hz Model Scale
63 Hz Full Scale

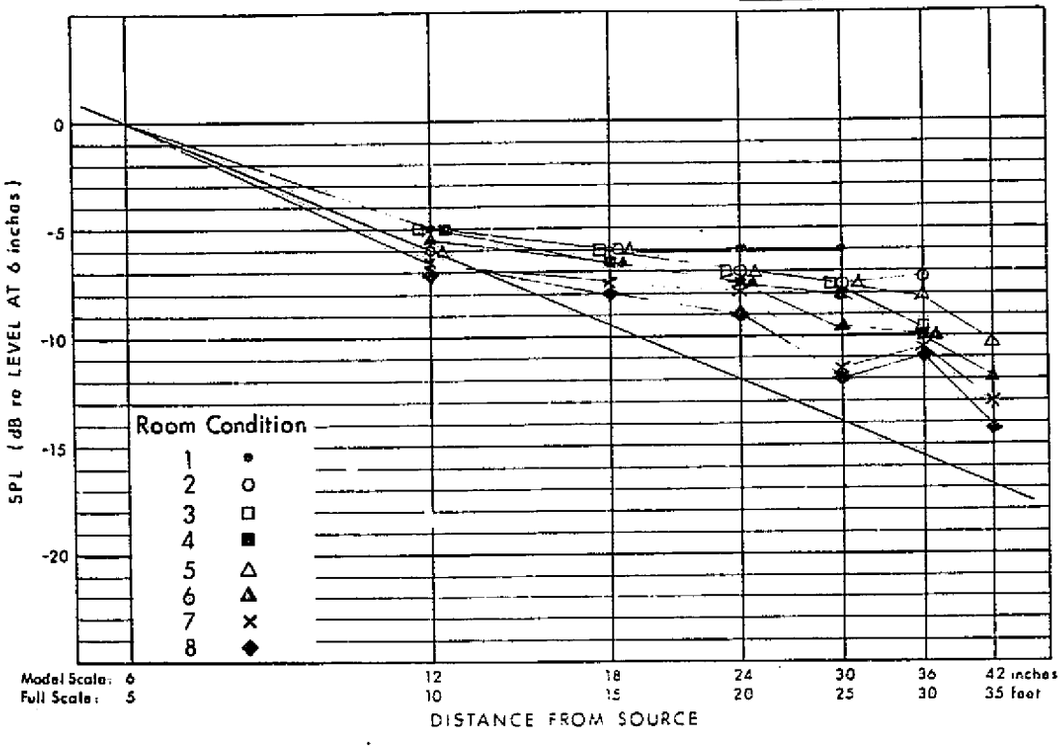

Fig. A-14 TRAVERSE C

Source Position 1
1250 Hz Model Scale
125 Hz Full Scale

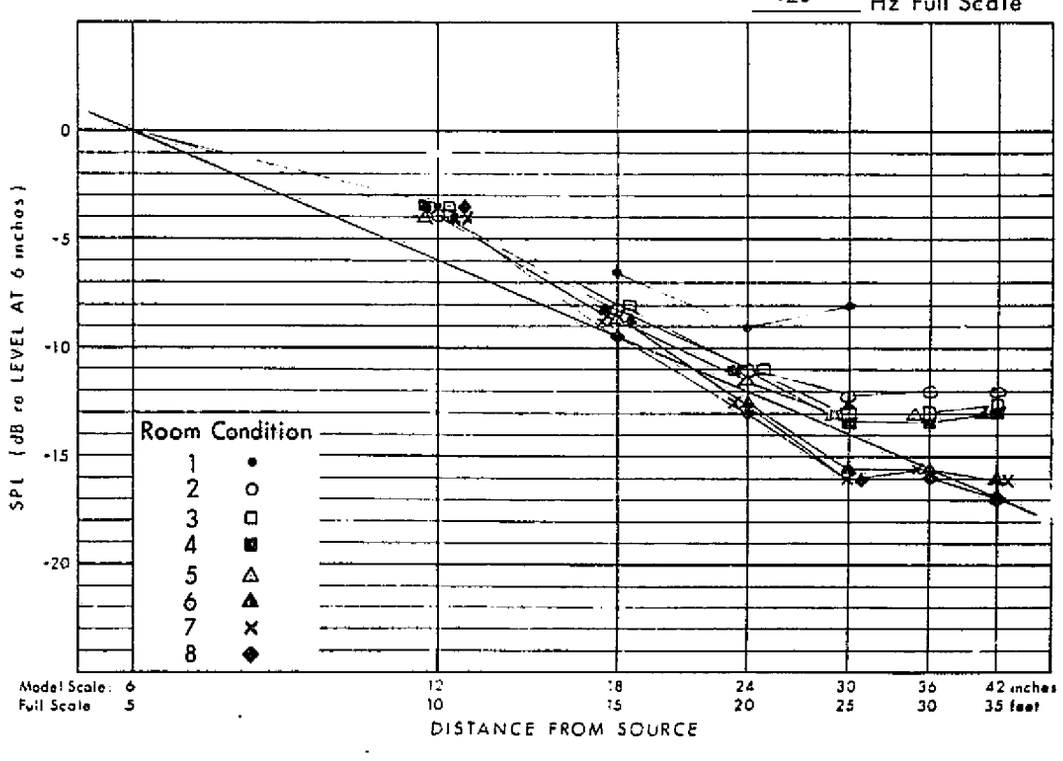

Fig A-15 TRAVERSE C

Source Position 1
2500 Hz Model Scale
250 Hz Full Scale

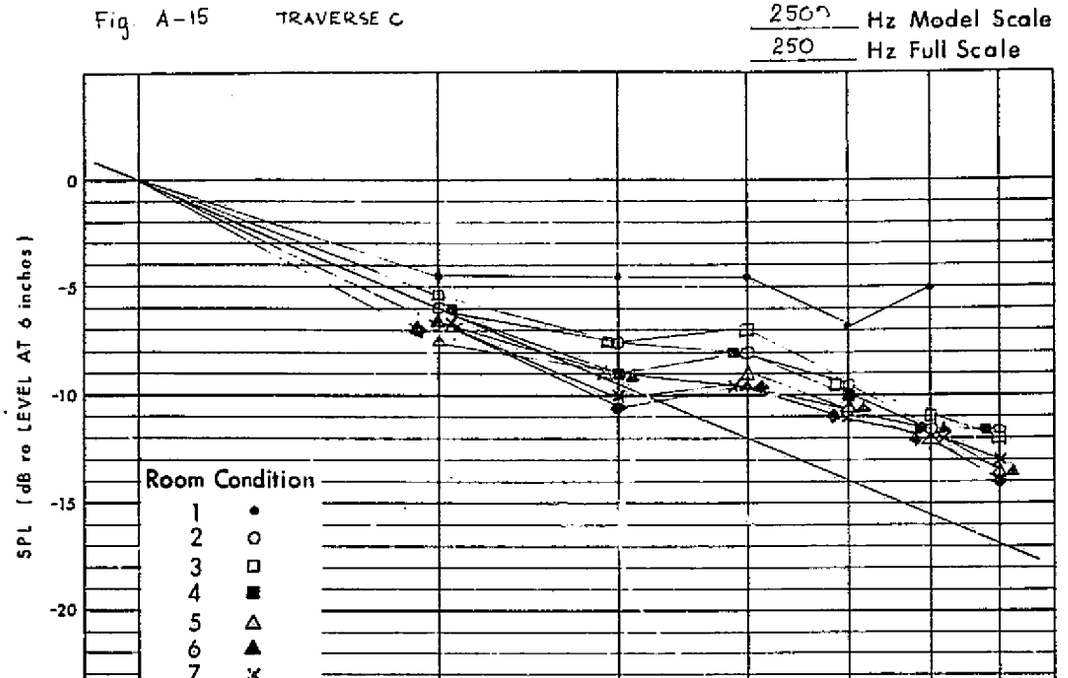

Fig A-16 TRAVERSE C

Source Position 1
5000 Hz Model Scale
500 Hz Full Scale

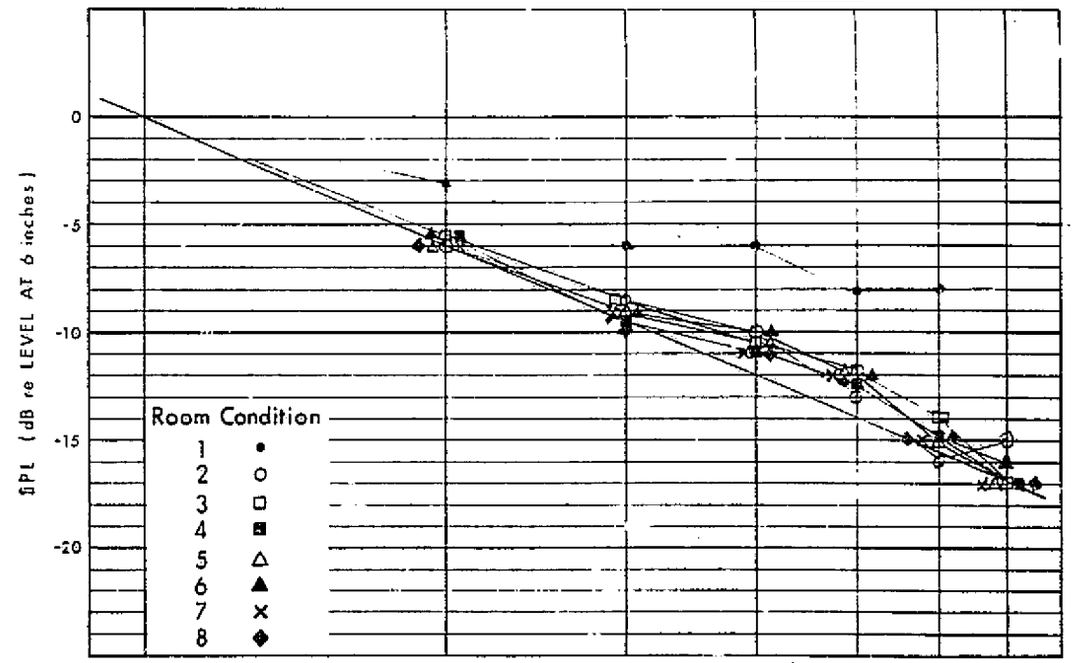

Fig. A-17 TRAVERSE C

Source Position 1
10,000 Hz Model Scale
1000 Hz Full Scale

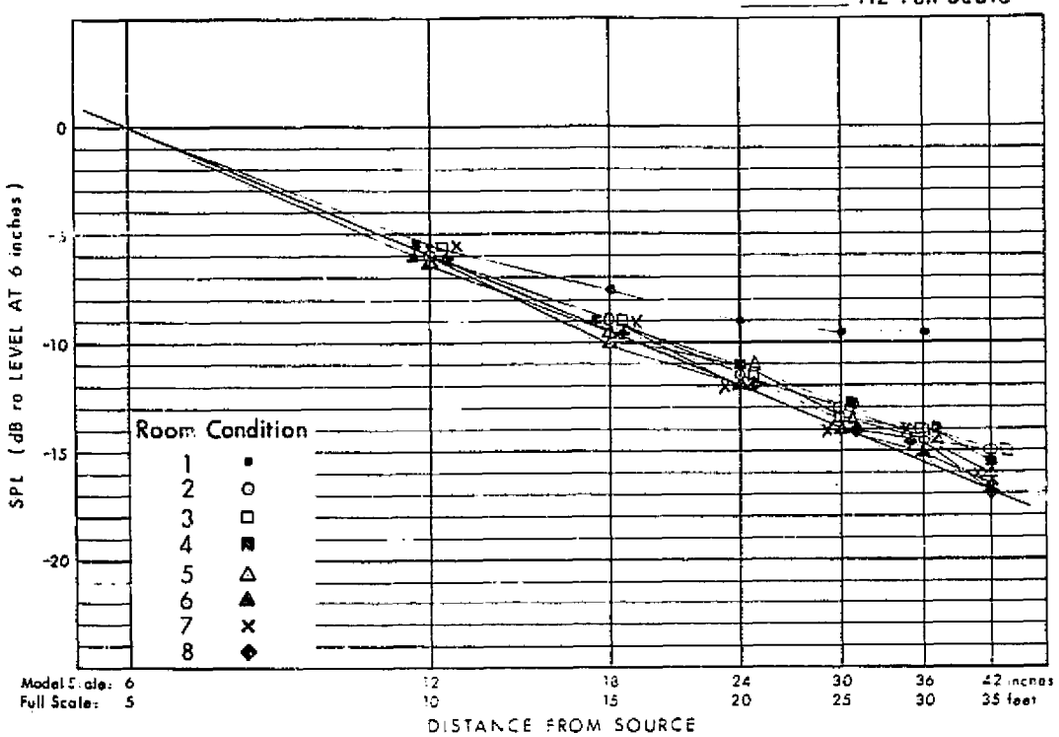

Fig. A-18 TRAVERSE C

Source Position 1
20,000 Hz Model Scale
2000 Hz Full Scale

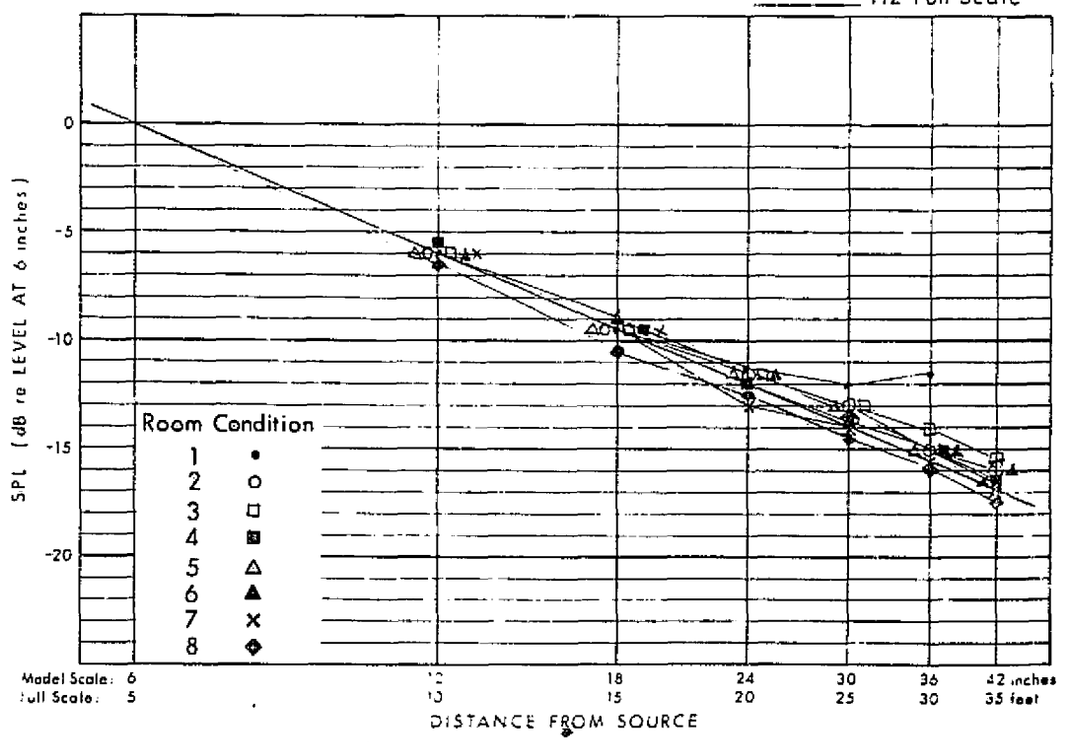

TRAVERSE D - 45° DOWNSTREAM TOWARD FAR WALL

Figure No.	Model-Scale Frequency, Hz
A-19	630
A-20	1250
A-21	2500
A-22	5000
A-23	10,000
A-24	20,000

Fig. A-19 TRAVERSE D

Source Position 1
630 Hz Model Scale
63 Hz Full Scale

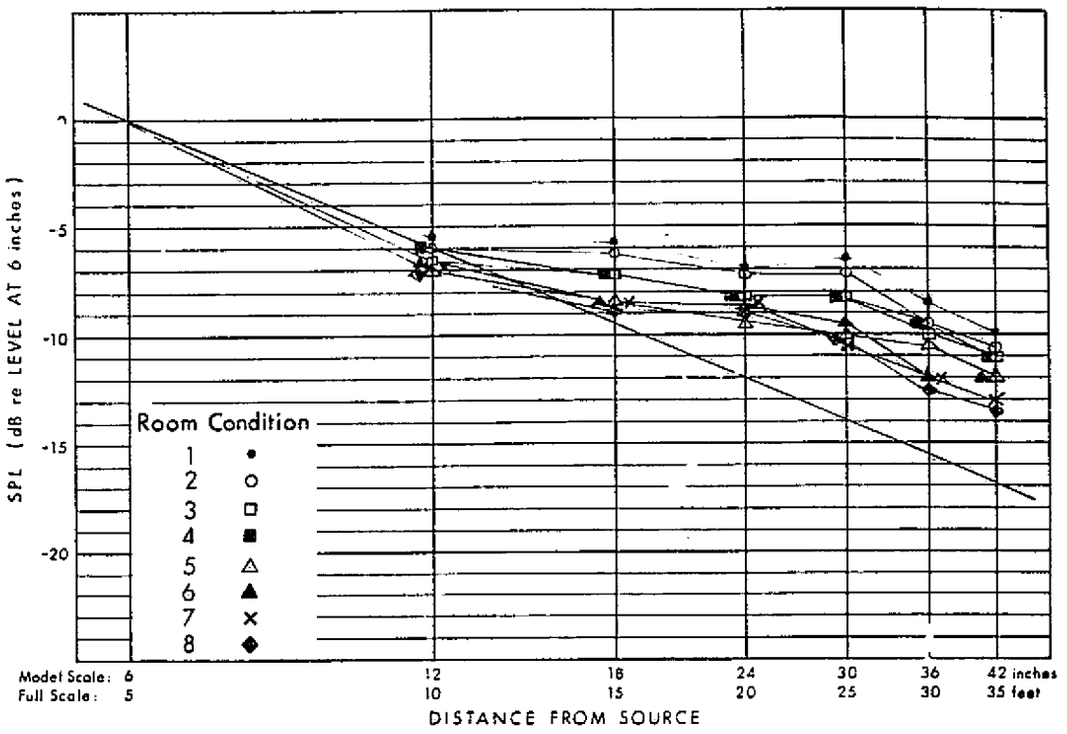

Fig. A-20 TRAVERSE D

Source Position 1
[illegible] Hz Model Scale
25 Hz Full Scale

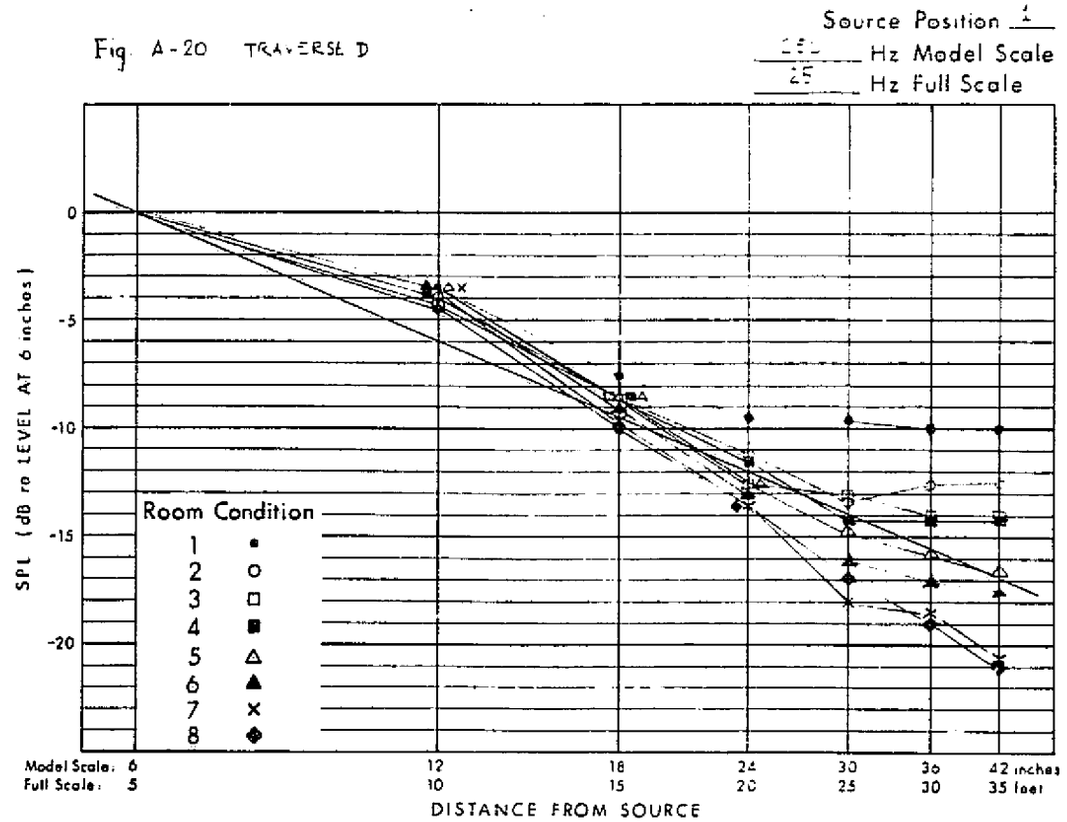

Fig A-21 TRAVERSE D

Source Position 1
2500 Hz Model Scale
250 Hz Full Scale

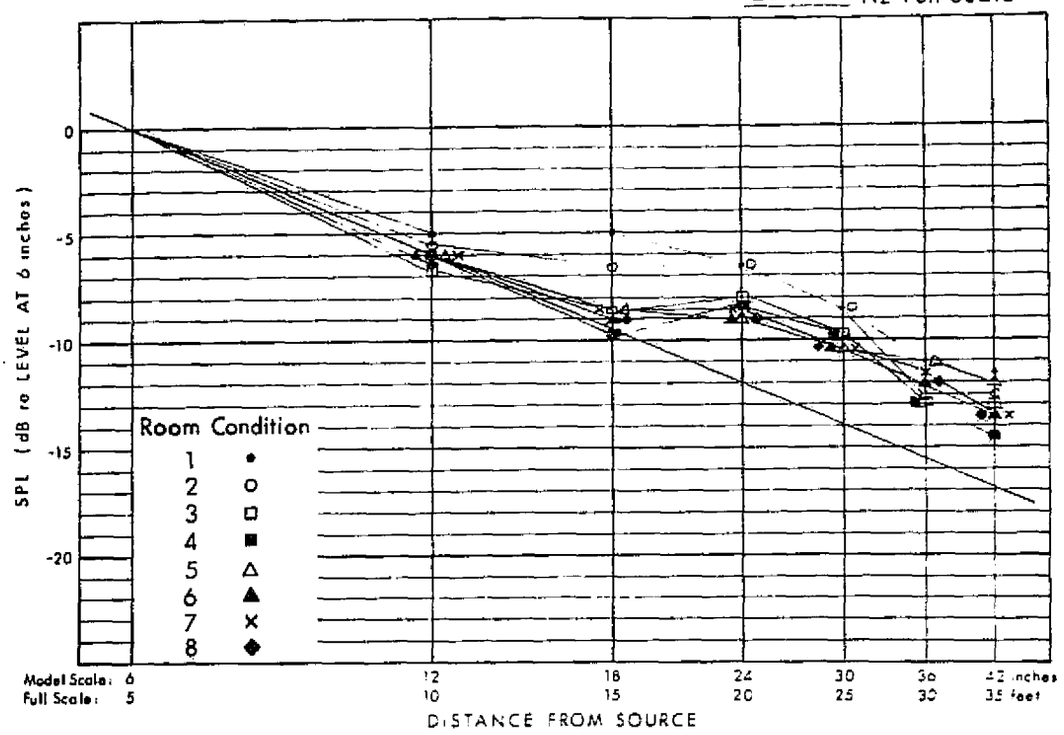

Fig A-22 TRAVERSE D

Source Position 1
5000 Hz Model Scale
500 Hz Full Scale

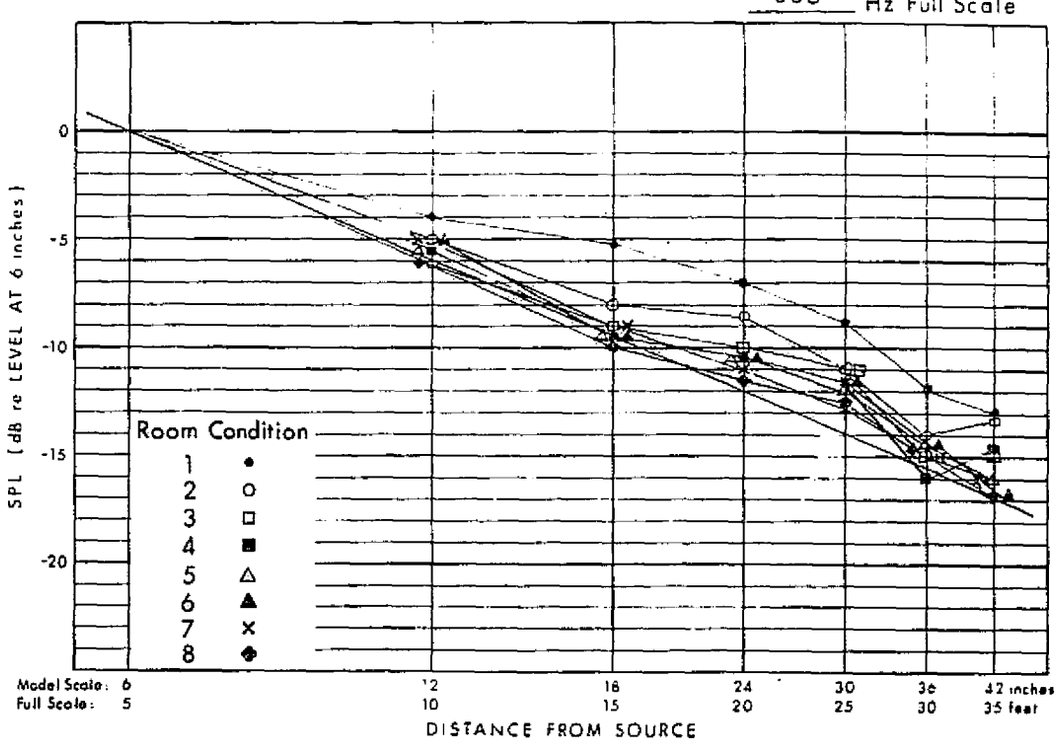

Fig. A-23 TRAVERSE D

Source Position 1
10,000 Hz Model Scale
1000 Hz Full Scale

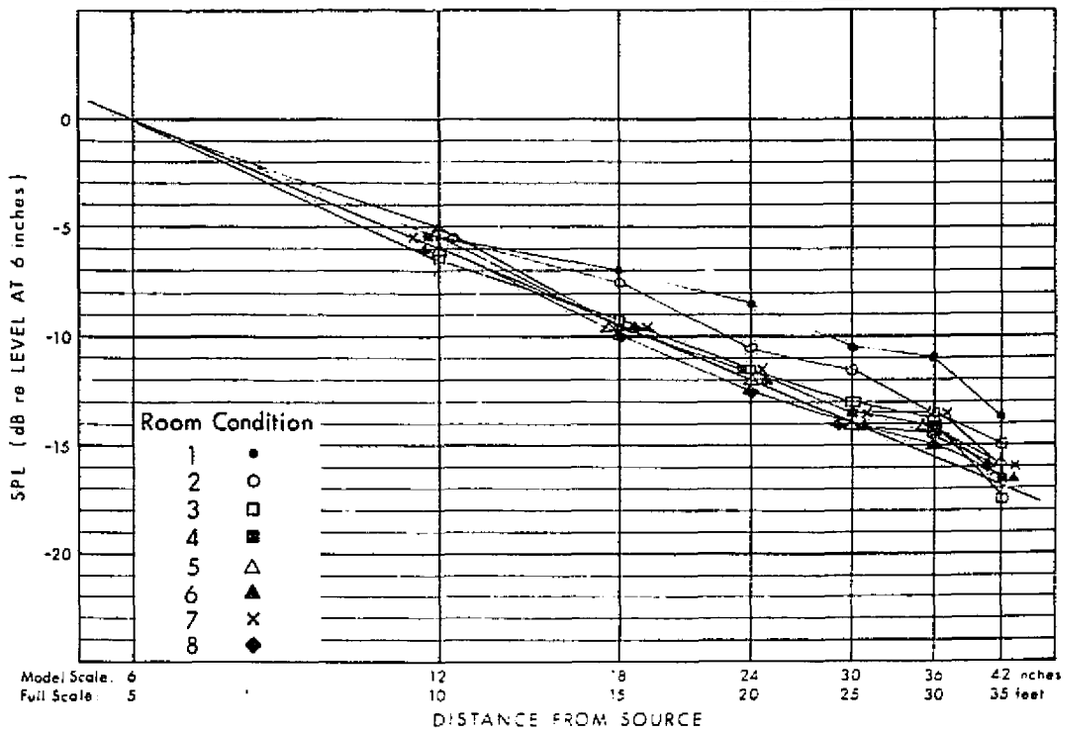

Fig A-24 TRAVERSE D

Source Position 1
20,000 Hz Model Scale
2000 Hz Full Scale

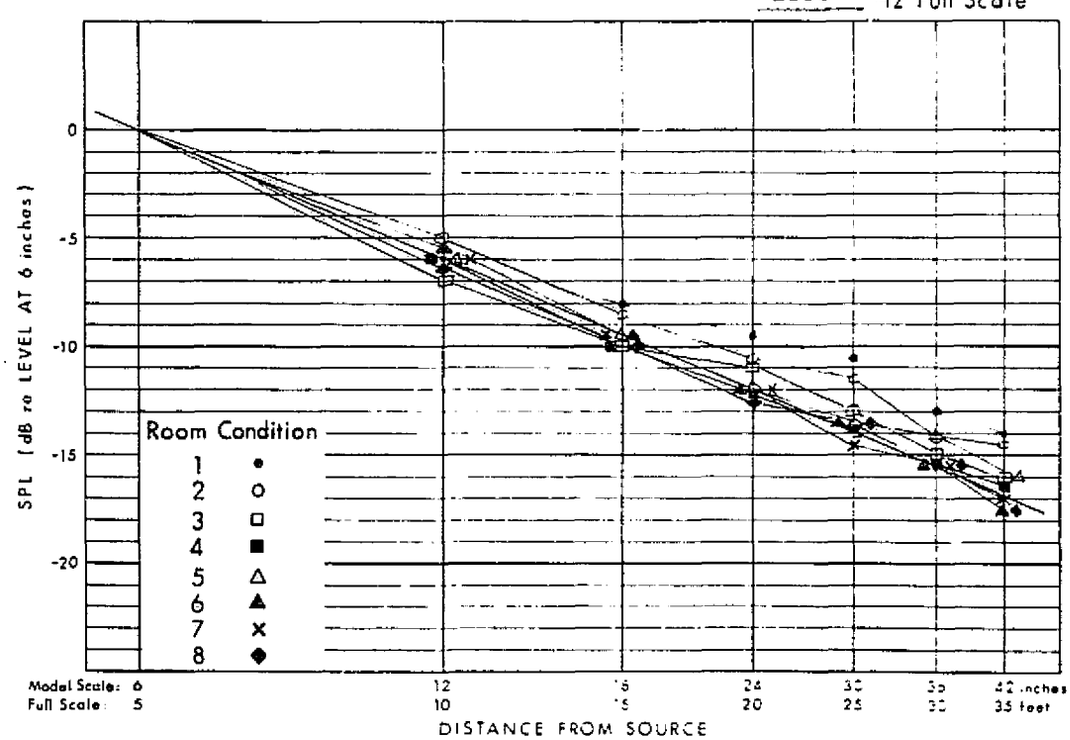

TRAVERSE E - 90° TOWARD FAR WALL

Figure No.	Model-Scale Frequency, Hz
A-25	630
A-26	1250
A-27	2500
A-28	5000
A-29	10,000
A-30	20,000

Fig. A-25 TRAVERSE E

Source Position 1
630 Hz Model Scale
630 Hz Full Scale

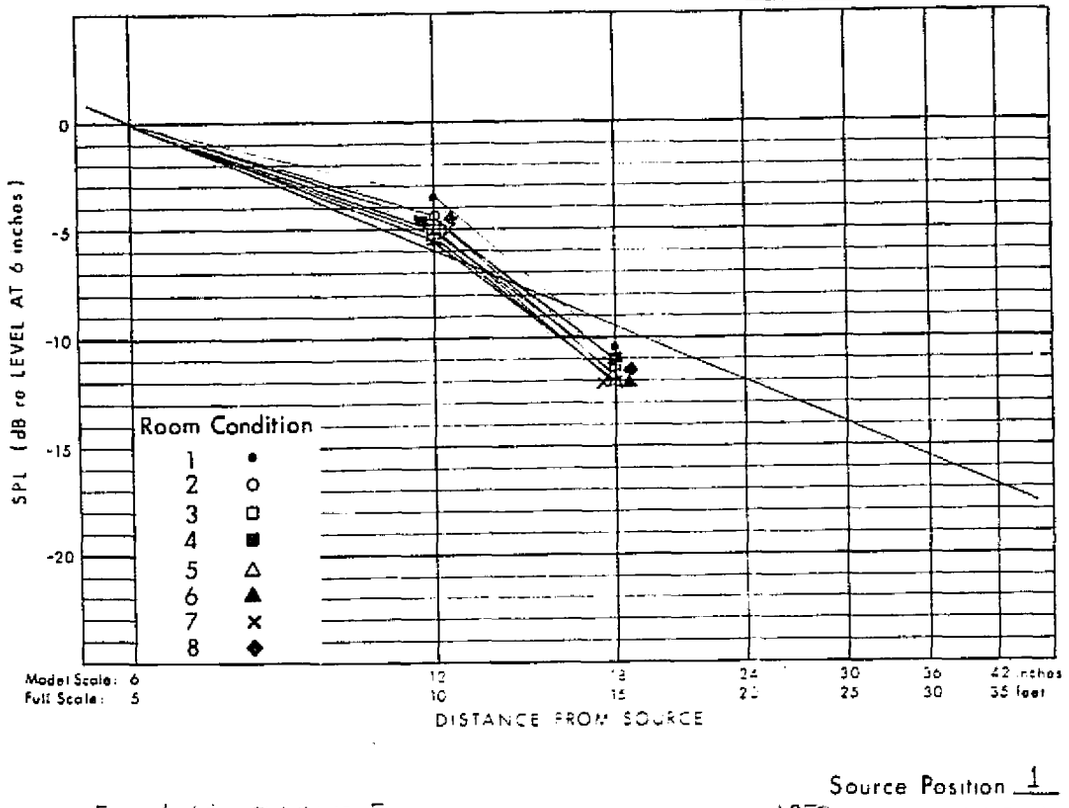

Fig. A-26 TRAVERSE E

Source Position 1
1250 Hz Model Scale
25 Hz Full Scale

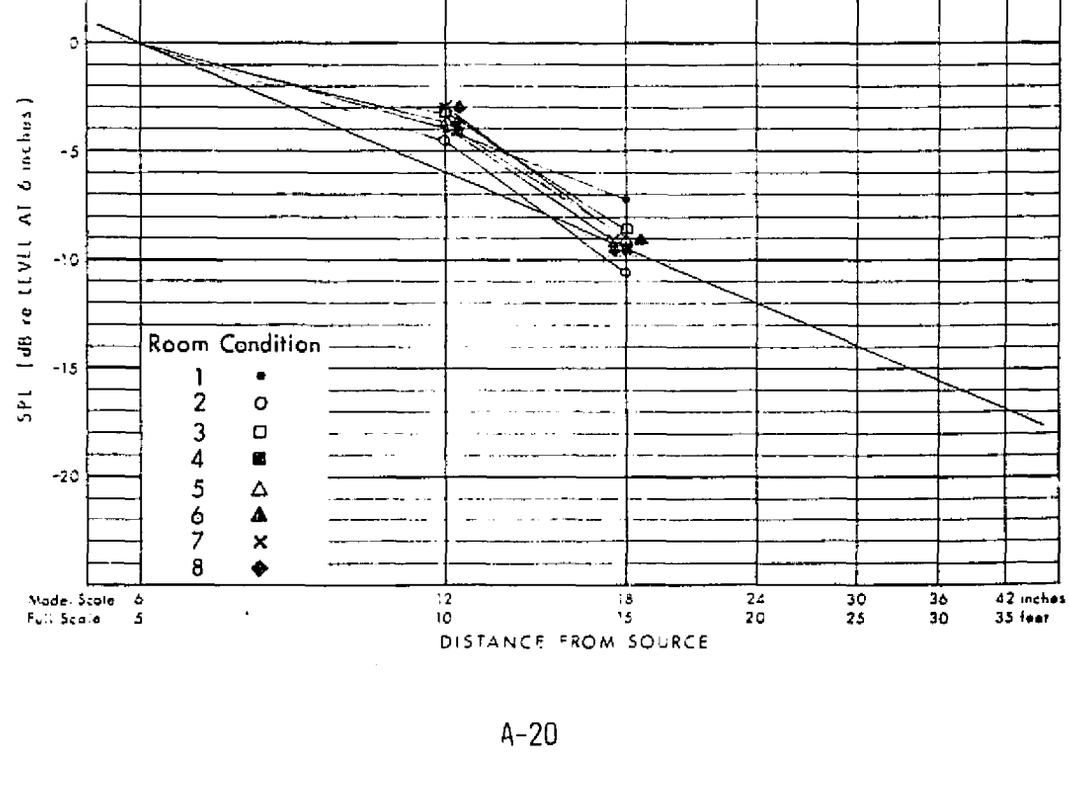

Fig. A-27 TRAVERSE E

Source Position 1
2500 Hz Model Scale
250 Hz Full Scale

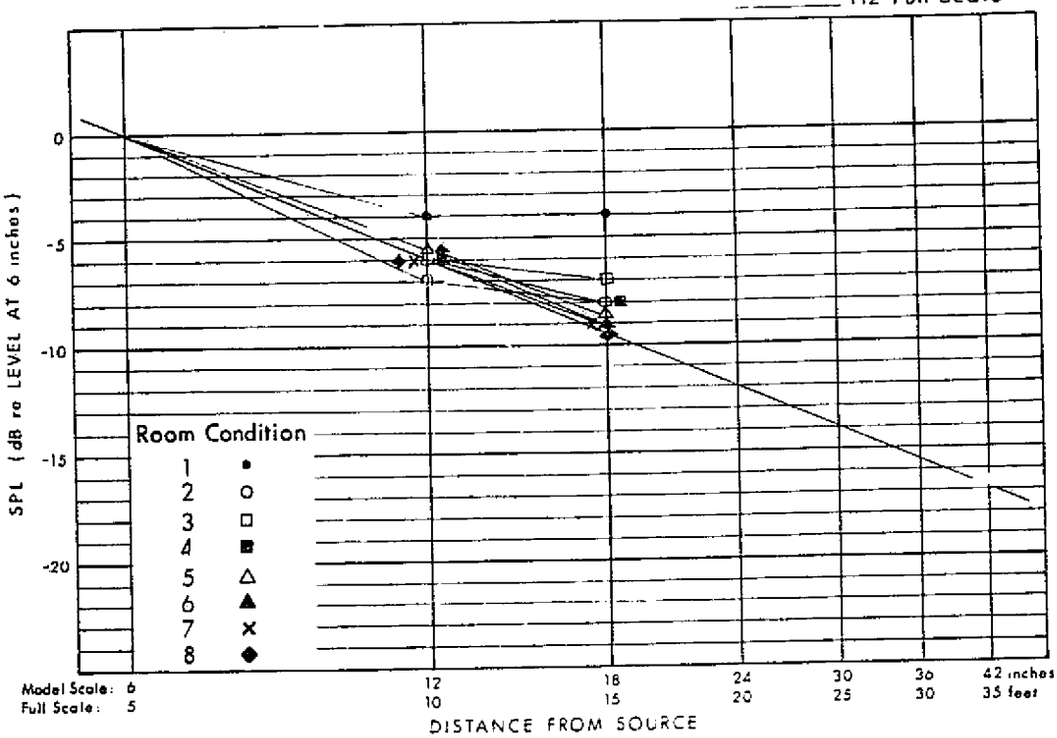

Source Position 1
5000 Hz Model Scale
500 Hz Full Scale

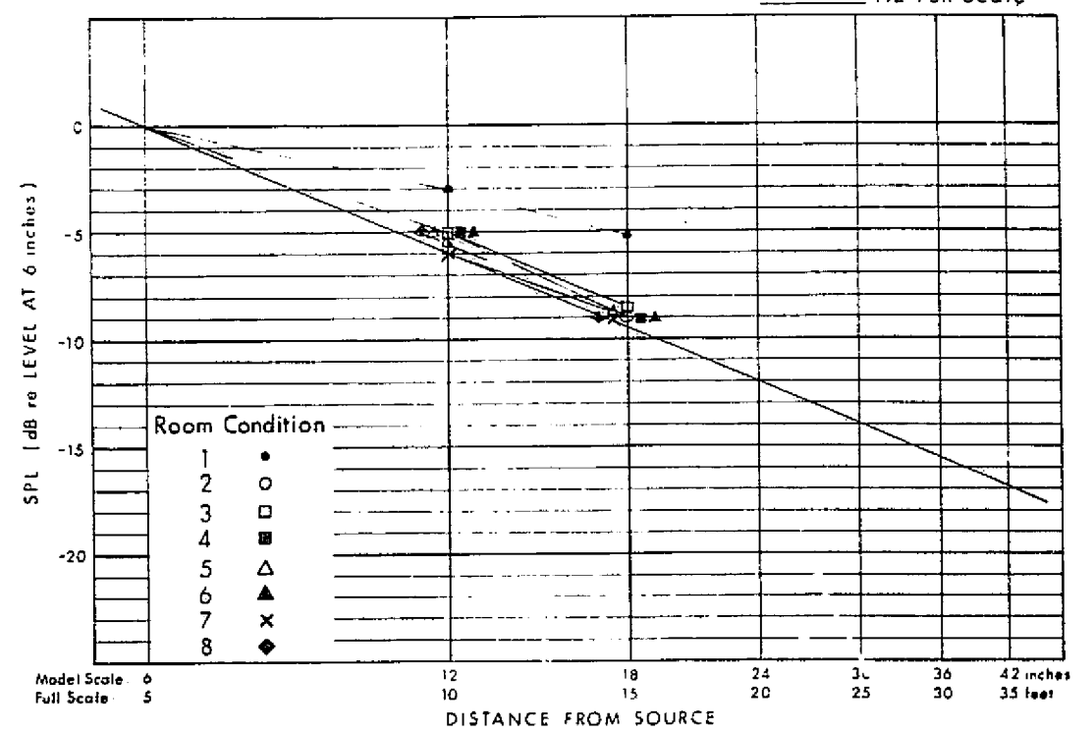

Fig. A-29 TRAVERSE E

Source Position 1
10,000 Hz Model Scale
1000 Hz Full Scale

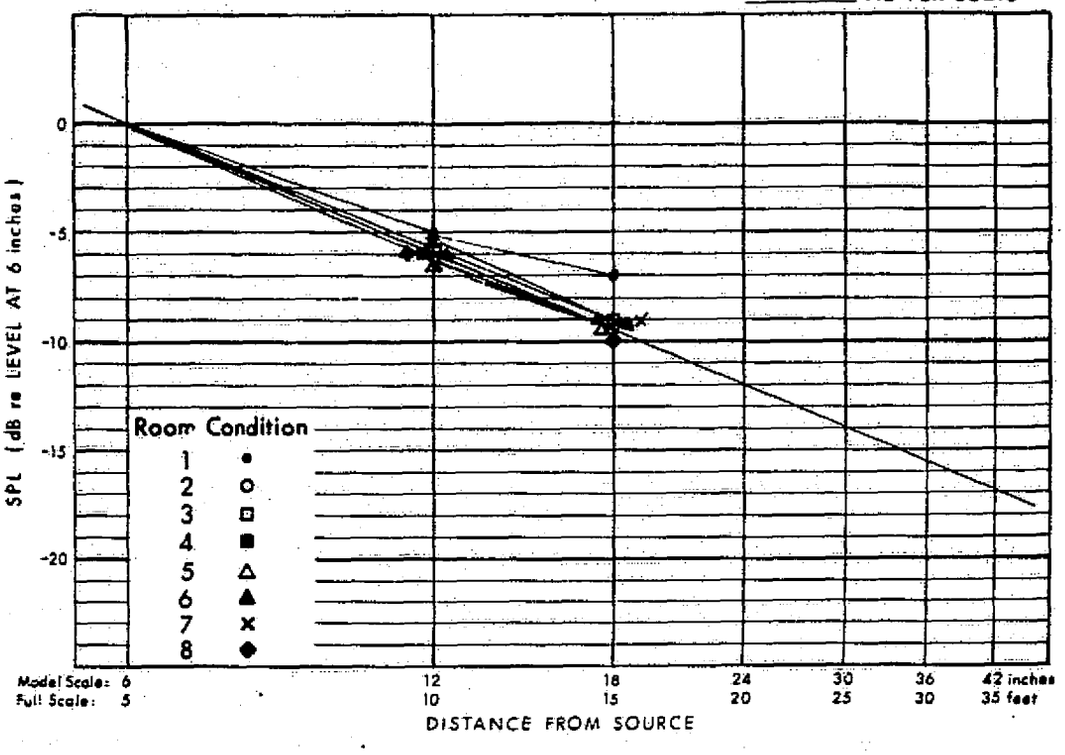

Fig. A-30 TRAVERSE E

Source Position 1
20,000 Hz Model Scale
2000 Hz Full Scale

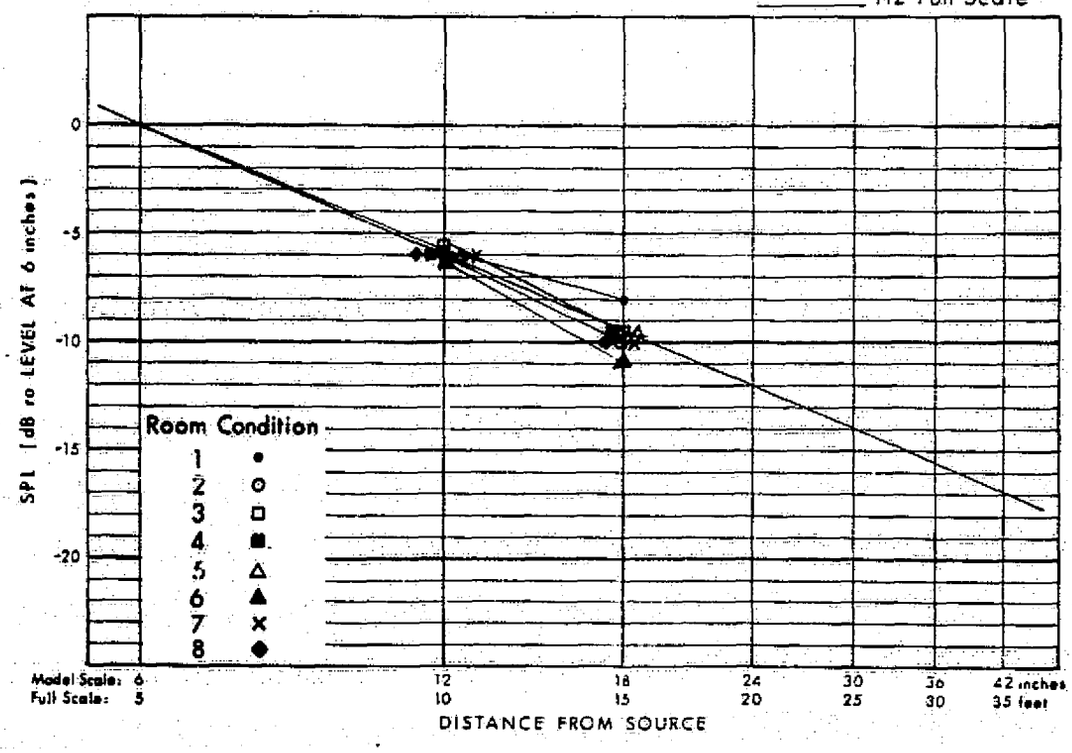

TRAVERSE F - STRAIGHT UPWARDS

Figure No.	Model-Scale Frequency, Hz
A-31	630
A-32	1250
A-33	2500
A-34	5000
A-35	10,000
A-36	20,000

Fig. A-31 TRAVERSE F

Source Position 1
630 Hz Model Scale
63 Hz Full Scale

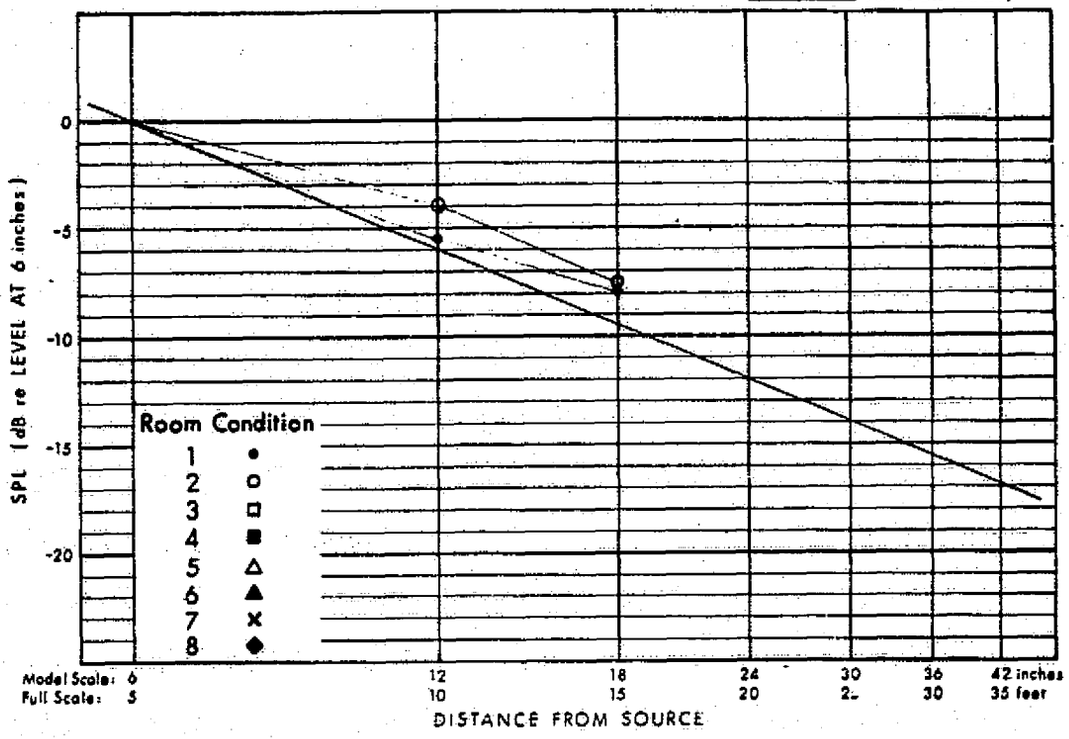

Fig. A-32 TRAVERSE F

Source Position 1
1250 Hz Model Scale
125 Hz Full Scale

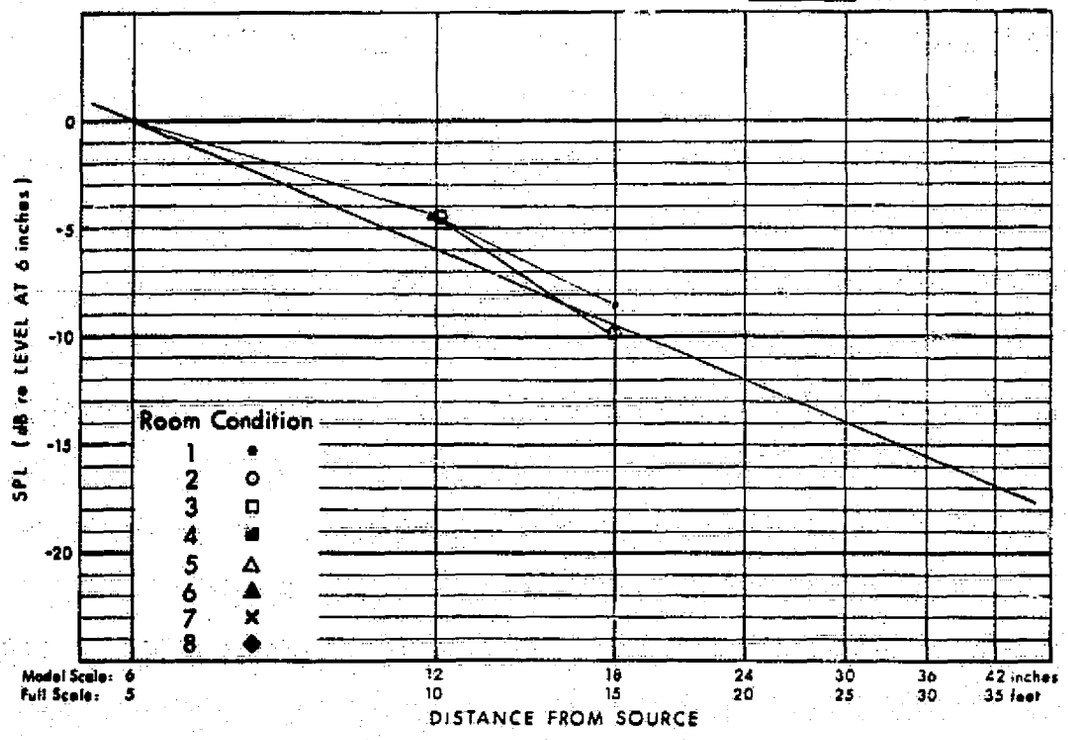

Fig. A-33 TRAVERSE F

Source Position 1
2500 Hz Model Scale
250 Hz Full Scale

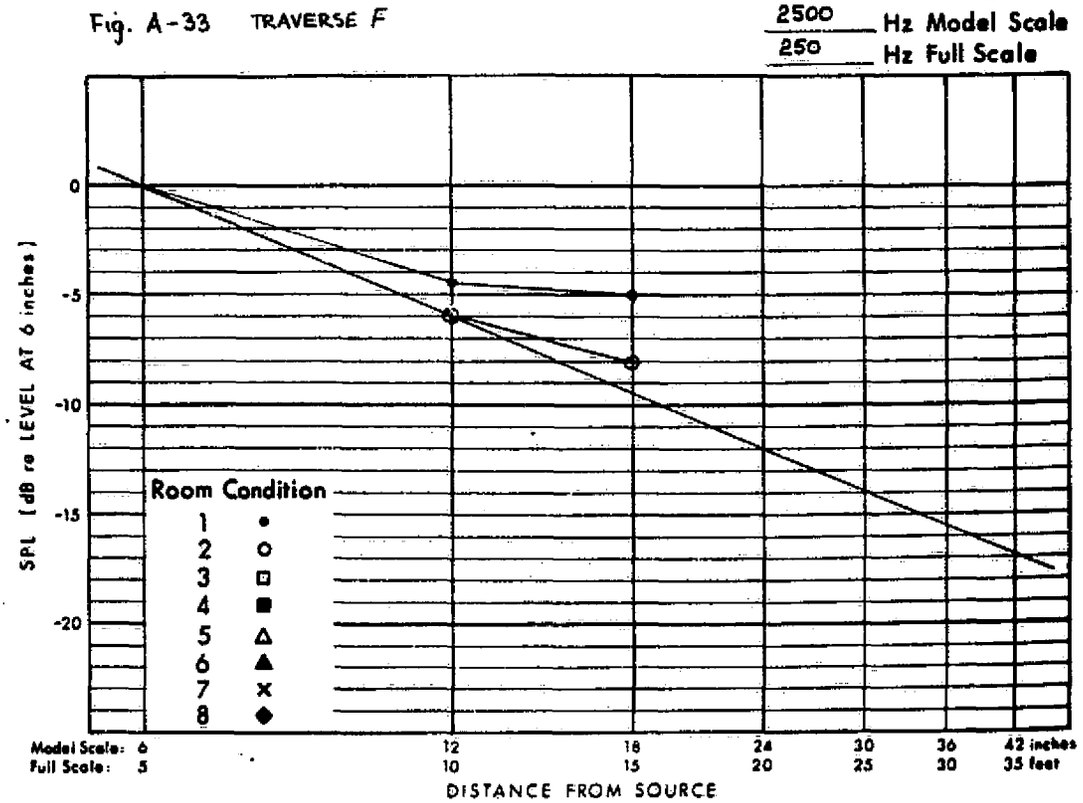

Fig A-34 TRAVERSE F

Source Position 1
5000 Hz Model Scale
500 Hz Full Scale

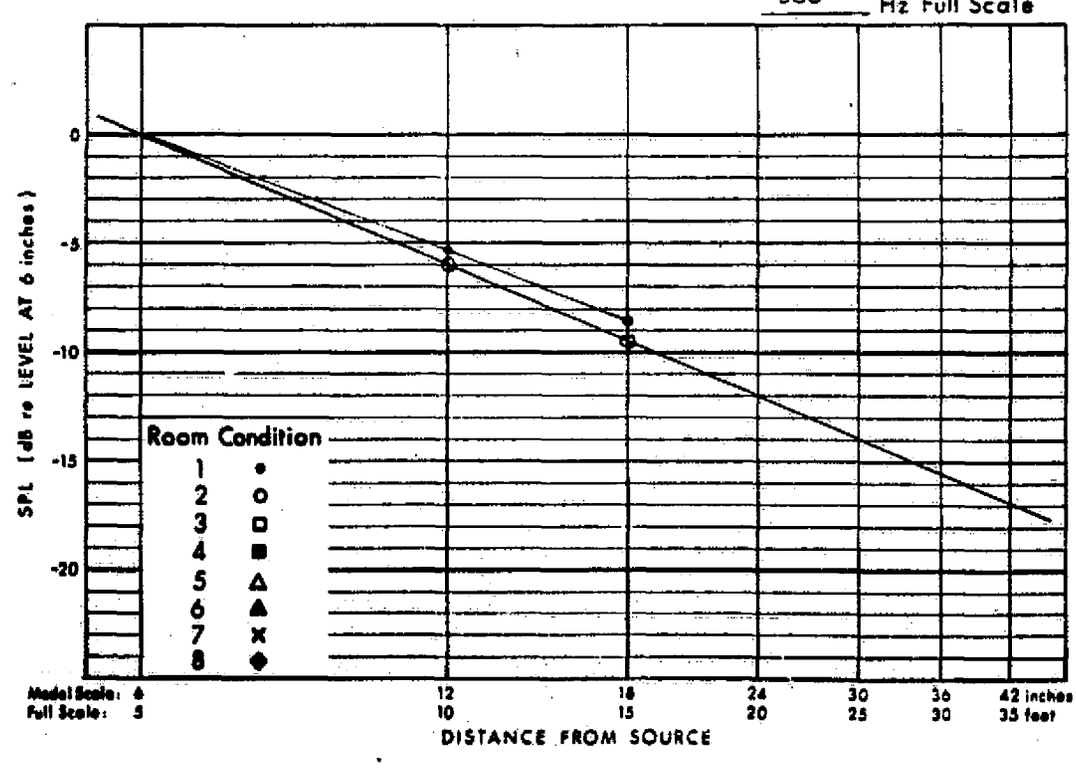

C.2

Fig. A-35 TRAVERSE F

Source Position 1
10,000 Hz Model Scale
1000 Hz Full Scale.

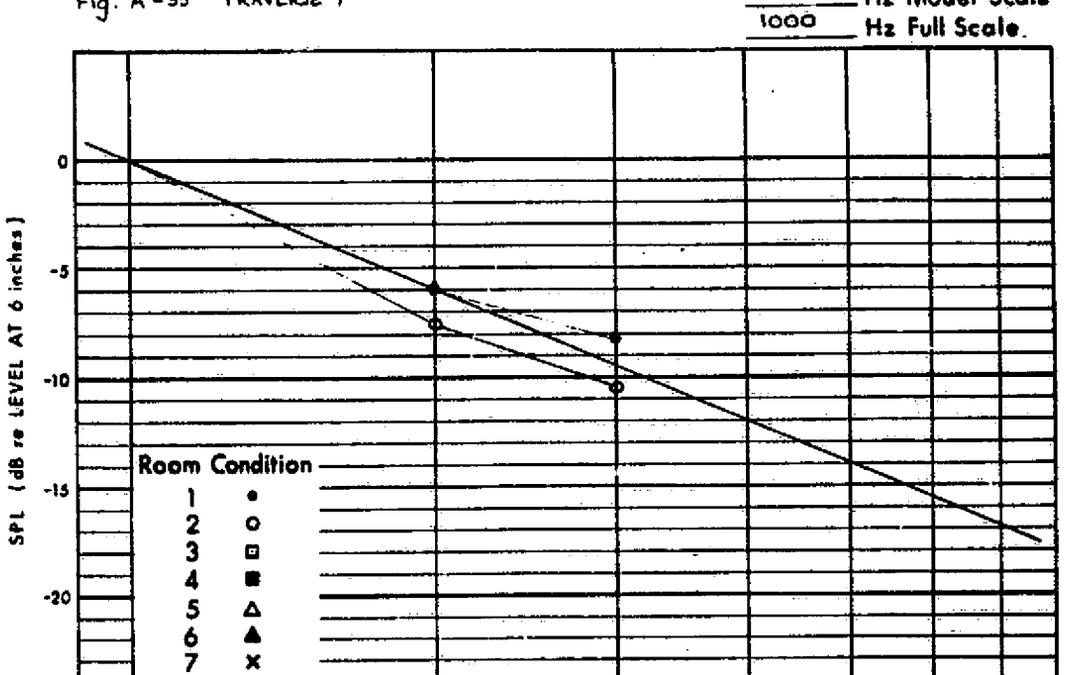

Fig. A-36 TRAVERSE F

Source Position 1
20,000 Hz Model Scale
2000 Hz Full Scale

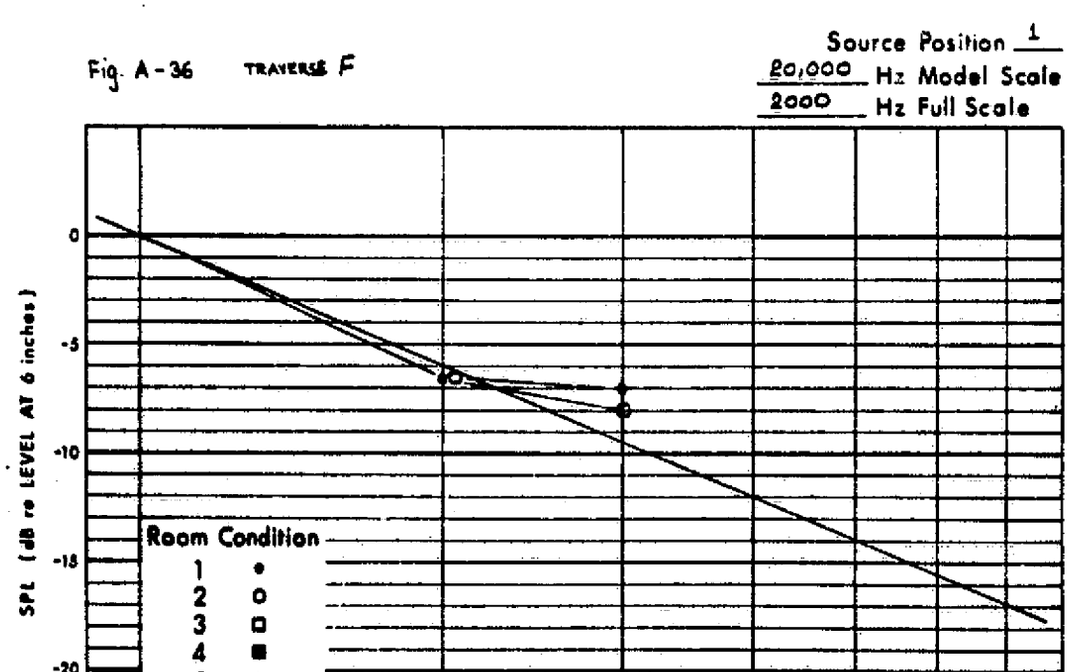

SOURCE POSITION 2

TRAVERSE A' - UPSTREAM

Figure No.	Model-Scale Frequency, Hz
A-37	630
A-38	1250
A-39	2500
A-40	5000
A-41	10,000
A-42	20,000

Fig. A-37 TRAVERSE A'

Source Position 2
630 Hz Model Scale
63 Hz Full Scale

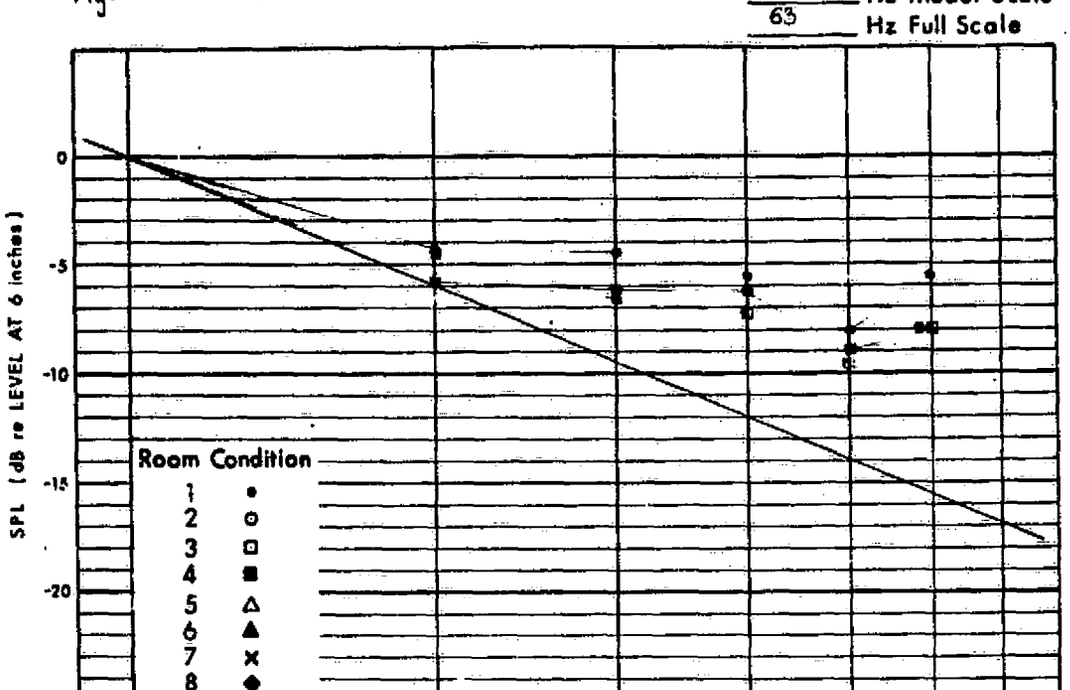

Fig. A-38 TRAVERSE A'

Source Position 2
1250 Hz Model Scale
125 Hz Full Scale

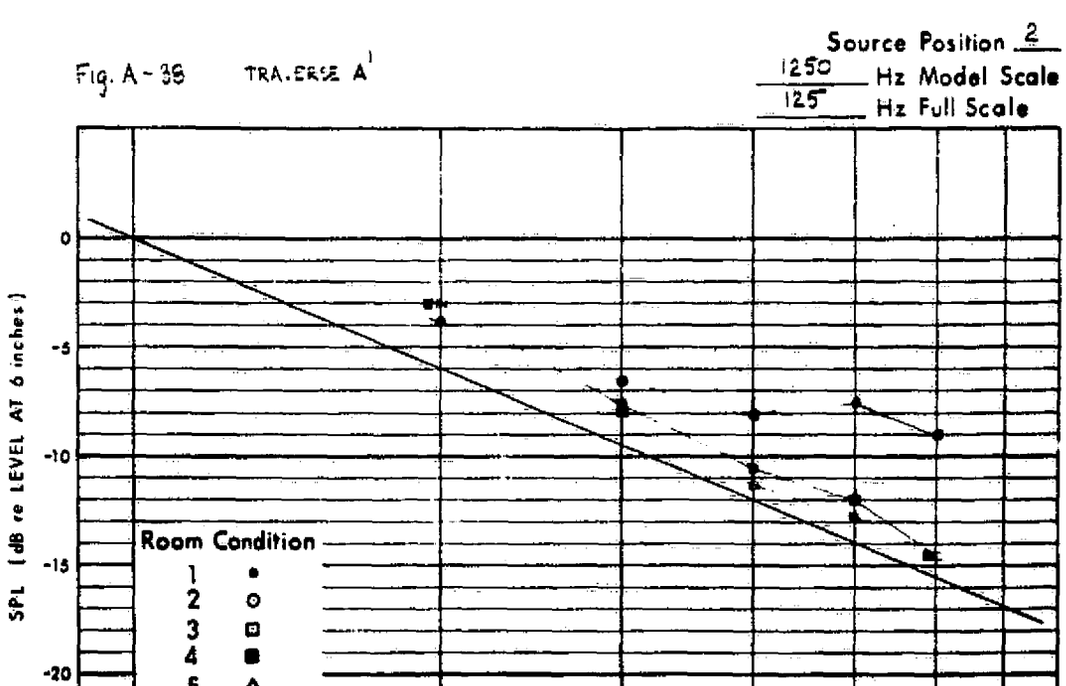

Fig. A-39 TRAVERSE A'

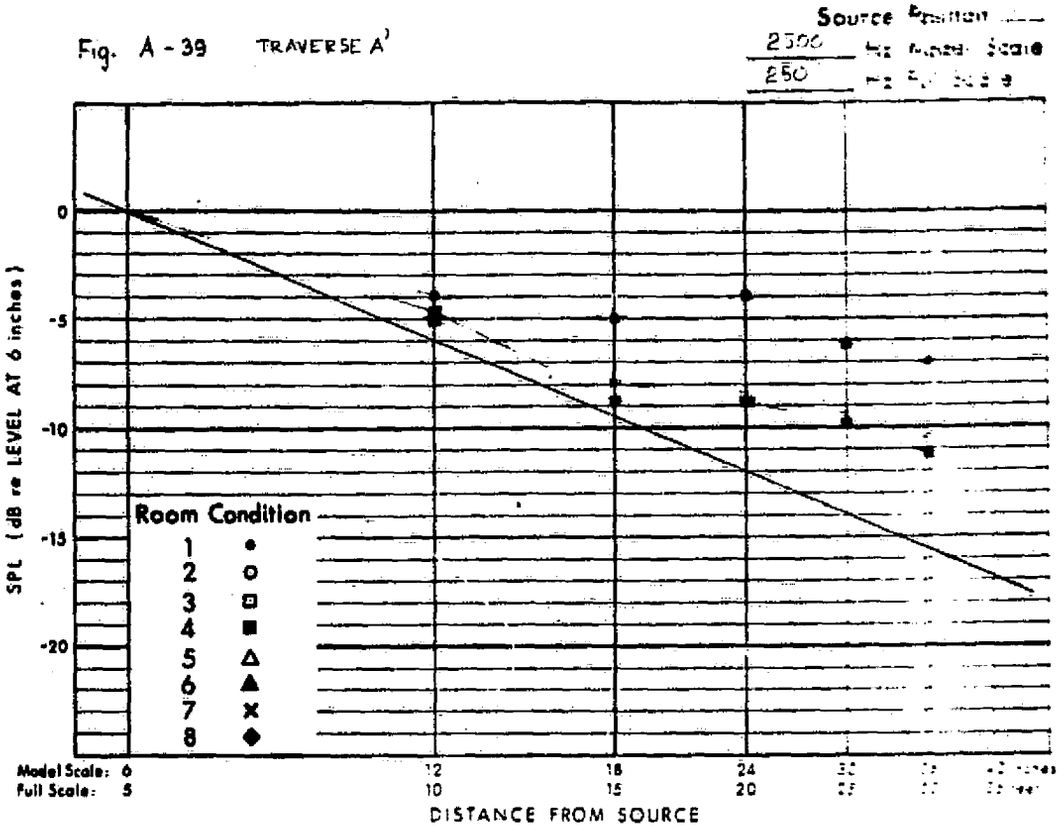

Fig. A-40 TRAVERSE A'

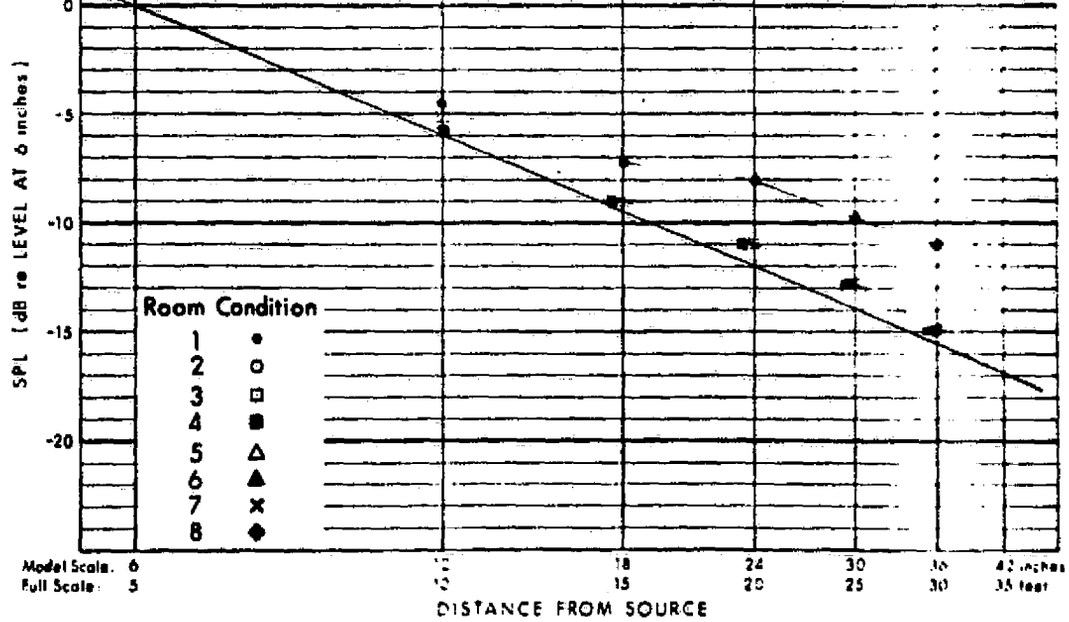

Fig. A-41 TRAVERSE A'

Source Position 2
10,000 Hz Model Scale
1000 Hz Full Scale

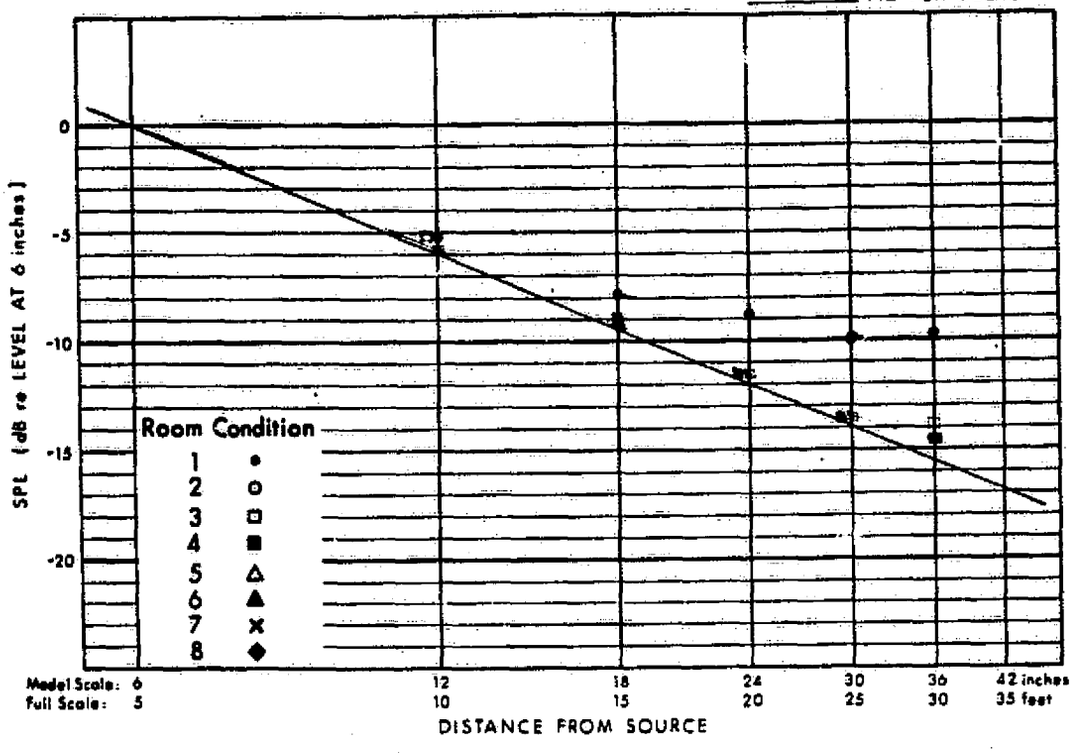

Fig. A-42 TRAVERSE A'

Source Position 2
20,000 Hz Model Scale
2000 Hz Full Scale

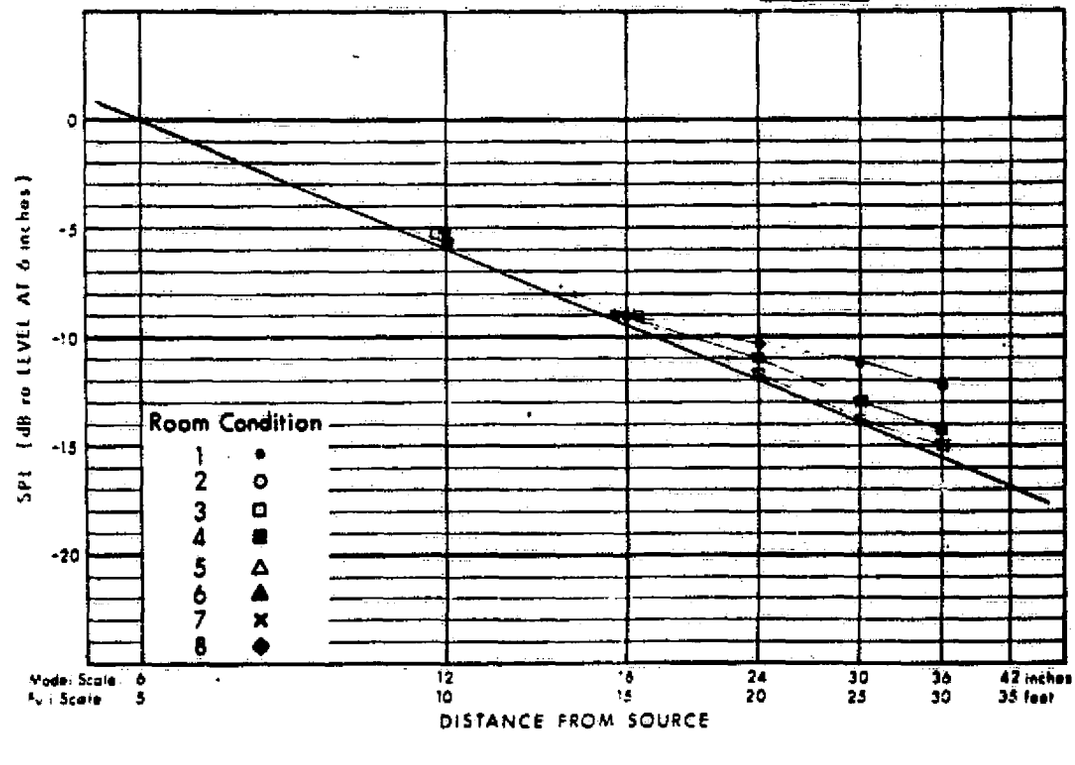

TRAVERSE C' - DOWNSTREAM

Figure No.	Model-Scale Frequency, Hz
A-43	630
A-44	1250
A-45	2500
A-46	5000
A-47	10,000
A-48	20,000

Fig. A-43 TRAVERSE 1

Source Position 1
630 Hz Model Scale
63 Hz Full Scale

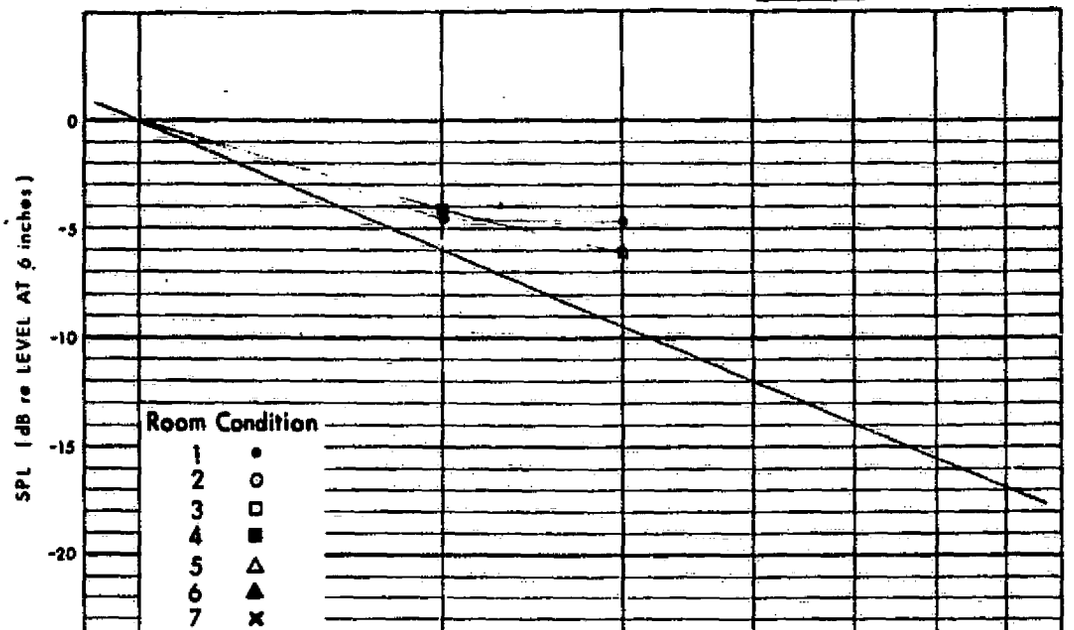

Fig. A-44 TRAVERSE 2

Source Position 2
1250 Hz Model Scale
125 Hz Full Scale

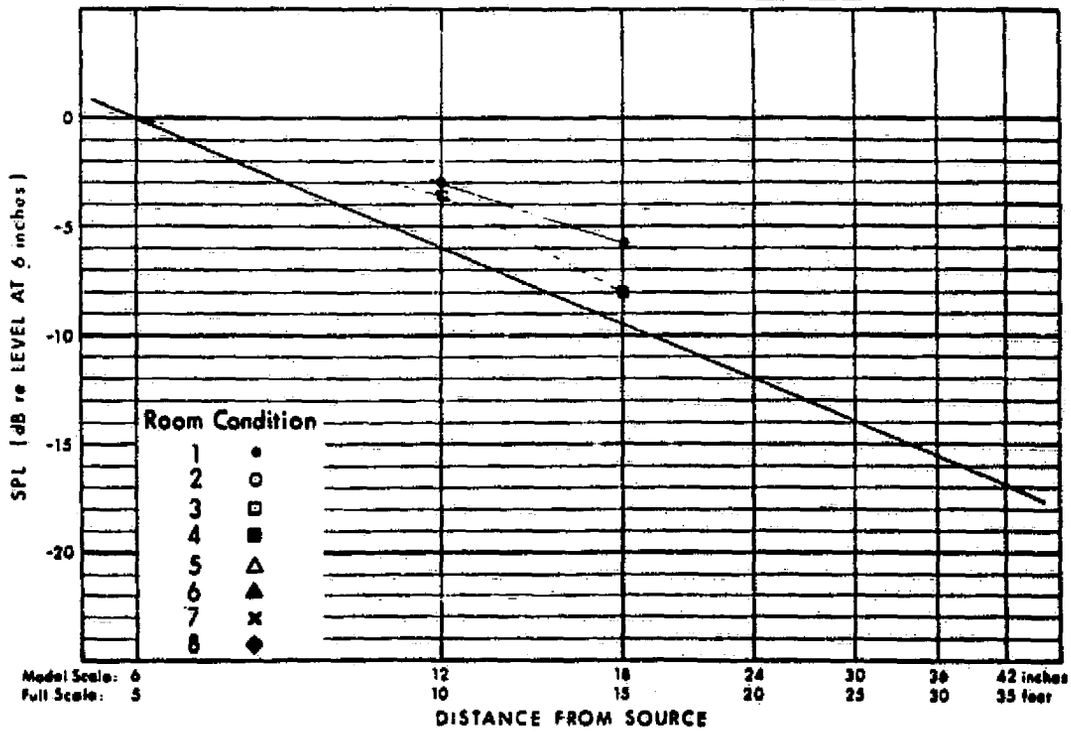

Fig. A-45 TRAVERSE c'

Source Position 2
2500 Hz Model Scale
250 Hz Full Scale

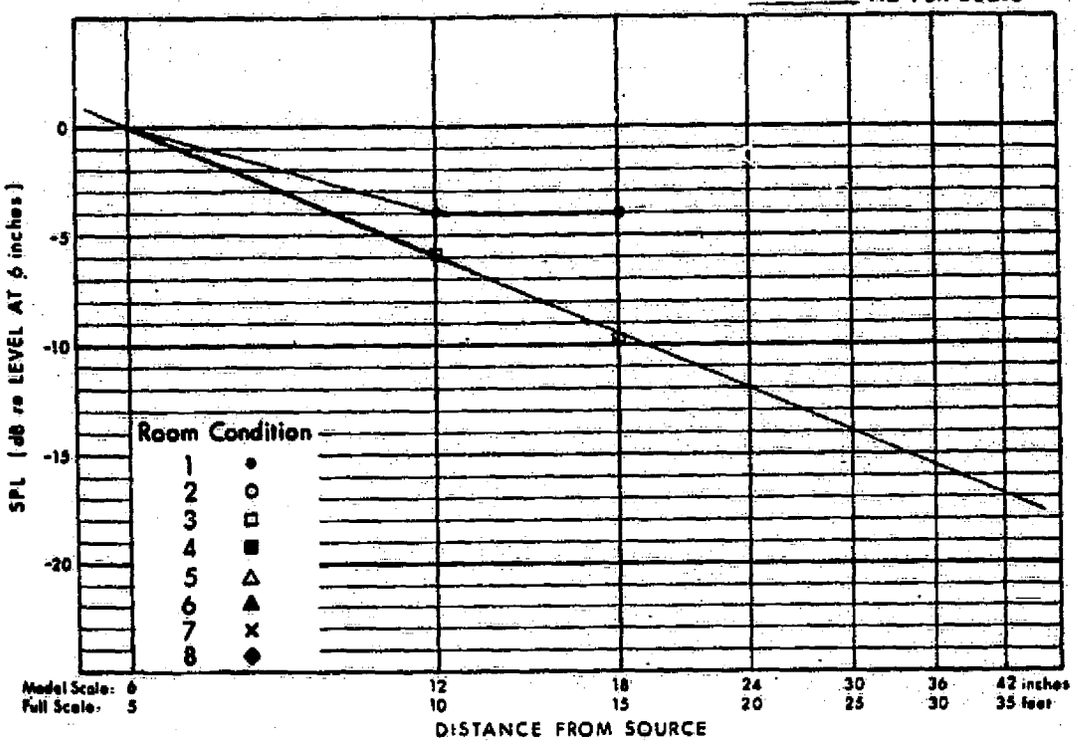

Fig. A-46 TRAVERSE c'

Source Position 2
5000 Hz Model Scale
500 Hz Full Scale

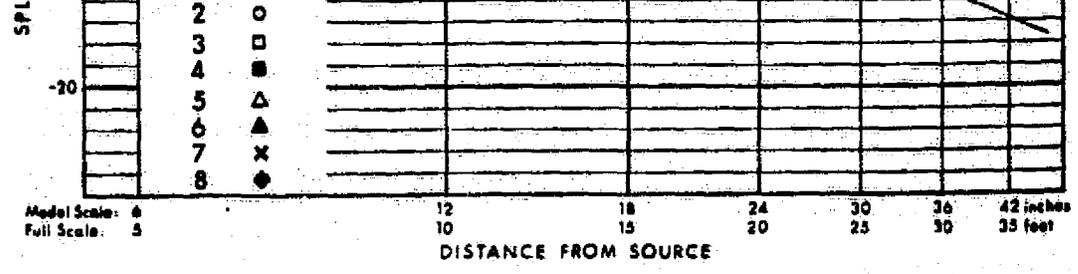

Fig. A-47 TRANSVERSE

Source Position 2
10,000 Hz Model Scale
1000 Hz Full Scale

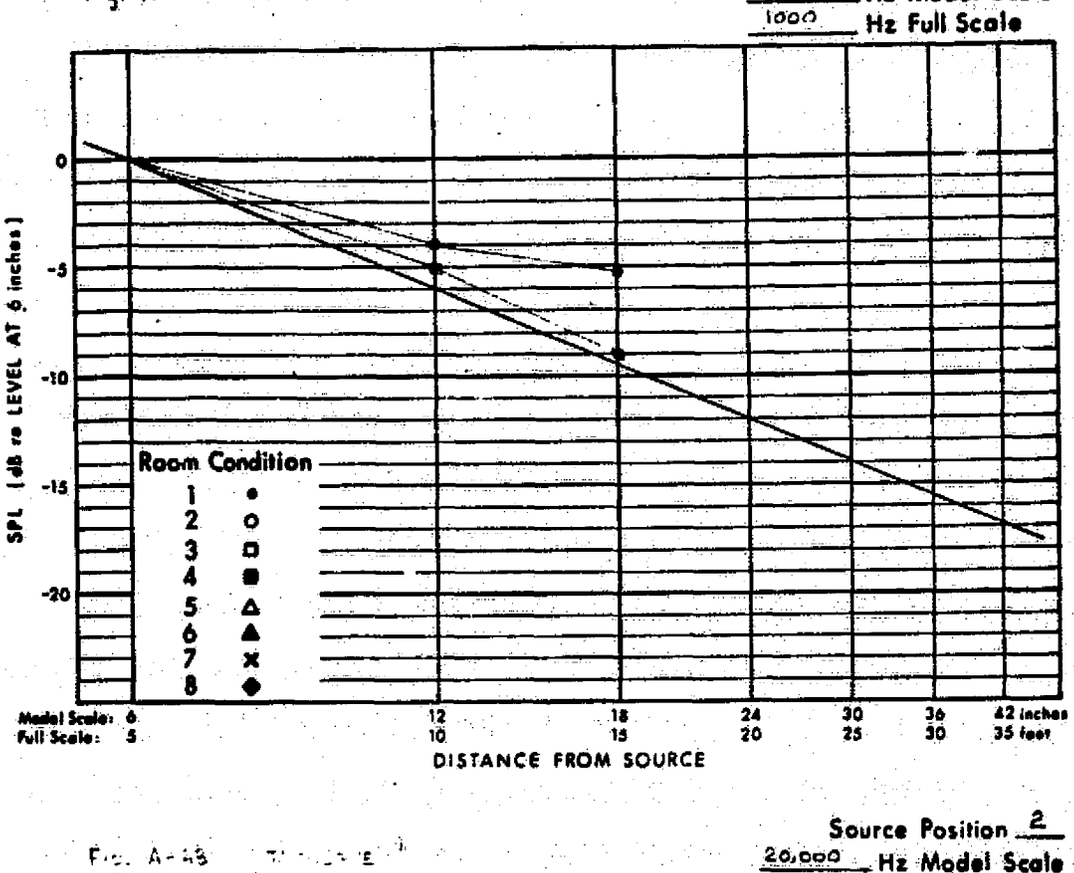

Fig. A-48 TRANSVERSE

Source Position 2
20,000 Hz Model Scale
2000 Hz Full Scale

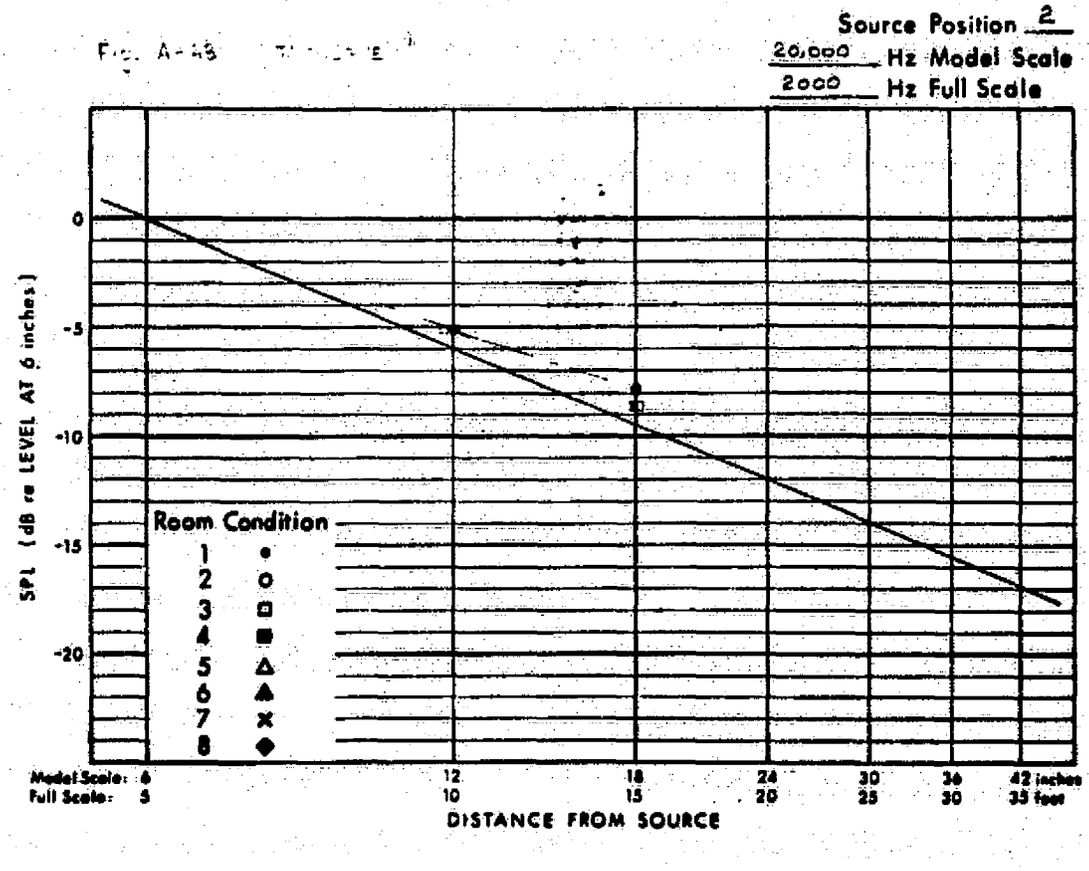

TRAVERSE E' - 90° TOWARD FAR WALL

Figure No.	Model-Scale Frequency, Hz
A-49	630
A-50	1250
A-51	2500
A-52	5000
A-53	10,000
A-54	20,000

Fig. A-49 TRAVERSE E'

Source Position 2
630 Hz Model Scale
63 Hz Full Scale

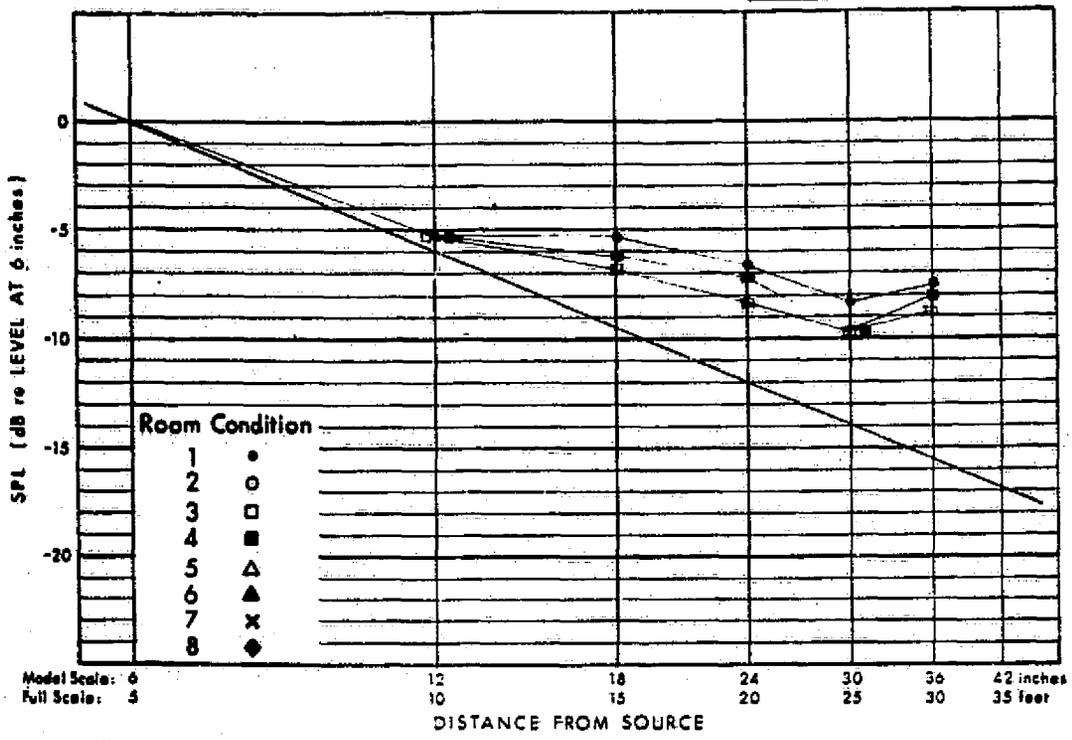

Fig. A-50 TRAVERSE E'

Source Position 2
1250 Hz Model Scale
125 Hz Full Scale

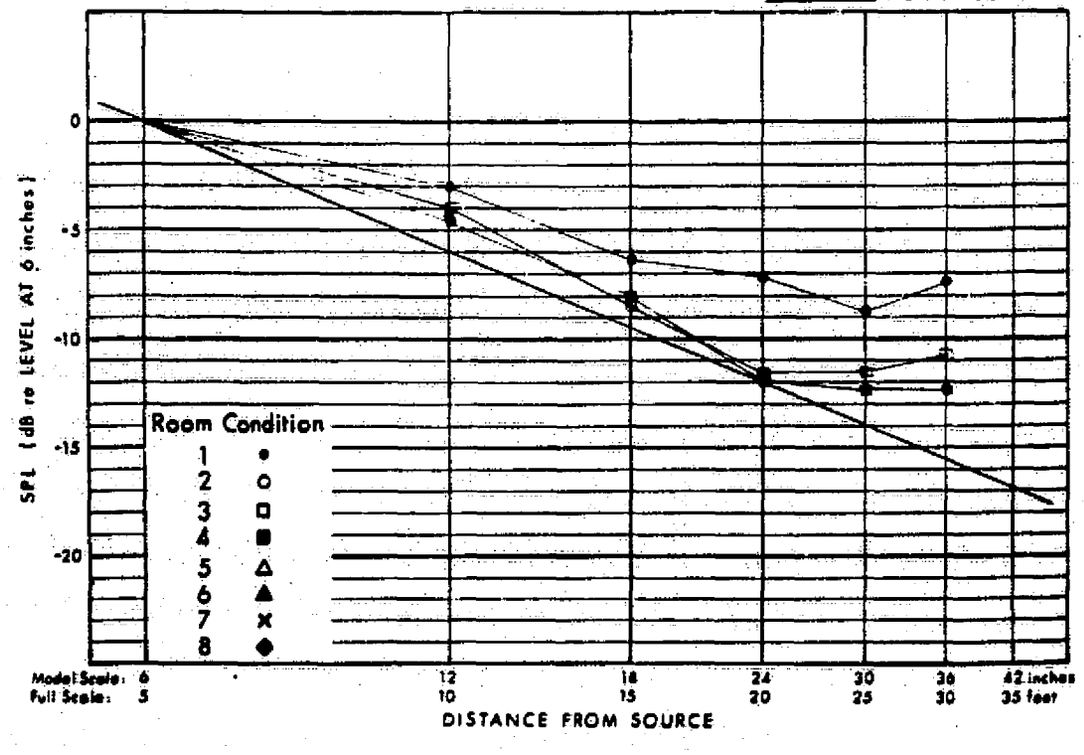

Fig. A-51 TRAVERSE E'

Source Position 3
2500 Hz Model Scale
250 Hz Full Scale

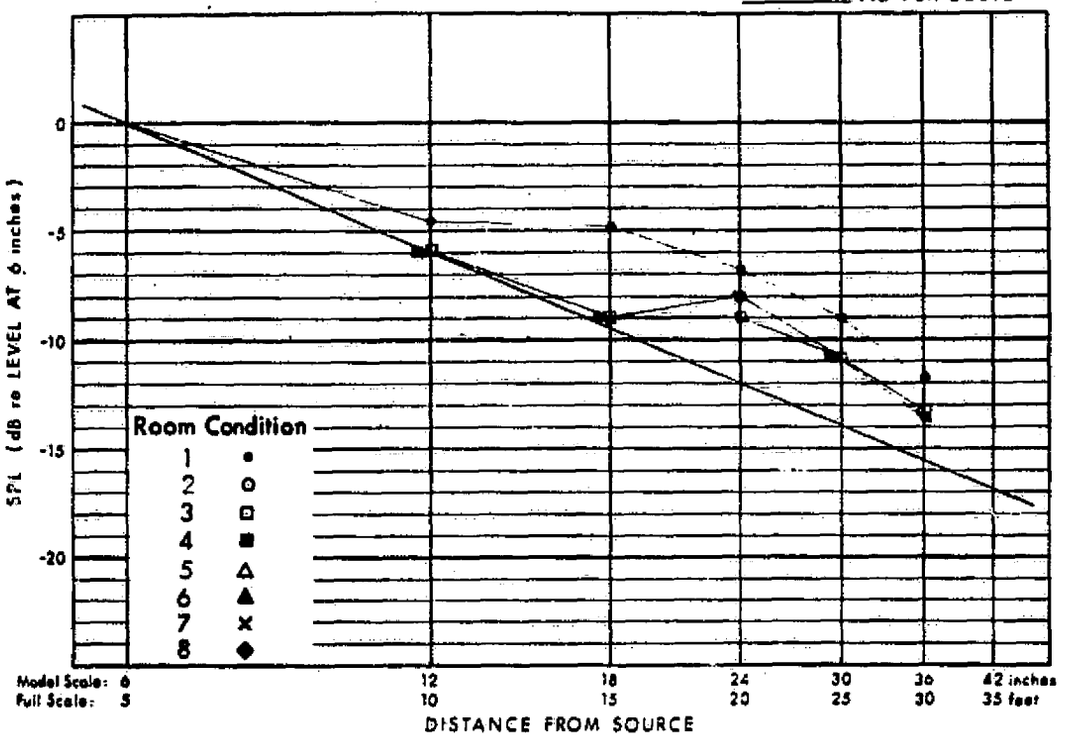

Fig. A-52 TRAVERSE E'

Source Position 2
5000 Hz Model Scale
500 Hz Full Scale

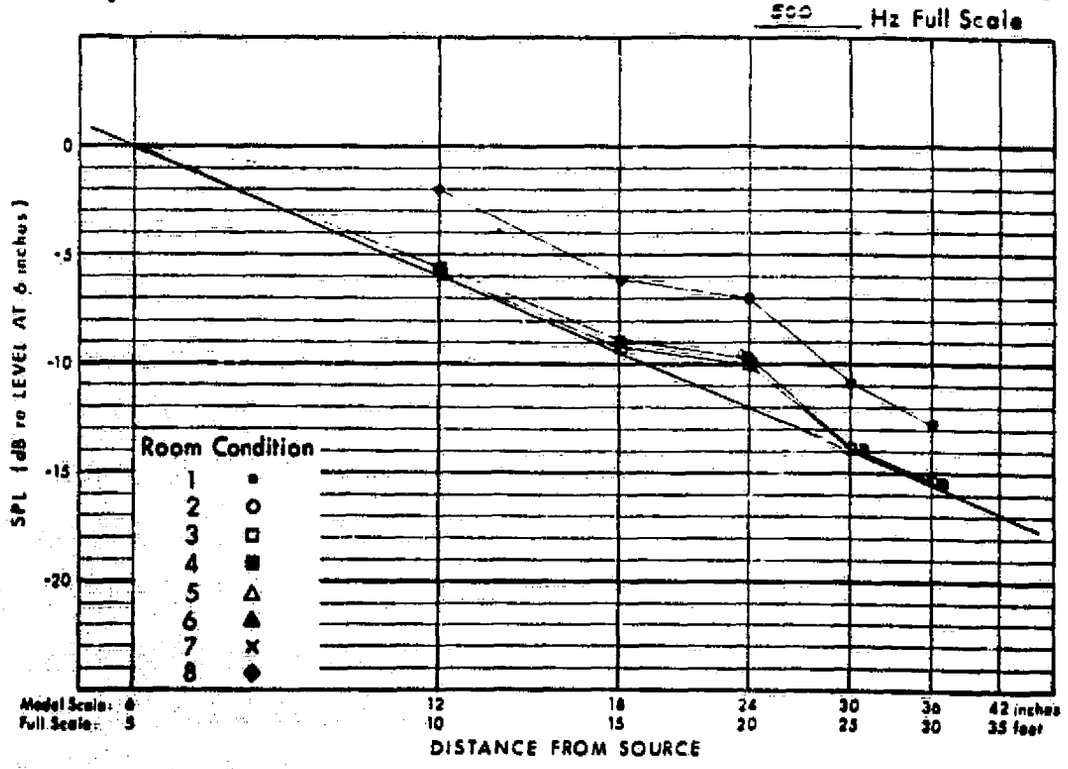

Fig. A-53 TRAVERSE E'

Source Position 2
10,000 Hz Model Scale
1000 Hz Full Scale

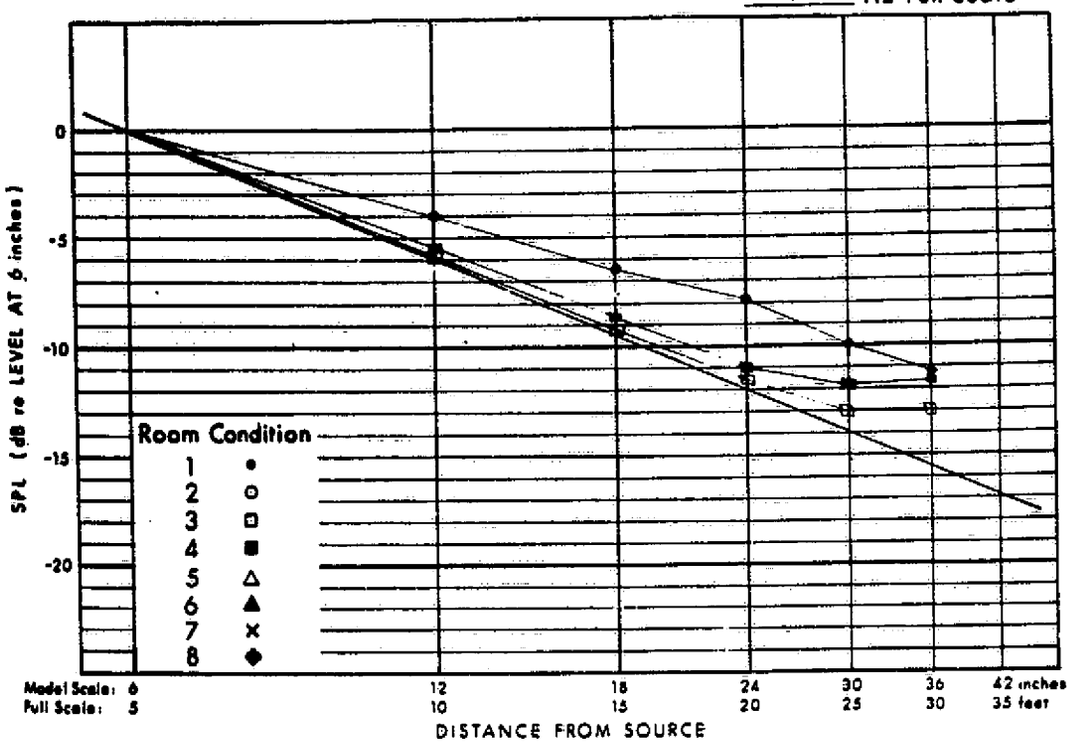

Fig. A-54 TRAVERSE E'

Source Position 2
20,000 Hz Model Scale
2000 Hz Full Scale

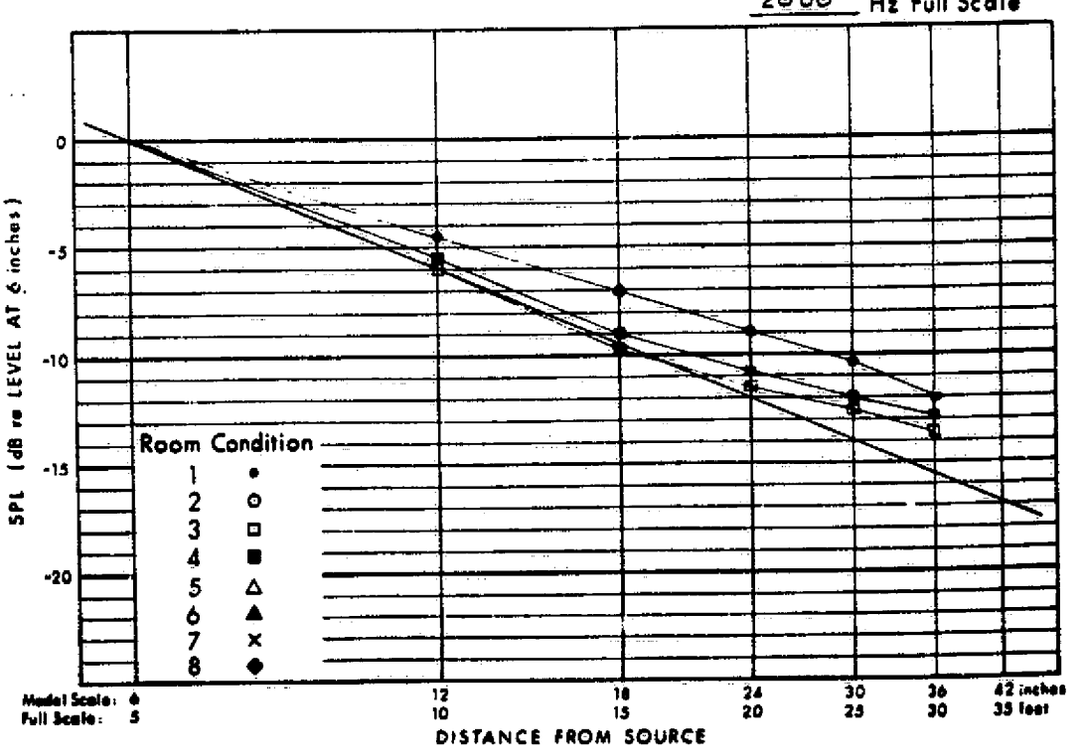

TRAVERSE G' - 45° UPSTREAM TOWARD FAR WALL

Figure No.	Model-Scale Frequency, Hz
A-55	630
A-56	1250
A-57	2500
A-58	5000
A-59	10,000
A-60	20,000

Fig. A-55 TRAVERSE G'

Source Position 2
630 Hz Model Scale
63 Hz Full Scale

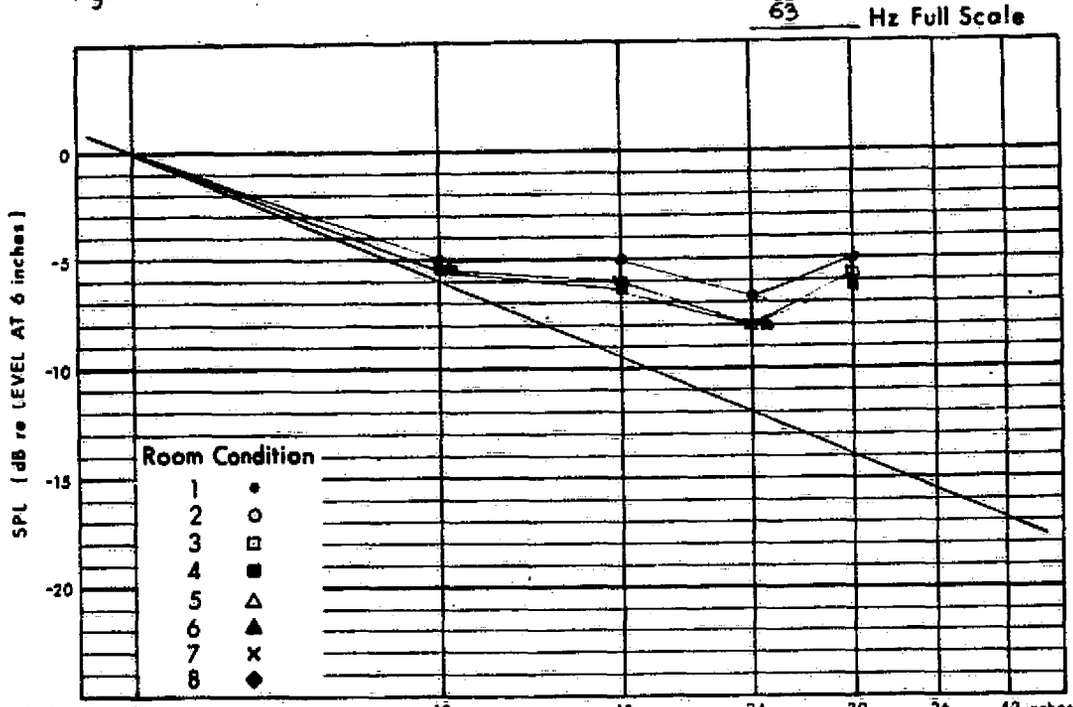

Fig. A-56 TRAVERSE G'

Source Position 2
1250 Hz Model Scale
125 Hz Full Scale

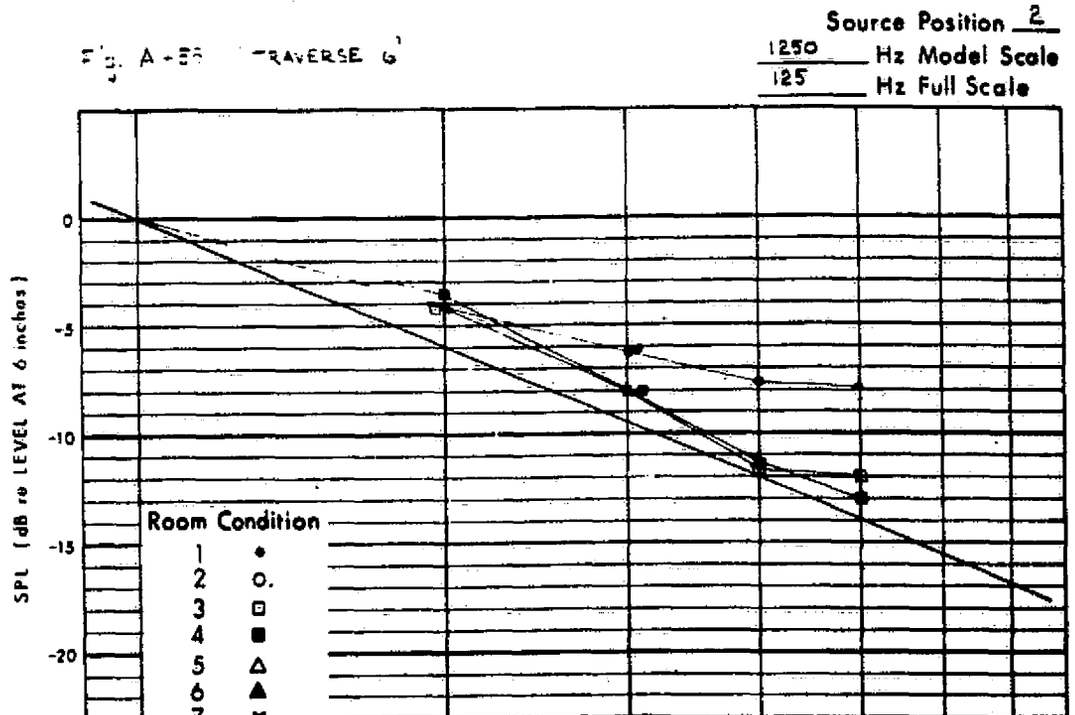

Fig. A-57 TRAVERSE G'

Source Position 2
2500 Hz Model Scale
250 Hz Full Scale

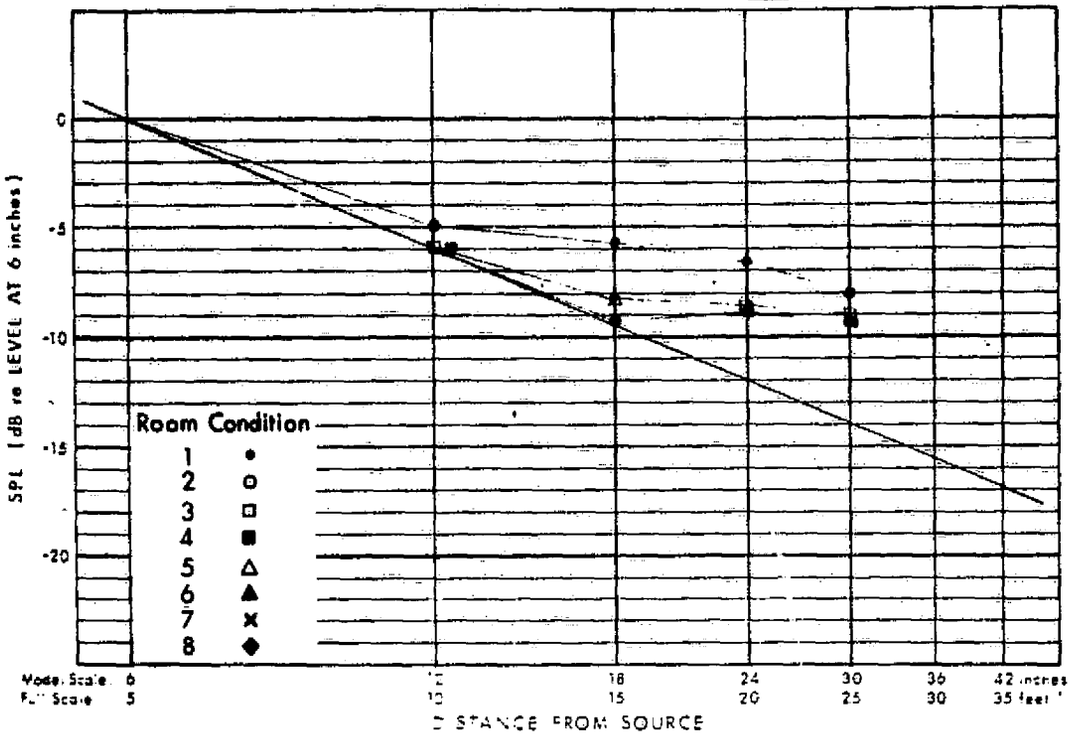

Fig. A-58 TRAVERSE G'

Source Position 2
5000 Hz Model Scale
500 Hz Full Scale

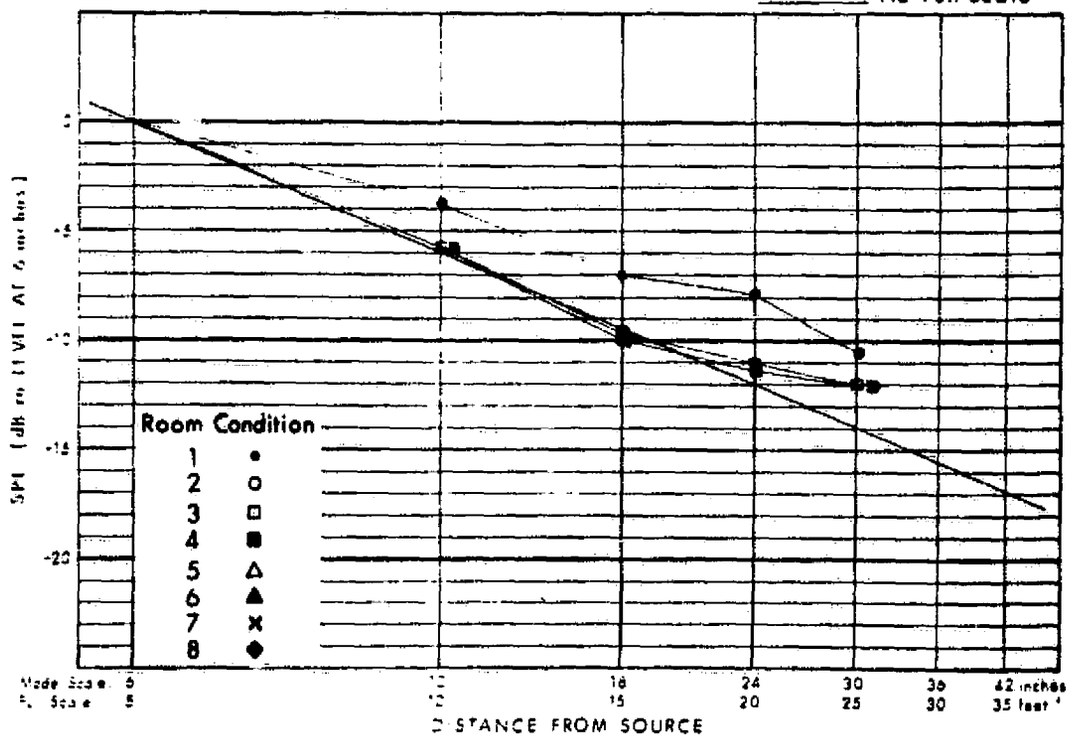

Fig A-53 TRAVERSE G'

Source Position 2
10,000 Hz Model Scale
1000 Hz Full Scale

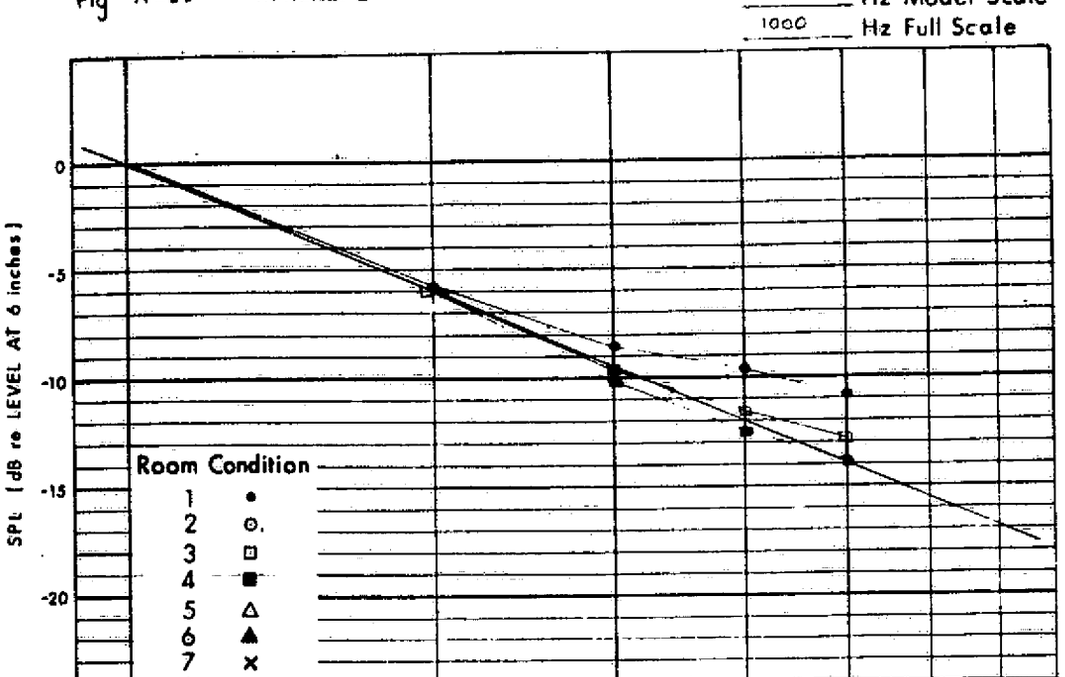

Fig. A-54 TRAVERSE G'

Source Position 2
20,000 Hz Model Scale
2000 Hz Full Scale